106p.

* mfs

N64-16521-N64-16525

NASA CODE-1

(NASA TMX-54562) OTS: #---

(MTP-AERO-63-70)
October 4, 1963

255

NASA.

GEORGE C. MARSHALL SPACE FLIGHT CENTER

HUNTSVILLE, ALABAMA

t; IMPLEMENTATION REPORT NO. 1
on Studies in the Fields of
Space Flight and Guidance Theory

Sponsored by Aero-Astrodynamics Laboratory
of the Marshall Space Flight Center

~~(auth.) W.E. Miner~~ 4 Oct. 1963 106p refs

OTS PRICE

XEROX $ 9.10 hc

MICROFILM $ 3.38 mf.

FOR INTERNAL USE ONLY

S

NATIONAL AERONAUTICS AND SPACE ADMINISTRATION

Avail thru N64-16525

MSFC - Form 523 (Rev. November 1960)

TABLE OF CONTENTS

GEORGE C. MARSHALL SPACE FLIGHT CENTER

MTP-AERO-63-70

October 4, 1963

IMPLEMENTATION REPORT NO. 1
on Studies in the Fields of
Space Flight and Guidance Theory

ASTRODYNAMICS AND GUIDANCE THEORY DIVISION
AERO-ASTRODYNAMICS LABORATORY

GEORGE C. MARSHALL SPACE FLIGHT CENTER

MTP-AERO-63-70

IMPLEMENTATION REPORT NO. 1
on Studies in the Fields of
Space Flight and Guidance Theory

Sponsored by Aero-Astrodynamics Laboratory
of the Marhall Space Flight Center

ABSTRACT

This volume contains reports of NASA sponsored studies in the area of space flight and guidance theory implementation. The studies are carried on by several industrial companies. This report covers the period from initiation of the studies until September 30, 1963. The technical supervisor of the contracts is W. E. Miner, Deputy Chief of the Astrodynamics and Guidance Theory Division, Aero-Astrodynamics Laboratory, George C. Marshall Space Flight Center.

GEORGE C. MARSHALL SPACE FLIGHT CENTER

MTP-AERO-63-70

IMPLEMENTATION REPORT NO. 1
on Studies in the Fields of
Space Flight and Guidance Theory

Sponsored by Aero-Astrodynamics Laboratory
of the Marshall Space Flight Center

SUMMARY

This volume contains reports of NASA sponsored studies in the area of space flight and guidance theory implementation. The studies are carried on by several industrial companies. This report covers the period from initiation of the studies until September 30, 1963. The technical supervisor of the contracts is W. E. Miner, Deputy Chief of the Astrodynamics and Guidance Theory Division of the Aero-Astrodynamics Laboratory, George C. Marshall Space Flight Center.

INTRODUCTION

This is the first of a series of reports dealing with the implementation of theory being developed by Astrodynamics and Guidance Theory Division of Aero-Astrodynamics Laboratory and the associated contractors.

The term Progress Report No. 1 (2, 3, 4) will be used for "Progress Reports on Studies in the Fields of Space Flight and Guidance Theory. The term Implementation Report will be used for "Implementation Report No. 1 on Studies in the Fields of Space Flight and Guidance Theory." These terms will be used for reference to the two companion series of reports.

Two problems are presented in this report. The first is that of determining feasibility of adaptive guidance for lunar orbital rendezvous ("LOR") type missions. The second is that of determining performance data as a basis for evaluating adaptive guidance in non-catastrophic abort from LOR type missions. Both works are preliminary and limited in scope.

Two papers are presented on the study of feasibility of adaptive guidance for LOR type missions. The first is by R. S. Polovitch and W. B. Morgan of Boeing Company. The second paper is by Dr. S. Hu of Northrop Corporation. The problem was arbitrarily defined by MSFC. No attempt was made to include the performance problem. Rather, the definition was made so that small maneuvers in yaw were required. This checked the guidance capability. Boeing was assigned the problem of launching into a space-fixed conic. This conic was defined as having circular velocity of a specified altitude with a 90° path angle (measured from vertical). It is realized that due to the earth's obliqueness, this will not define a specified conic. From the practical point of view, the simplified definition of the orbit was sufficient. From the point of injection into the circular orbit, Northrop Corporation developed the guidance to insertion into the lunar transit. This latter orbit was defined using the JPL lunar deck. Because of certain assumptions therein, the resulting lunar transits do not make up a continuous group. This caused large errors at the moon while having small errors compared to the defined end-conditions.

It is planned in the next implementation report to rework the problem utilizing a newly developed earth-moon deck and also to elaborate on performance considerations. In addition, various engineering constraints will be considered. It is also planned to extend the launch window study with a view toward determining whether or not additional holds on the launch pad are possible. Improvements in procedures will be incorporated, especially in the area of curve-fit techniques. Progress Reports 3 and 4 refer to articles in this area. In these two reports, many ideas are being checked and "packaged" for computer use. Lastly, experience alone will greatly improve the next results.

Two papers are presented on the study of performance data as a basis for evaluating adaptive guidance for non-catastrophic abort from LOR type missions. The first paper is by V. V. Moore and F. G. Bourque of Boeing Company. The second paper on reentry is by Ann Muzyka and H. Elmore Blanton of Raytheon Company. These two studies are complementary. The Raytheon study should define acceptable reentry conditions and maximum and minimum ranges for free flight through the atmosphere. These reentry conditions then become the desired end-conditions for the Boeing work. The parameters to be matched here are path angle (γ), velocity (v), and altitude (y or h). The last parameter (h) has been arbitrarily frozen and will only be opened at

a very late date. Several points of mismatch can be seen in the work. These will be corrected in future work. It may be noted that even for preliminary evaluation both papers should be considered simultaneously. Both papers offer modifications and extensions. Many of these will be followed for future work. Not clearly stated is the fact that in many cases return to some specified orbit and a later return to the earth is possible. This will greatly reduce the size of the required landing area. Future work will expand as discussed above and then add the full guidance problem.

Future implementation reports will add the efforts of several other contractors.

THE BOEING COMPANY Seattle, Wash.

SATURN BOOSTER BRANCH

AEROBALLISTIC UNIT

PATH ADAPTIVE GUIDANCE FOR SATURN V THREE-DIMENSIONAL ASCENT TO ORBIT

by

R. S. Polovitch and

W. B. Morgan

In NASA, Marshall Space Flight Center ~~Implementation~~ Rept. No. 1 on Studies in the Flight and Guidance Theory Fields of Space ~~Huntsville~~, Alabama 1963 P 5-30 refs

(See N64-16521 08 22) OTS: ~~OTS:~~

as

6

THE BOEING COMPANY
SATURN BOOSTER BRANCH
AEROBALLISTICS UNIT
Huntsville, Alabama

PATH-ADAPTIVE GUIDANCE FOR SATURN V THREE-DIMENSIONAL ASCENT TO ORBIT

by
R. S. Polovitch
W. B. Morgan

16522

SUMMARY

A

Pitch and yaw guidance polynomials for the Saturn V vehicle have been generated. These polynomials are designed to steer the vehicle into a space-fixed orbit at an altitude of 100 n.mi. The polynomials are capable of acceptable orbit injection at any time during a one hour launch window. They also allow for variations in thrust, specific impulse and weight in any of the stages as well as perturbations due to winds during Stage 1 flight.

AUTHOR

INTRODUCTION

An empirical method of implementing the path adaptive guidance scheme involves the development of steering polynomials. These polynomials must be able to steer the vehicle toward a predetermined end condition in an optimum manner.

The purpose of this study is to calculate a set of steering polynomials capable of acceptable injection into a 100 n.mi. orbit. These polynomials allow for launch at any time during a one-hour launch window. Perturbations due to thrust, specific impulse and weight variations in any of the stages and the effect of winds during first stage are included in the development of the polynomials.

The assumptions involved in the study are as follows:

1. Saturn V Vehicle

The launch vehicle is a typical three-stage Saturn V. Only that portion of the third stage required to achieve the proper orbital conditions is utilized during boost. The remainder of the propellant

is retained for use during insertion into the lunar trajectory. Vehicle characteristics used in the study are given in the following table.

	Stage 1	Stage 2	Stage 3
Thrust (lbs)	7,500,000.(s.l.)	1,000,000.(vac)	200,000.(vac)
Liftoff Weight (lbs)	6,000,000.	1,366,078.	359,267.
Propellant Weight (lbs)	4,224,210.	919,011.	(minimized)
Specific Impulse (sec)	Classified		

2. Trajectory Optimization

All of the trajectories used to generate the polynomials have been optimized for maximum burnout weight.

3. Spaced-fixed Waiting Orbit

The target orbit is a 100 n.mi. circular orbit with an inclination of 28.52 degrees. The space-fixed orbit is oriented so that its nodal line is coincident with the line of nodes of the lunar plane at the date of launch.

4. Launch Window

A launch window one hour in duration was selected for this study.

ANALYSIS

The analysis consists of two principal parts:

1. Determination of optimum trajectories which meet the desired end conditions.

2. Fitting pitch and yaw steering polynomials which steer the vehicle along these optimum trajectories.

1. Determination of Optimum Trajectories

A zero lift trajectory is flown during Stage 1 flight. However, during the early portion of the flight a pitch maneuver must be performed to turn the vehicle from the vertical. This pitch maneuver, as well as the launch azimuth, must be optimized. No thrust is applied in the yaw direction during Stage 1. Consequently, except for perturbations due to oblateness and earth's rotation, the first

stage flight is two-dimensional.

Upper stage trajectories are optimized by a three-dimensional calculus of variations analysis with an oblate earth model. The optimization criterion for all phases of the flight is maximum burnout weight.

The desired cut-off condition corresponds to the level of energy and angular momentum associated with a 100 n.mi. circular orbit over a spherical earth. On an oblate earth, this will result in an orbit whose radius from the center of the earth will vary in a periodic manner.

Discussion of the optimization of the first stage pitch maneuver involves several variables which require definition. These are as follows:

a) Tilt angle (α_p)~This is a measure of the rate at which the vehicle is turned away from vertical attitude. A pre-programmed turn is made early in first stage flight with α following the pattern indicated in the following sketch.

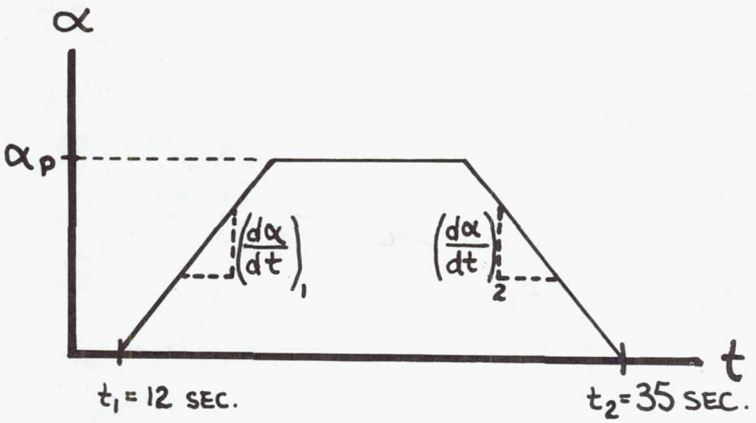

The values for t_1, t_2, $\left(\frac{d\alpha}{dt}\right)_1$, $\left(\frac{d\alpha}{dt}\right)_2$ are fixed. Consequently, the only parameter which affects the "steepness" of the first stage flight path and the ensuing first stage burnout conditions is α_p.

b) Launch Azimuth (A_z)~The vehicle azimuth at launch is measured clockwise from north. For purposes of this study, it is assumed that the pitch plane of the vehicle is always aligned with the launch azimuth. This eliminates the need for considering any roll during the vertical rise portion of the trajectories.

c) Co-nodal time ~ At the instant of liftoff the launch azimuth and latitude define a hypothetical orbit plane. If an azimuth of 90° is used, there is one time each day when the line of nodes of the instantaneously established plane will be coincident with the line of nodes of the target orbit. This time is defined as the co-nodal time.

d) Launch time (Δt_L) ~ This parameter is a measure of the location within the launch window of the launch site at the instant of liftoff. For this study the space fixed target orbit has an inclination equal to the launch latitude. This assumption places the launch site in the plane of the target orbit only once each day. This time corresponds to the co-nodal time defined previously and establishes an unique point, i.e., $\Delta t_L = 0$. Early and late launches are respectively characterized by negative and positive values of Δt_L. In the following sketch, Δt_L is depicted as an angle. This is the angle through which the earth rotates between the time of vehicle liftoff and the co-nodal time.

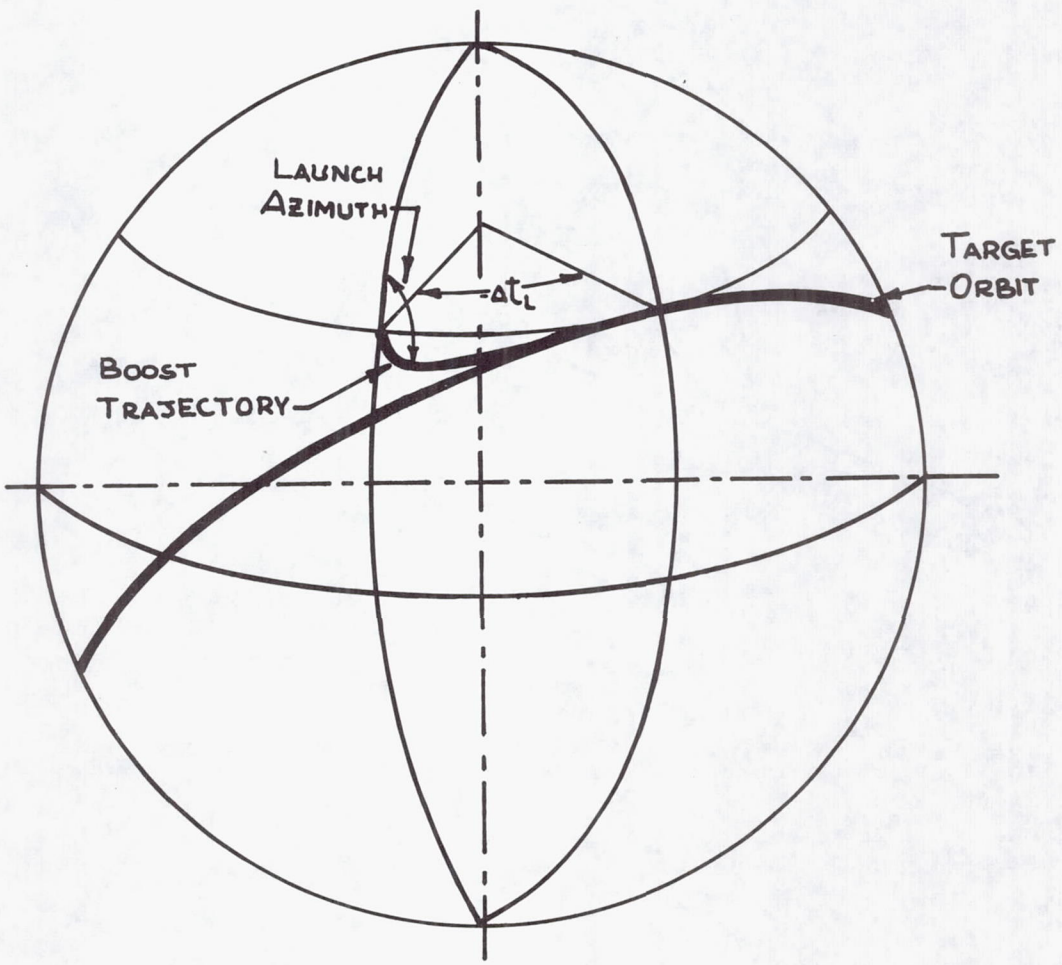

e) Plumbline coordinate system ~This coordinate system has its origin at the center of the earth. The y_p axis is parallel to the gravity gradient which passes through the launch site. The x_p axis is parallel to the launch azimuth and the z_p axis is perpendicular to the x_p-y_p plane forming a right hand system.

f) Steering Angles (χ_p, χ_y, χ_r) Eulerian angles which locate the missile axis with respect to the plumbline coordinate system.

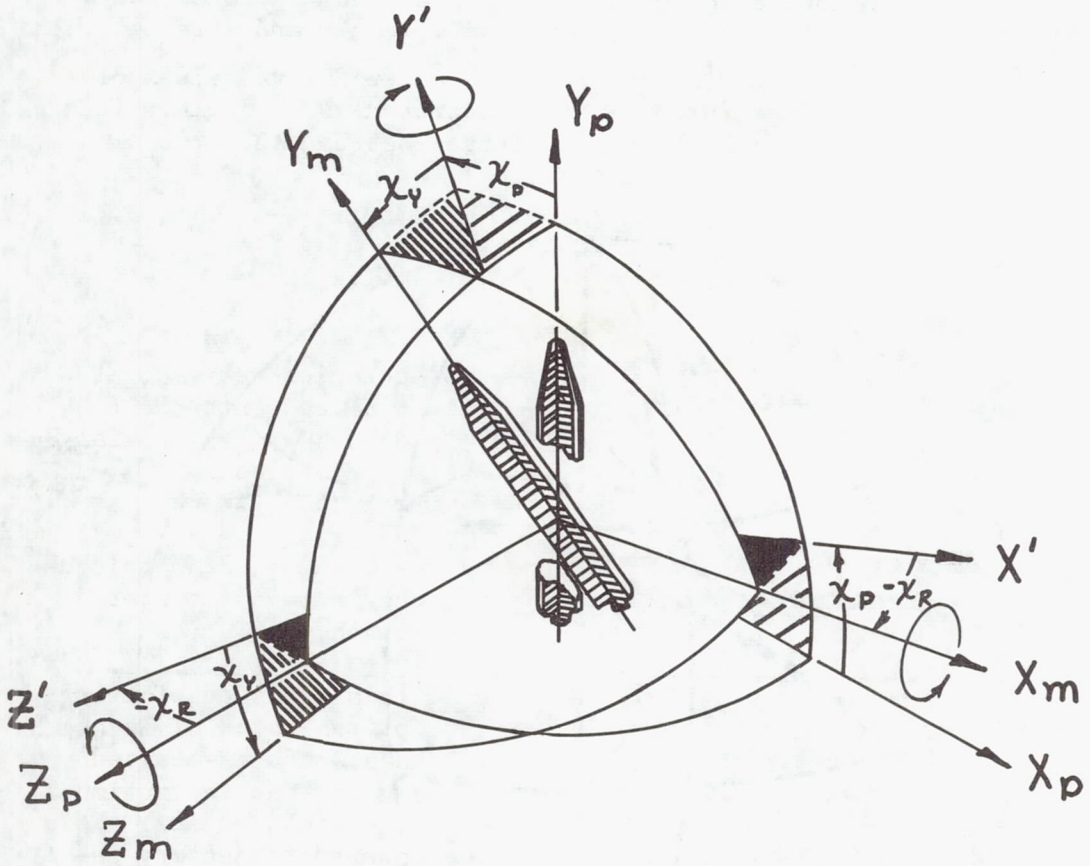

The launch window studied is one hour wide, i.e., $-30 \text{ min} \leq \Delta t_L \leq +30 \text{ min}$. For each selected value of Δt_L, the parameters A_z and α_p must be optimized. Studies indicated that the optimum value of α_p is quite insensitive to variations in A_z and Δt_L. This was a fortuitous result since an actual first stage flight may use an open-loop χ_p versus time guidance which is invariant with launch time and launch azimuth. A fifth order polynomial in time for χ_p was written to fit the nominal χ_p versus time table. This polynomial which was used to guide all of the first stage trajectories flown in this study is shown below.

First Stage χ_p Polynomial

$$\chi_p = a_o + a_1 t + a_2 t^2 + a_3 t^3 + a_4 t^4 + a_5 t^5$$

$a_o = +0.3835668$ $\qquad$ $a_3 = -0.9412463 \times 10^{-4}$

$a_1 = -0.2384704$ $\qquad$ $a_4 = -0.6213386 \times 10^{-7}$

$a_2 = +0.1633698 \times 10^{-1}$ $\qquad$ $a_5 = +0.1104191 \times 10^{-8}$

For each value of Δt_L studied, trajectories were run at several launch azimuths to determine the weight placed into orbit by a nominal vehicle. These trajectories followed the χ_p polynomial during first stage and were optimized in the upper stages by the calculus of variations to obtain maximum burnout weight.

A similar analysis in Reference 1 discusses a parametric study involving variations in launch time, launch azimuth, target orbit inclination and altitude on a spherical earth.

Figure 1 illustrates the results of this study by plotting A_z versus weight in orbit. For each Δt_L an optimum value of launch azimuth is clearly defined. The optimum launch azimuth associated with each value of Δt_L is given in Figure 2. Note that the optimum azimuth for $\Delta t_L = 0$ is 89.15° and not 90° as one might expect. This result is due primarily to the fact that the powered trajectory required a finite time (about 12 minutes) and that the analysis was performed using an oblate earth model. As shown in the following sketch, the gravity gradient is resolved into two components, one directed toward the center of the earth and one perpendicular to the geocentric radius.

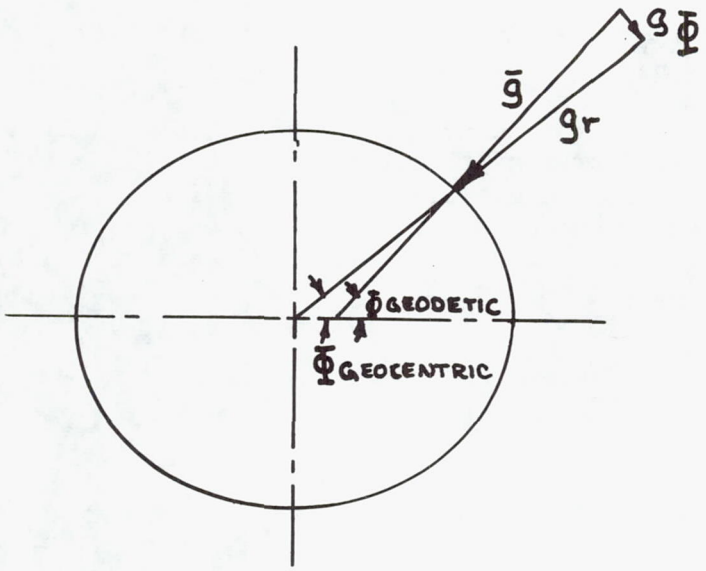

A vehicle launched due east ($A_z = 90°$) at $\Delta t_L = 0$ would tend to leave its plane because of the gravity component, g_Φ. In order to maintain flight in the desired plane, thrust would be required in the yaw direction. In effect, this would be a three dimensional trajectory. When the launch direction is slightly north of east, gravity draws the vehicle into the target plane without any expenditure of propellant. Consequently, although a small plane change is performed, the total energy expended in reaching the desired end condition is a minimum.

In Figure 3, the maximum weight which can be placed in orbit at each value of Δt_L is given. This curve indicates that the best launch time with respect to weight in orbit is $\Delta t_L = +17$ min. This corresponds to a launch azimuth of 91.9° and appears contrary to the expected optimum of 90°. Explanation of this result involves a trade between the effect of the gravity component, g_Φ, previously discussed and the contribution of the earth's rotation to the total energy imparted to the vehicle. As launch azimuth is varied from north to south, the effect of the gravity component becomes more pronounced. In fact, if this effect is the only one considered, a launch direction of due south is optimum. However, the tangential velocity imparted to the vehicle due to earth's rotation is a maximum when the launch direction is due east. When the effects of earth's rotation and gravity are considered simultaneously, the optimum launch azimuth becomes some angle south of east. Since the earth's rotational effect is so much larger than the gravity effect, the

optimum launch direction is slightly south of east.

Empirical implementation of the path adaptive guidance scheme involves forcing the vehicle to follow an optimum path. The guidance system continually monitors the vehicle's state variables, i.e., position and velocity components, thrust acceleration, time, and Δt_L. The on-board computer carries prestored guidance polynomials which allow calculation of the optimum required thrust direction as a function of the state variables. Prior to flight, a volume of optimum trajectories is generated using the calculus of variations. These trajectories, when flown, place the vehicle at the desired end condition in an optimum manner. Polynomials are written to fit the optimum χ history of these trajectories.

Two basic considerations were involved in the selection of optimum trajectories contained in the volume used to write the polynomials. These considerations are size and content. It is desirable to make the volume large enough to adequately cover the range of variables required and small enough to prevent the solution from becoming too cumbersome. It is also desirable to vary the vehicle and flight parameters to assure that any given vehicle, whose characteristics are within their allowable tolerances, will fly a trajectory enclosed in the volume studied. The range of dispersions used is as follows:

	Stage 1	Stage 2	Stage 3
Thrust	$\pm$ 3%	$\pm$ 3%	$\pm$ 3%
Isp	$\pm$ 4 sec.	$\pm$ 6.36 sec.	$\pm$ 6.36 sec.

Stage one trajectories were also perturbed by the presence of head, tail, and cross winds. The wind profile assumed is maximum design wind at an altitude of 12 Km. This wind is defined in Reference 2.

The volume chosen included vehicles with off-nominal values of thrust and specific impulse in each stage, taken one at a time; i.e., when Stage 1 was assumed off-nominal, Stages 2 and 3 were flown as nominal. In addition, extreme variations were included by assuming that the vehicle parameters all varied simultaneously in the same direction. For instance, negative dispersions in both thrust and specific impulse in all three stages were considered. The trajectories flown with winds included vehicle variations in first stage with all nominal upper stages. For each vehicle variation studied, optimum trajectories are flown for $-30 \text{ min} \leq \Delta t_L \leq +30$ min. in ten minute intervals. This volume resulted in a total of 339 optimum trajectories.

Table 1 illustrates the range of first stage burnout conditions generated by the volume of vehicle and flight dispersions. The increments of position and velocity vector components referenced to the completely nominal vehicle are shown. An indication of the large size of the volume may be obtained from the maximum and minimum variations denoted by asterisks.

2. Curve Fit

Once the volume of optimum trajectories has been calculated, the next step involves generating guidance polynomials capable of steering the vehicle during boost to an acceptable orbit injection. Pitch and yaw steering polynomials must be written. In addition, a polynomial which calculates the required time remaining to burnout during the latter portion of the third stage flight is also written.

Steering and cutoff polynomials for the Saturn C-1 vehicle are presented in Reference 3. In this study, liftoff always occurs when the launch site is in the target plane. Three dimensional turning during upper stage flight is required primarily to eliminate out-of-plane perturbations caused by the earth's rotation and oblateness.

The polynomials are of the following form:

$$\chi = A_o + A_1 X + A_2 Y + A_3 Z + A_4 \dot{X} + A_5 \dot{Y} + \ldots$$

$$\chi_p = f(x, y, z, \dot{x}, \dot{y}, \dot{z}, F/M, t, \Delta t_L)$$

$$\chi_y = f(x, y, z, \dot{x}, \dot{y}, \dot{z}, F/M, t, \Delta t_L)$$

$$t_c = f(x, y, z, \dot{x}, \dot{y}, \dot{z}, F/M, t, \Delta t_L)$$

where $x, y, z,$ = components of position vector in plumbline coordinate system (meters)

$\dot{x}, \dot{y}, \dot{z},$ = components of velocity vector in plumbline coordinate system (meters/sec)

F/M = thrust/mass (meters/sec^2)

t = time from liftoff (seconds)

Δt_L = launch window (minutes)

χ_p, χ_y = Eulerian angles defining thrust vector direction in the pitch and yaw planes. (degrees)

t_c = time remaining to engine cutoff (sec)

All combinations of the nine state variables to third order, plus a constant, result in 220 terms.

Selected points from the 339 optimum trajectories in the volume are used to write the steering and cutoff polynomials. A cross-section of the 220 possible terms is chosen up to a maximum of 50. Using those terms, a least squares curve fit technique is utilized to generate the desired polynomials.

RESULTS

A number of different polynomials were calculated for pitch, yaw, and cutoff. Separate polynomials were calculated for second and third stage. A preliminary comparison between polynomials may be based on the root-mean-sum of the difference between χ as defined by the optimum trajectories and χ as calculated by the polynomial. Past experience indicated that if RMS is less than approximately 0.3, the polynomial would be acceptable and would result in an acceptable trajectory. In the course of running actual trajectory simulations with guidance commands provided by the polynomials, it was found that RMS is not too valuable an indication of their validity. Comparison between two polynomials often indicates that the one with the lower value of RMS results in greater deviations from the desired end condition.

Typical polynomials are presented in Tables 2 through 6. The coefficients for each variable are given. The term Y found in the polynomials is defined as $Y_p - R$ where Y_p = value for Y in the plumbline coordinate system and R = radius of earth. The number of terms in each polynomial and its corresponding RMS are tabulated below.

	No. of terms	RMS
Second Stage Pitch	48	.136 Deg.
Second Stage Yaw	45	.081 Deg.
Third Stage Pitch	45	.854 Deg.
Third Stage Yaw	45	.191 Deg.
Third Stage Cutoff	38	.118 Sec.

In order to adequately test the validity of the polynomials, a number of 3-dimensional digital flight simulations were run. These simulations actually used the steering and cutoff polynomials to guide the flight path. The check trajectories were chosen to encompass each of the variations used to generate the initial volume.

The desired cutoff conditions are as follows:

Velocity (V)	= 7794.58 m/sec.
Radius (r)	= 6555200. meters
Flight Path Angle (θ)	= 90°
Orbital Inclination (i)	= 28.52°

The results of this check, using the polynomials already presented, are given in Table 7. Errors in altitude, velocity, flight path angle and orbit inclination are presented for each vehicle dispersion. The RMS of each error is also given.

An indication of the amount of plane change required for liftoff anywhere in the launch window is presented in Figure 4. The angle $\Delta\phi$ is defined as the angle between the target plane and the plane established if an orbit is instantaneously attained at any given launch latitude and azimuth. Data are given for launch azimuth from 86 degrees to 94 degrees and for the optimum launch azimuth associated with each value of Δt_L.

Ground tracks of boost trajectories for Δt_L = 0 and -30 min. are illustrated in Figure 5. For comparison, the ground track of the target orbit is also shown. The tracks are plotted in Mercator projection on a non-rotating earth.

CONCLUSIONS AND RECOMMENDATIONS

1. When launch occurs at the co-nodal time, the optimum launch azimuth is 89.15°. Maximum weight is placed in orbit if launch is delayed until 17 minutes after the co-nodal time.

2. Guidance polynomials have been written which successfully steer the vehicle into a space fixed orbit. Liftoff may take place anywhere within a one hour launch window.

3. Perturbations in the nominal boost trajectory due to vehicle variations in thrust, specific impulse and weight are easily handled by the polynomials. Perturbations due to winds during boost are also readily handled.

4. Simulation of typical boost trajectories steered by the reported guidance polynomials results in RMS errors of approximately 1 km. in altitude, 0.1° in flight path angle, 0.4 m/sec. in velocity, and 0.007° in orbit inclination.

5. The selection of terms for use in the polynomials has involved a trial and error process. Errors considerably smaller than

those presented can result if the proper selection of terms is made. Development of an efficient scheme for determining the most significant terms is desirable.

6. Curve fit techniques other than least squares should be investigated.

7. Comparison between polynomials on an RMS basis has been found to be ineffective. Consequently, in this study comparison has been based only on a digital flight simulation using the polynomials to steer the vehicle. An attempt to find a better statistical comparison should be made. If some polynomials can be eliminated by the use of a statistical comparison, the amount of digital computer time required to determine the best combination of terms in the polynomial would be greatly reduced.

TABLE 1

FIRST STAGE CUT-OFF CONDITIONS

Δt_L = -30 Min. A_Z = 86.1 Deg.

RUN NO.	FIRST STAGE DISPERSION			FIRST STAGE CUT-OFF						
	F	Isp	Wind	ΔX (m)	ΔY (m)	ΔZ (m)	ΔX (m/s)	ΔY (m/s)	ΔZ (m/s)	Δt_c (sec)
A-1	+3%	+1.5%	None	- 1133	+3971	- 56**	+20.93	+70.60	- .28	-2.1
A-15	+3%	-1.5%	"	-10398	+1808	- 167	-85.65	+81.65	- .005**	-6.5
A-43	-3%	+1.5%	"	+11157	-2311	+ 177	+85.29	-86.13	- .02	+6.9
A-57	-3%	-1.5%	"	+ 1014**	-4060	+ 58	-24.94	-69.92**	+ .08	+2.3
B-1	+3%	+1.5%	Head	- 2294	+4365	- 112	+ 8.63**	+74.39	- .82	-2.1
B-3	+3%	-1.5%	"	-11517	+2186	- 221	-98.28*	+85.45	- .55	-6.5
B-34	-3%	+1.5%	Tail	+12228*	-2704	+ 227	+95.74	-89.22*	+ .41	+6.9
B-36	-3%	-1.5%	"	+ 2046	-4442*	+ 106	-14.38	-73.10	+ .51	+2.3
B-57	+3%	-1.5%	Lf.Cross	-10474	+1807	+1105	-86.76	+81.58	+13.44	-6.5
B-61	-3%	+1.5%	" "	+11072	-2312	+1588*	+84.38	-86.22	+13.22	+6.9
B-82	+3%	+1.5%	Rt.Cross	- 1121	+3946	-1372	+20.99	+70.33	-13.62*	-2.1
B-84	+3%	-1.5%	" "	-10386	+1784**	-1434	-85.82	+81.38	-13.41	-6.5

Nominal Case $X = 151216$ $Y = 6435131$ $Z = 22224$

$\dot{X} = 2563.69$ $\dot{Y} = 855.93$ $\dot{Z} = 17.71$

$t_c = 153.7$ $\chi_p = 56.6°$ $\chi_y = .791°$

* Maximum Variation

** Minimum Variation

TABLE 2

YAW STEERING POLYNOMIAL

SECOND STAGE

TERM	COEFFICIENT	TERM	COEFFICIENT	TERM	COEFFICIENT
A_o (Deg)	-9.3163288	YT	$-7.8257465 \times 10^{-8}$	$\dot{X}\dot{Y}$ F/M	$-5.0942913 \times 10^{-9}$
X (M)	$+1.0195762 \times 10^{-5}$	ZT	$-2.7299943 \times 10^{-6}$	$Y\dot{Z}$ F/M	$+9.0348244 \times 10^{-9}$
Y (M)	$+3.1438830 \times 10^{-5}$	$\dot{X}$T	$+3.7748143 \times 10^{-6}$	$\dot{Z}^2$F/M	$+5.1456394 \times 10^{-7}$
Z (M)	$+8.2167335 \times 10^{-4}$	$\dot{Y}$T	$-8.9242263 \times 10^{-6}$	Y$(F/M)^2$	$+1.1035070 \times 10^{-8}$
$\dot{X}$ (M/S)	$-1.6089329 \times 10^{-3}$	$\dot{Z}$T	$-2.5124504 \times 10^{-5}$	Z$(F/M)^2$	$-4.1817956 \times 10^{-8}$
$\dot{Y}$ (M/S)	$-7.4887707 \times 10^{-3}$	F/M T	$-3.7529165 \times 10^{-4}$	Y^2T	$-4.0329277 \times 10^{-14}$
$\dot{Z}$ (M/S)	$+3.5143001 \times 10^{-3}$	T^2	$+4.5386163 \times 10^{-5}$	XZT	$+9.5624569 \times 10^{-13}$
F/M(M/S^2)	$+2.4306434 \times 10^{-1}$	YΔt_L	$-7.3868989 \times 10^{-7}$	YZT	$+4.7792121 \times 10^{-12}$
T (Sec)	$+6.0046996 \times 10^{-3}$	ZΔt_L	$-7.1529175 \times 10^{-6}$	Z^2T	$+2.1335529 \times 10^{-12}$
Δt_L (Min)	$+3.2836861 \times 10^{-1}$	$\dot{Y}\Delta t_L$	$-2.6115389 \times 10^{-5}$	XZΔt_L	$+5.9335804 \times 10^{-12}$
YZ	$-1.0479217 \times 10^{-9}$	$\dot{Z}\Delta t_L$	$-6.7082010 \times 10^{-5}$	YZ Δt_L	$+2.0924695 \times 10^{-11}$
$Z\dot{Y}$	$+2.4622173 \times 10^{-7}$	F/MΔt_L	$-9.2781489 \times 10^{-4}$	$Z^2\Delta t_L$	$-1.7755862 \times 10^{-11}$
$\dot{X}\dot{Y}$	$+1.0077969 \times 10^{-6}$	TΔt_L	$-6.0591885 \times 10^{-4}$	$X\dot{Y}\Delta t_L$	$+6.9803377 \times 10^{-11}$
$Y\dot{Z}$	$-4.0146217 \times 10^{-7}$	XY F/M	$-1.6504575 \times 10^{-13}$	$Y\dot{Y}\Delta t_L$	$+1.3324114 \times 10^{-10}$
XT	$-3.8593084 \times 10^{-8}$	YZ F/M	$-4.3819295 \times 10^{-11}$	$Z\dot{Y}\Delta t_L$	$-1.3949240 \times 10^{-10}$

$Y = Y_p - R$ where $R = 6373337.2$ meters

092463

TABLE 3

PITCH STEERING POLYNOMIAL

SECOND STAGE

TERM	COEFFICIENT	TERM	COEFFICIENT	TERM	COEFFICIENT
A_o	$-2.5197237 \times 10^{+1}$	$\dot{Y}\Delta t_L$	$+1.1918824 \times 10^{-6}$	Z^2F/M	$-1.0571918 \times 10^{-12}$
X	$+1.4428352 \times 10^{-6}$	$\dot{Z}\Delta t_L$	$+7.9003317 \times 10^{-6}$	$Y\dot{X}\ F/M$	$-8.4894779 \times 10^{-10}$
Y	$+8.5079440 \times 10^{-5}$	$F/M\Delta t_L$	$-3.2709072 \times 10^{-4}$	$\dot{Z}(F/M)^2$	$-8.9403287 \times 10^{-7}$
Z	$+3.2921825 \times 10^{-6}$	$T\Delta t_L$	$+1.1509458 \times 10^{-5}$	X^2T	$-1.4671355 \times 10^{-13}$
$\dot{Y}$	$+1.5740623 \times 10^{-2}$	XY^2	$+1.6779022 \times 10^{-16}$	XYT	$+4.5312886 \times 10^{-13}$
$\dot{Z}$	$+3.1747471 \times 10^{-4}$	Y^3	$+4.6502831 \times 10^{-16}$	$Y\dot{Y}T$	$+4.2224126 \times 10^{-10}$
F/M	$+7.7751782$	$X^2\dot{Y}$	$-5.3540472 \times 10^{-15}$	$\dot{X}YT$	$+3.5908920 \times 10^{-9}$
Δt_L	$+2.3433923 \times 10^{-3}$	$Y\dot{Y}^2$	$+5.6684405 \times 10^{-11}$	$Y\dot{Z}T$	$+5.8405668 \times 10^{-11}$
Y^2	$+3.1233771 \times 10^{-10}$	$\dot{Y}^3$	$+5.0011765 \times 10^{-9}$	XT^2	$+5.0728903 \times 10^{-10}$
$Z\dot{Y}$	$+2.8067417 \times 10^{-9}$	$Y^2\dot{Z}$	$+4.7123697 \times 10^{-14}$	$\dot{X}T^2$	$+1.4796217 \times 10^{-7}$
$Y\dot{Z}$	$-3.3963735 \times 10^{-8}$	$Z^2\dot{Z}$	$-1.8458686 \times 10^{-12}$	$\dot{Y}T^2$	$-1.8725866 \times 10^{-7}$
$Z\dot{Z}$	$+3.4187530 \times 10^{-8}$	$Y\dot{Z}^2$	$-1.5884291 \times 10^{-11}$	$F/M\ T^2$	$-4.2467833 \times 10^{-5}$
$\dot{Z}^2$	$+4.3455238 \times 10^{-6}$	$\dot{Z}^2Z$	$+2.8702789 \times 10^{-10}$	T^3	$-8.6560105 \times 10^{-7}$
$X\Delta t_L$	$-3.3188386 \times 10^{-9}$	$\dot{Y}\dot{Z}^2$	$+1.2542381 \times 10^{-9}$	$XY\Delta t_L$	$+2.0395705 \times 10^{-14}$
$Y\Delta t_L$	$-2.2090197 \times 10^{-8}$	$XY\ F/M$	$-7.1365936 \times 10^{-12}$	$Y^2\Delta t_L$	$+4.1764537 \times 10^{-14}$
$Z\Delta t_L$	$-5.4797011 \times 10^{-8}$	Y^2F/M	$-2.0949745 \times 10^{-12}$	$X\dot{X}\Delta t_L$	$+8.1906996 \times 10^{-13}$

$Y = Y_p - R$ where $R = 6373337.2$ meters

092463

TABLE 4

YAW STEERING POLYNOMIAL

THIRD STAGE

TERM	COEFFICIENT	TERM	COEFFICIENT	TERM	COEFFICIENT
A_o	-4.8682864	YT	$+2.6615327 \times 10^{-8}$	$\dot{X}\dot{Y}$ F/M	$+2.5244878 \times 10^{-8}$
X	$+1.8170245 \times 10^{-5}$	ZT	$-3.7271234 \times 10^{-6}$	$Y\dot{Z}$ F/M	$+4.2969013 \times 10^{-8}$
Y	$+1.7919258 \times 10^{-5}$	$\dot{X}T$	$-3.7089316 \times 10^{-6}$	$\dot{Z}^2$F/M	$+4.8997438 \times 10^{-6}$
Z	$+1.3527021 \times 10^{-3}$	$\dot{Y}T$	$-1.5211184 \times 10^{-5}$	$Y(F/M)^2$	$+1.7803666 \times 10^{-7}$
$\dot{X}$	$+1.5742798 \times 10^{-3}$	$\dot{Z}T$	$+7.5556900 \times 10^{-4}$	$Z(F/M)^2$	$+4.6359573 \times 10^{-6}$
$\dot{Y}$	$+1.2294579 \times 10^{-2}$	F/MT	$+2.4599282 \times 10^{-4}$	Y^2T	$-8.7370124 \times 10^{-15}$
$\dot{Z}$	$-3.7419080 \times 10^{-1}$	T^2	$+1.1840582 \times 10^{-4}$	XZT	$+3.3831325 \times 10^{-13}$
F/M	$-9.0590695 \times 10^{-1}$	$Y\Delta t_L$	$-7.6782971 \times 10^{-7}$	YZT	$+4.7031745 \times 10^{-13}$
T	$-4.3223290 \times 10^{-2}$	$Z\Delta t_L$	$-9.6857025 \times 10^{-7}$	Z^2T	$-4.9203751 \times 10^{-13}$
Δt_L	$+2.3549313 \times 10^{-1}$	$\dot{Y}\Delta t_L$	$-2.1159120 \times 10^{-4}$	$XZ\,\Delta t_L$	$-7.7466600 \times 10^{-14}$
YZ	$-1.2218951 \times 10^{-9}$	$\dot{Z}\Delta t_L$	$+2.0292869 \times 10^{-4}$	$YZ\,\Delta t_L$	$-1.8050161 \times 10^{-12}$
$Z\dot{Y}$	$+4.5606823 \times 10^{-8}$	F/M Δt_L	$+3.9146195 \times 10^{-2}$	$Z^2\Delta t_L$	$-2.9903261 \times 10^{-12}$
$\dot{X}\dot{Y}$	$-6.0549310 \times 10^{-7}$	$T\Delta t_L$	$-1.0972316 \times 10^{-3}$	$X\dot{Y}\,\Delta t_L$	$+1.1857600 \times 10^{-10}$
$Y\dot{Z}$	$+8.7691277 \times 10^{-8}$	XY F/M	$-5.8519842 \times 10^{-13}$	$Y\dot{Y}\,\Delta t_L$	$+2.1859794 \times 10^{-10}$
XT	$-2.5318894 \times 10^{-8}$	YZ F/M	$-4.2464884 \times 10^{-11}$	$Z\dot{Y}\,\Delta t_L$	$+1.8029512 \times 10^{-10}$

$Y = Y_p - R$ where R = 6373337.2 meters

092463

TABLE 5

PITCH STEERING POLYNOMIAL

THIRD STAGE

TERM	COEFFICIENT	TERM	COEFFICIENT	TERM	COEFFICIENT
A_o	$-4.0546367 \times 10^{+3}$	$\ddot{X}\dot{Y}$	$+1.9631275 \times 10^{-4}$	XY F/M	$+1.0527299 \times 10^{-12}$
X	$-1.9664022 \times 10^{-3}$	$\dot{Y}^2$	$+3.4629657 \times 10^{-4}$	$\dot{Y}\dot{X}$ F/M	$-2.1355763 \times 10^{-8}$
Y	$+7.3941658 \times 10^{-3}$	Y F/M	$+1.8056825 \times 10^{-4}$	X^2T	$+2.5336599 \times 10^{-12}$
Z	$-2.9962813 \times 10^{-5}$	XT	$-2.9404846 \times 10^{-6}$	XYT	$+4.1216178 \times 10^{-12}$
$\dot{X}$	$+2.5675969 \times 10^{-1}$	YT	$-3.3249322 \times 10^{-5}$	Y^2T	$-7.1577965 \times 10^{-12}$
$\dot{Y}$	$-4.9720504 \times 10^{-1}$	$X \Delta t_L$	$+3.643889 \times 10^{-8}$	$\dot{X}^2T$	$+7.3205544 \times 10^{-8}$
$\dot{Z}$	$+2.6498565 \times 10^{-3}$	$Y \Delta t_L$	$-9.1311300 \times 10^{-8}$	$\dot{Y}YT$	$+2.6467831 \times 10^{-10}$
F/M	-7.4008585	$Z \Delta t_L$	$+1.0703024 \times 10^{-6}$	$\ddot{X}YT$	$-7.3210298 \times 10^{-8}$
T	$+1.3721689 \times 10^{+1}$	$\dot{Y} \Delta t_L$	$+2.2959069 \times 10^{-5}$	XT^2	$-9.8167372 \times 10^{-9}$
Δt_L	$+4.9925804 \times 10^{-2}$	$\dot{Z} \Delta t_L$	$-1.9619938 \times 10^{-4}$	$\dot{X}T^2$	$-2.5073155 \times 10^{-6}$
XY	$+5.2647937 \times 10^{-9}$	F/M Δt_L	$+2.6763259 \times 10^{-4}$	F/M T^2	$+4.4789852 \times 10^{-5}$
Y^2	$+1.0047664 \times 10^{-8}$	$T \Delta t_L$	$-1.7694321 \times 10^{-4}$	T^3	$+1.6061421 \times 10^{-5}$
$X\dot{X}$	$+4.2551235 \times 10^{-7}$	$X^2\dot{Y}$	$+6.7001801 \times 10^{-14}$	$XY \Delta t_L$	$-1.3385831 \times 10^{-14}$
$Y\dot{X}$	$-3.0180819 \times 10^{-8}$	$Y\dot{Y}^2$	$-3.2219629 \times 10^{-10}$	$Y^2 \Delta t_L$	$-5.8639033 \times 10^{-14}$
$\dot{X}^2$	$-3.7110768 \times 10^{-5}$	$\dot{Y}^3$	$+6.9654744 \times 10^{-8}$	$X\dot{X} \Delta t_L$	$-1.9954698 \times 10^{-12}$

$Y = Y_p - R$ where R = 6373337.2 meters

092463

TABLE 6

CUTOFF TIME POLYNOMIAL

THIRD STAGE

TERM	COEFFICIENT	TERM	COEFFICIENT	TERM	COEFFICIENT
A_o	$+2.4983850 \times 10^{+4}$	$\dot{Z}F/M$	$-1.1256042 \times 10^{-3}$	$\dot{Z}^3$	$-3.4314616 \times 10^{-9}$
$\dot{X}$	$-1.0576426 \times 10^{+1}$	$(F/M)^2$	$+2.4077407 \times 10^{+1}$	$\dot{X}(F/M)^2$	$-3.1809302 \times 10^{-3}$
$\dot{Y}$	-4.3829501	$\dot{X}T$	$+6.2334678 \times 10^{-3}$	$\dot{Y}(F/M)^2$	$+5.3836821 \times 10^{-4}$
$\dot{Z}$	$+4.8057398 \times 10^{-3}$	$\dot{Y}T$	$+2.7125073 \times 10^{-4}$	$\dot{Z}(F/M)^2$	$+8.1422970 \times 10^{-5}$
F/M	$-4.9569286 \times 10^{+2}$	T^2	$-1.3807829 \times 10^{-2}$	$\dot{X}^2T$	$-6.4530036 \times 10^{-7}$
T	$-1.3299996 \times 10^{+1}$	$\dot{X}\Delta t_L$	$-1.6312105 \times 10^{-7}$	$\dot{Y}^2T$	$-9.7423446 \times 10^{-8}$
Δt_L	$-1.3622844 \times 10^{-3}$	$\dot{Y}\Delta t_L$	$+2.1012181 \times 10^{-6}$	$\dot{Z}^2T$	$-3.6915943 \times 10^{-9}$
$\dot{X}^2$	$+1.5076425 \times 10^{-3}$	$T\Delta t_L$	$+1.4034174 \times 10^{-5}$	$\dot{X}T^2$	$+2.1615007 \times 10^{-6}$
$\dot{X}\dot{Y}$	$+1.4542013 \times 10^{-3}$	$(\Delta t_L)^2$	$+1.5633668 \times 10^{-4}$	$\dot{Y}T^2$	$-3.0226162 \times 10^{-7}$
$\dot{Y}^2$	$+2.5875335 \times 10^{-4}$	$(\dot{X})^3$	$-7.0478323 \times 10^{-8}$	$\dot{Z}T^2$	$+1.7156491 \times 10^{-10}$
$\dot{Z}^2$	$-5.8075911 \times 10^{-6}$	$\dot{X}^2\dot{Y}$	$-1.1930620 \times 10^{-7}$	$\dot{Y}^2\Delta t_L$	$+1.2791656 \times 10^{-10}$
$\dot{X}F/M$	$+6.2449482 \times 10^{-2}$	$\dot{X}\dot{Y}^2$	$-3.6179801 \times 10^{-8}$	$(\Delta t_L)^3$	$+6.2766209 \times 10^{-7}$
$\dot{Y}F/M$	$-1.7262958 \times 10^{-2}$	$\dot{Y}^3$	$-7.6967234 \times 10^{-9}$		

$Y = Y_p - R$ where $R = 6373337.2$ meters

092463

TABLE 7

CUTOFF ACCURACY

DESIRED CUTOFF CONDITIONS: Radius (r) = 6,555,200 Meters
Flight Path Angle (θ) = 90.0 Degrees
Velocity (V) = 7794.58 Meters/Second
Inclination (i) = 28.52 Degrees

RUN No.	Δt_L (Min)	DISPERSION	Δr (KM)	$\Delta\theta$ (Deg.)	ΔV (M/Sec.)	Δi (Deg.)
1	0	Nominal	+0.66	-0.06	+0.11	-0.009
2	0	-2% in Stage 1 Thrust	+1.63	-0.24	+0.16	-0.009
3	0	-1% in Stage 1 Isp	+1.05	-0.08	+0.34	-0.005
4	0	+10% in Stage 1 Inert Wt.	+1.69	-0.17	+0.31	-0.004
5	0	-2% in Stage 2 Thrust	-0.28	+0.09	+0.50	-0.007
6	0	-1% in Stage 2 Isp	+1.48	-0.14	+0.20	-0.009
7	0	+10% in Stage 2 Inert Wt.	-1.01	+0.12	+1.16	-0.006
8	0	-2% in Stage 3 Thrust	+0.62	-0.05	+0.22	-0.008
9	0	-1% in Stage 3 Isp	+0.67	-0.06	+0.11	-0.009
10	0	+10% in Stage 3 Inert Wt.	+0.26	-0.18	+0.39	-0.007
11	0	Head Wind	-0.55	+0.06	+0.52	-0.002
12	0	Left Cross Wind	-0.82	-0.07	+0.13	-0.008
13	-30	Δt_L = -30 Minutes	+0.70	-0.06	+0.11	+0.002
RMS			0.99	0.12	0.43	0.007

092463

SATURN V LOR MISSION

Δt_L ~ LAUNCH TIME RELATIVE TO CO-NODAL INSTANT

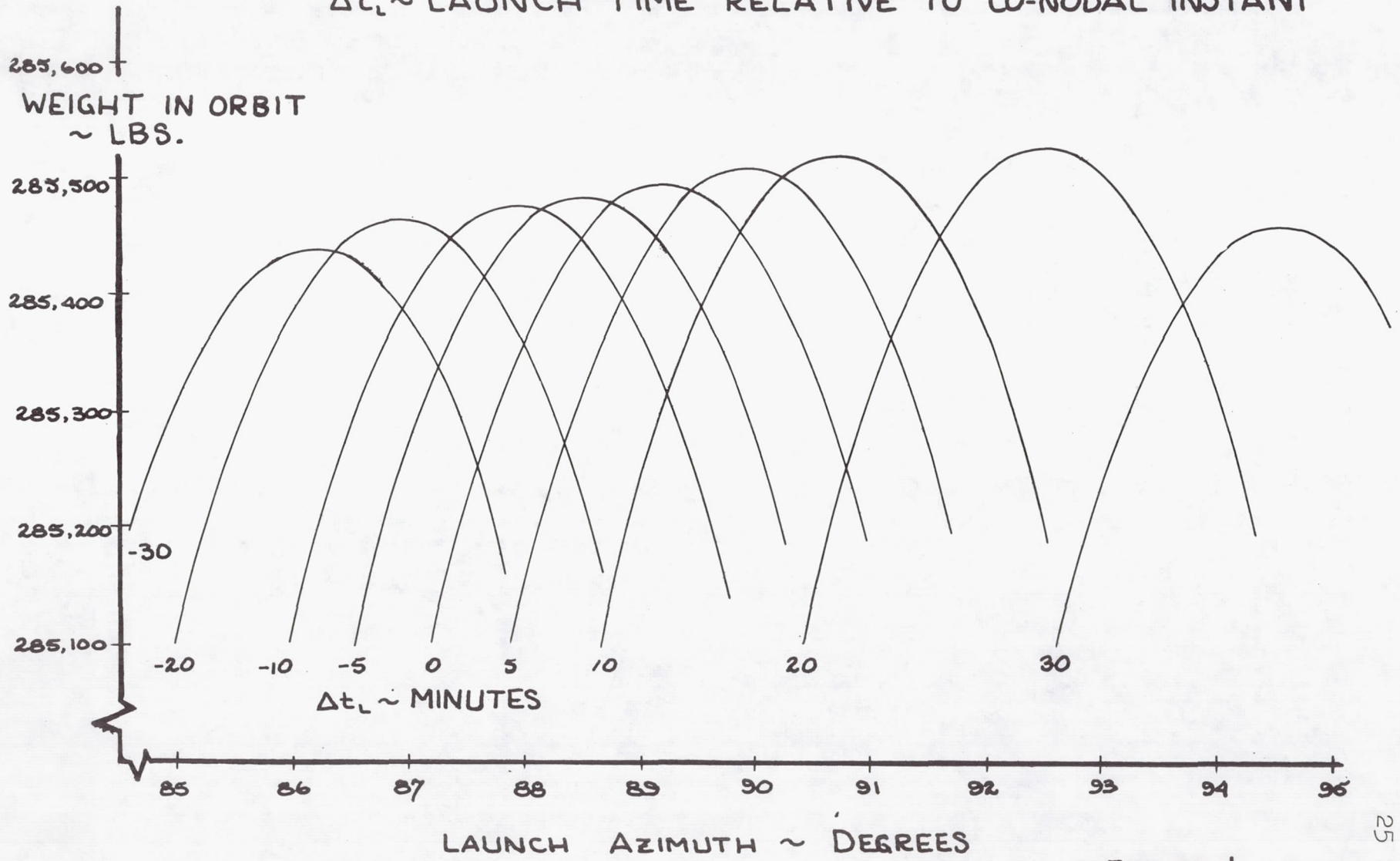

FIGURE 1

SATURN V LOR MISSION

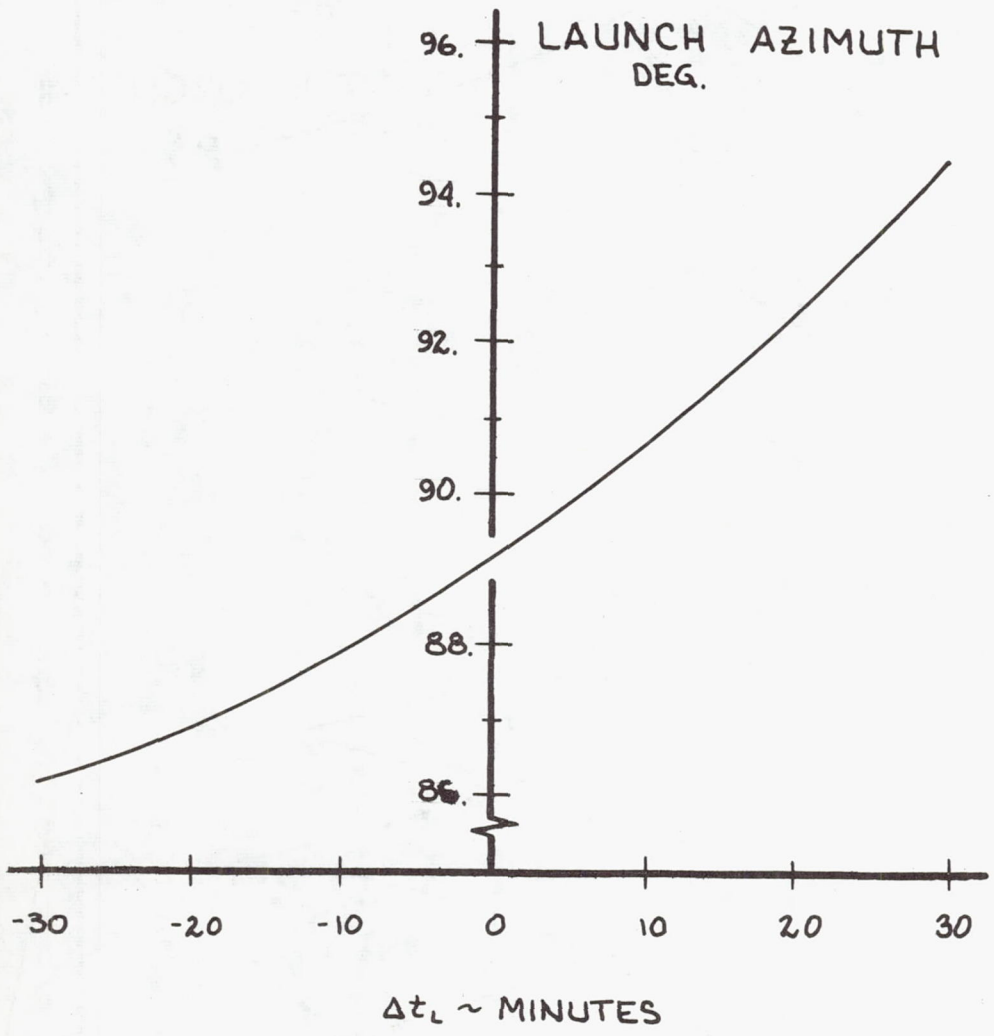

Δt_L ~ LAUNCH TIME RELATIVE TO CONDAL INSTANT

FIGURE 2

SATURN V LOR MISSION

Δt_L ~ LAUNCH TIME RELATIVE TO CO-NODAL INSTANT

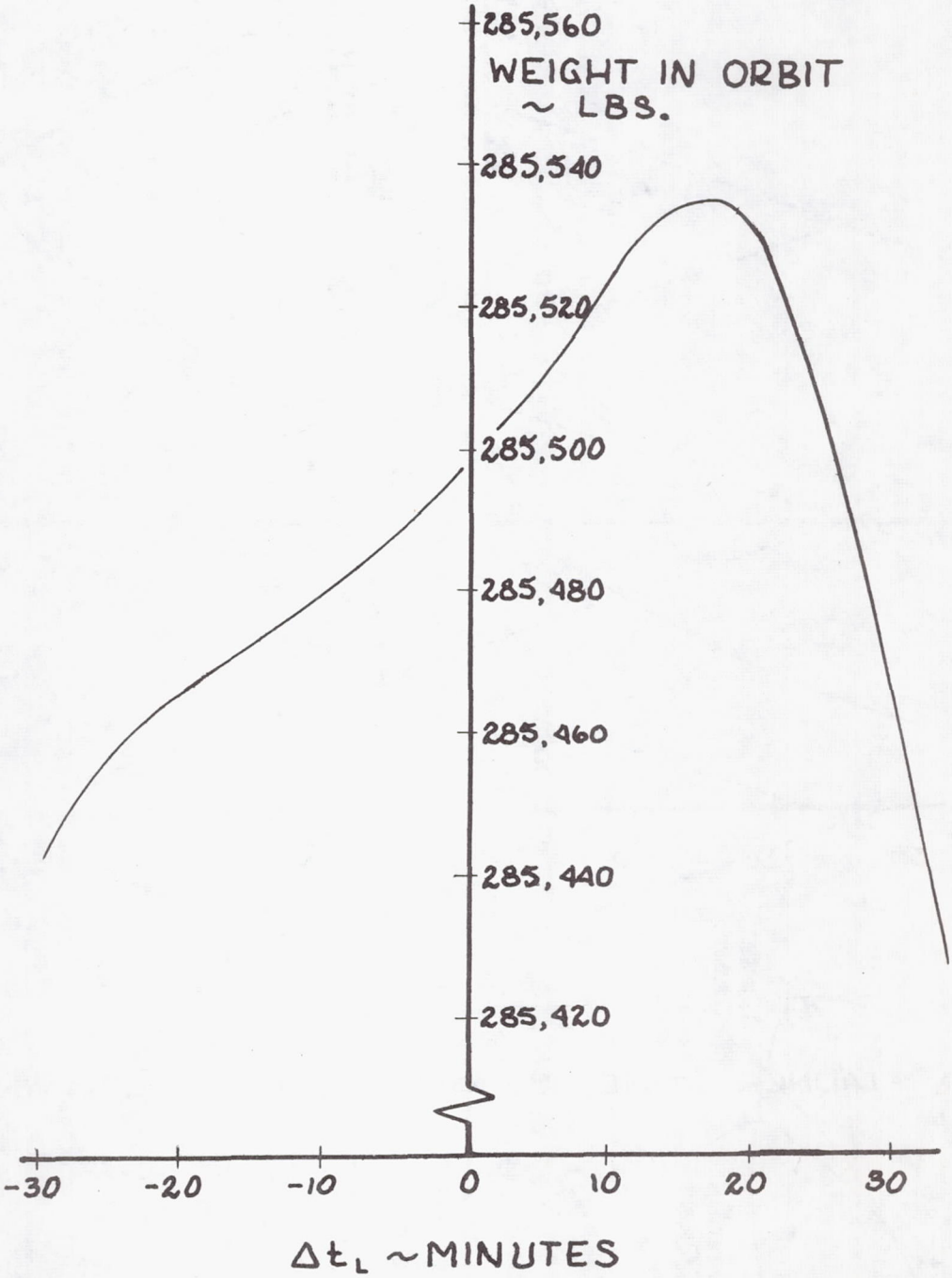

FIGURE 3

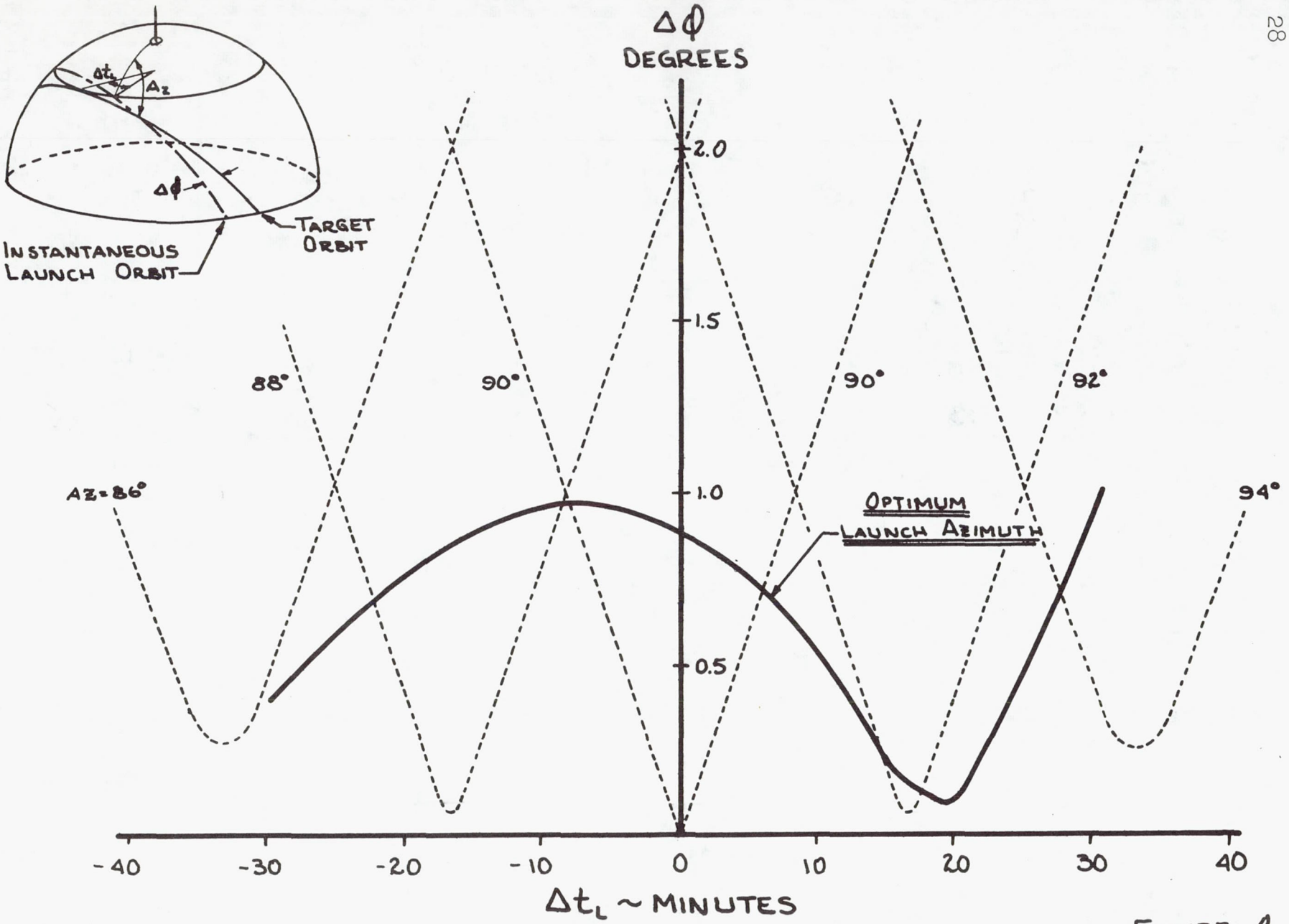
Δφ
DEGREES
2.0
1.5
1.0
0.5
88°
90°
90°
92°
94°
AZ=86°
OPTIMUM
LAUNCH AZIMUTH
-40
-30
-20
-10
0
10
20
30
40
Δt_L ~ MINUTES
Δt_L
A_Z
Δφ
TARGET
ORBIT
INSTANTANEOUS
LAUNCH ORBIT

FIGURE 4

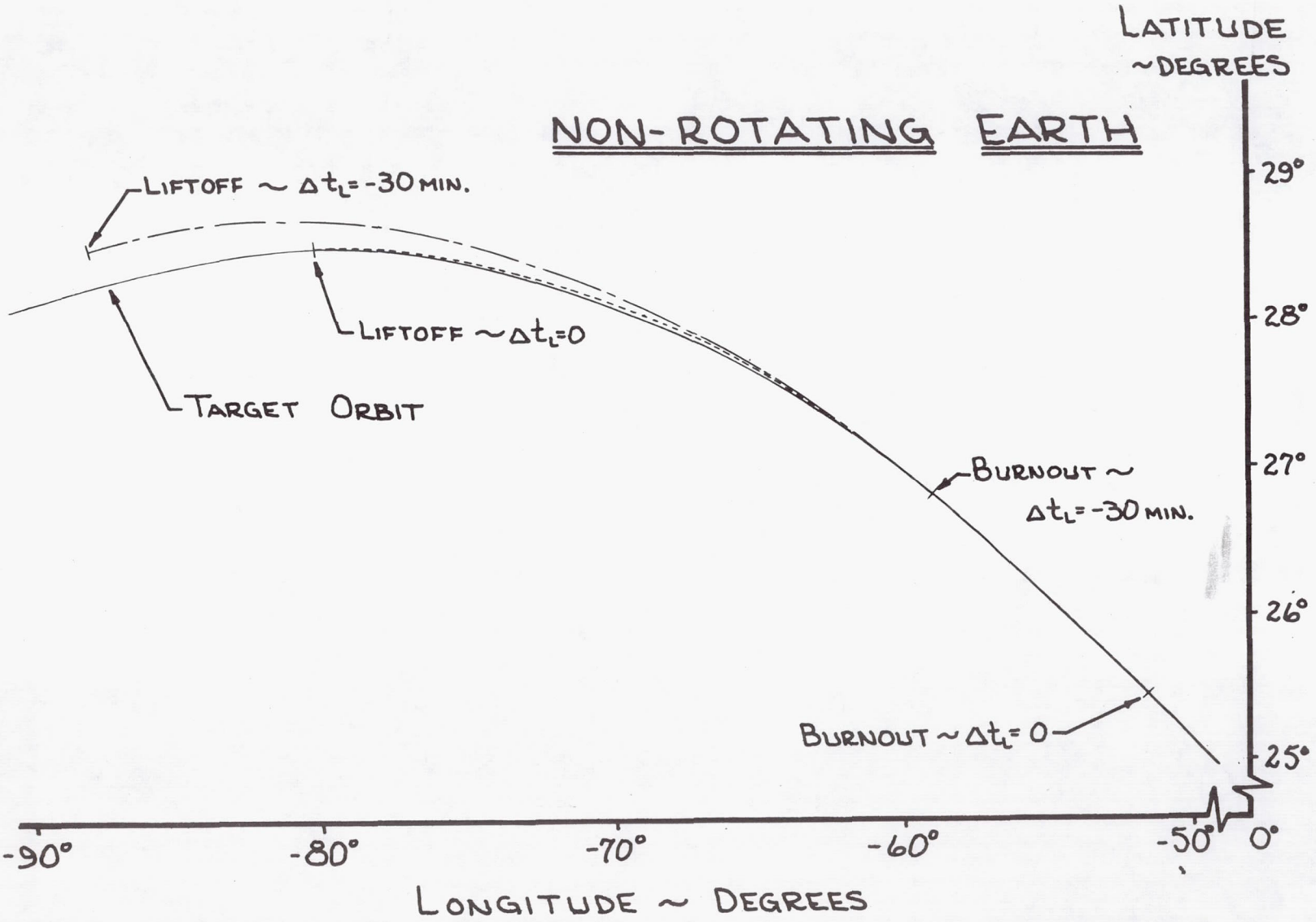
NON-ROTATING EARTH
LATITUDE ~DEGREES
LIFTOFF ~ Δt_L=-30 MIN.
LIFTOFF ~Δt_L=0
TARGET ORBIT
BURNOUT ~ Δt_L=-30 MIN.
BURNOUT ~Δt_L= 0
29°
28°
27°
26°
25°
-90°
-80°
-70°
-60°
-50°
0°
LONGITUDE ~ DEGREES

FIGURE 5

REFERENCES

1. Miner, W. E., and Silber, Robert, "Launch Window Studies Employing Variational Calculus to Determine Optimum Three Dimensional Trajectories Leading to Injection into a Space-Fixed Circular Orbit", ARS 17th Annual Meeting and Space Flight Exposition, Los Angeles, California, November, 1962.

2. Geissler, E. D., "Revision of Natural Environmental Design Criteria, In-Flight Wind Conditions, Saturn C-5 Vehicle." M-AERO-G-24-62, Marshall Space Flight Center, Sept. 4, 1962.

3. Ingram, Hugo, "Path-Adaptive Guidance Applied to Saturn C-1 Block II: Three Dimensional Steering Functions and Cutoff Functions for a Circular Orbit Mission". AIN-7-63, Marshall Space Flight Center, February 15, 1963.

RESEARCH-ANALYSIS SECTION
NORTHROP/HUNTSVILLE DEPARTMENT
NORTHROP SPACE LABORATORIES

Northrop Corp., Hawthorne, Calif
174 1412

t; SATURN V GUIDANCE EQUATIONS FOR POWER FLIGHT FROM PARKING ORBIT TO EARTH-TO-MOON TRANSIT

by

S. HU In ... 1963 p31-70
(See ...) OTS;

Huntsville, Alabama

ACKNOWLEDGEMENT

The work described in this report was performed by the Northrop/ Huntsville Lunar Flight Analysis Study Team. The members of this team are S. Hu, R. E. Bray, R. D. Gilbertson, E. J. Holmbeck, W. J. Reilly, H. J. Wilcox, D. L. Cooper, and E. L. Bailey.

RESEARCH-ANALYSIS SECTION

NORTHROP/HUNTSVILLE DEPARTMENT
NORTHROP SPACE LABORATORIES

SATURN V GUIDANCE EQUATIONS FOR POWER FLIGHT FROM PARKING ORBIT TO EARTH-TO-MOON TRANSIT

by

S. Hu

16523

Summary

A

A set of guidance equations for power flight of the third stage of the Saturn V from parking orbit to earth-to-moon transit conic have been developed. This set consists of four polynomial expressions in terms of time and the state and vehicle performance variables. These equations provide the time of leaving the parking orbit, pitch and yaw steering angles during power flight and time remaining to third stage cutoff. The method utilized to obtain these guidance equations is based upon the calculus of variations.

AUTHOR

INTRODUCTION

The purpose and object of this report is to present the work involved and the results obtained to date concerning the development of a set of guidance equations for properly guiding a Saturn V third-stage vehicle to: (1) take off from a perturbed parking orbit, (2) boost through a 3-dimensional optimal twisted powered flight, and (3) inject into a properly selected earth-moon transit conic, so that the vehicle will free-fall into the vicinity of the moon, passing the moon at a pre-determined minimum altitude over a pre-determined point on the moon's surface. These guidance equations would command the control system of the vehicle in terms of "when" and "how": (1) when to re-ignite the third-stage rocket, (2) how to steer the rocket thrust in pitch and yaw, and (3) when to finally cut off the rocket thrust, thereby, effectively carrying out the optimal 3-dimensional post-orbital boost to transit.

Briefly, the report first describes and discusses: (1) the basic desired unperturbed optimal trajectory, (2) various unavoidable perturbations including analysis of perturbed parking orbits, and (3) the 3-dimensional post-orbital boost which was studied following the perturbed parking orbits and other perturbation studies. A large volume of perturbed trajectories was computed on the basis of all types of perturbation combinations. This spectrum of perturbed optimal trajectories was analyzed at every time interval and was reduced into a representative statistical model. All controlling guidance parameters were expressed in the form of multi-term polynomials of the vehicle's state and performance variables. These guidance polynomials may be used to convert instantly sensed state and control elements of the vehicle into command signals to enable the vehicle to follow a newly selected optimal path from instant to instant. Finally, each of these polynomial guidance functions is analyzed: (1) in terms of its own accuracy as to how closely it represents all of the perturbed optimal trajectories by

the root-mean-square value of their value differences at all time intervals, and (2) in terms of its guidance accuracy as to how far off is the cutoff performance of the vehicle when it is steered by these guidance polynomials as compared with the cutoff performance if it is steered by the theoretical function of variational calculus optimization.

PRE-SELECTED UNPERTURBED NOMINAL OPTIMAL TRAJECTORY

The desired and nominal trajectory chosen for this study represents a 72-hour space flight path to the moon on October 13, 1966. This date was chosen because there was an angular difference between the minimum-inclination parking orbit from Cape Canaveral launch site (90° azimuth over Cape Canaveral) and the earth-moon plane, thereby illustrating the 3-dimensional feature of the guidance functions to be developed in this paper.

This nominal trajectory will pass the moon at a minimum radius (periselenum) of 1885 km (from the moon's center) over a predetermined point on the moon's surface, which is 5° latitude N. and 167° longitude E. from the zero point at the mean earth-moon-line. (Note: The said 167° longitude E. is in the rear side of the moon as viewed from the earth; and the zero point at the mean earth-moon-line is in the Sinus of Medii which can be seen from the earth at all times.) By n-body celestial mechanics or by 6-body J.P.L. programming, a proper earth-moon transit may be approached by Cape Canaveral launching at 10h 36m 6 sec (Greenwich time) on October 10, 1966. The vehicle will be inserted eastward into a 90° azimuth 100-nautical mile parking orbit. It will then coast 1-2/3 orbit, and then inject into this earth-moon transit for free flight to the moon, passing the pre-selected point in the vicinity of the moon.

The point of interest involved in this project centered in the duration of the parking orbit waiting period and the post-orbital boost to earth-moon transit. The trajectory to be optimized will have both ends variable. It starts from the perturbed parking orbit in the 2/3-orbit region and ends on the time-varying earth-moon transit (see figure 2). The vehicle, under the adaptive guidance, will seek and follow an optimal path from instant-to-instant based on instaneous state and control variables sensed, until it reaches the transit conic and starts free flight.

Figure 2 described this desired and preselected nominal and undisturbed optimal trajectory.

PERTURBATIONS SURVEY AND PARKING ORBIT ANALYSIS

It is usually impossible to fly along the above-mentioned preselected nominal optimal trajectory, because there are many unavoidable perturbations. To start with, there are perturbations due to a launch window of $\pm$ 30 minutes for time to launch. Then, there are the initial errors of position and velocity vectors at the time of insertion into parking orbit. This insertion error, in terms of variations of velocity, altitude, and path angle, $\Delta v, \Delta r, \Delta\theta$, will be modified and enlarged during the parking orbit coasting period due to earth oblateness and controlled venting effects of the vehicle's propellant tank. Therefore, errors of Δv, Δr, $\Delta\theta$ at the time of re-ignition or at the end of parking-orbit coasting may be greater than at the time of insertion. Besides, there are perturbations due to the orbital boost window; i.e., one period advance or one period delay for the time of re-ignition. In other words, the vehicle may be ignited in the region of the 2/3 orbit, 1-2/3 orbit, or 2-2/3 orbit.

It is to be noted that the variation in yaw (out-of-plane motion) was assumed to be negligible for this first-cut investigation and was not included in parking orbit insertion errors. The out-of-plane yaw effect, however, was properly included in the studies of parking orbit perturbations due to earth oblateness and related factors.

After the third stage re-ignition, there are further perturbations due to the imperfections of post-orbital-boost's propulsion system in terms of variations of thrust and specific impulse, $\pm \Delta F$, $\pm \Delta I_{sp}$. This, together with other perturbations as mentioned in previous paragraphs, will prevent the vehicle from following the exact preselected nominal optimal trajectory in reaching the final third stage cutoff point on the earth-moon transit.

The study of this complex picture of perturbations may best be approached by the study of the parking orbit perturbations. During

parking orbit coasting, there are two external variable forces acting on the vehicle. They are: (1) gravitational force due to the oblate earth, and (2) assumed axial thrust force due to the controlled venting of the vehicle's propellant tank. As the pressure in the propellant tank rises, due to aerodynamic heating and solar heating, it must be released from time to time in order to prevent it from exceeding certain limits. Figure 3 illustrates the general venting mechanism of the third-stage vehicle; and figure 4 illustrates the force function due to the axial venting. The venting is assumed to start after 12 minutes from the time of insertion. It exerts a 300-pound thrust for 90 seconds, shuts off for 16 minutes, and vents again for 90 seconds. This venting cycle will be repeated until the time of re-ignition.

The parking orbit perturbation due to initial insertion error was studied on the basis of this assumed venting-force function together with oblate earth effect. The plumbline coordinate system, the pitch plane diagram, as well as the orbital pitching rate of the vehicle adopted for the study, are illustrated in figures 4, 5, and 6.

The initial insertion error in terms of Δr, Δv, and θ was assumed to be $\pm$ 1 km, $\pm$ 2 m/sec, and $\pm$ 0.02 degree. A total of ten trajectories for parking orbit coasting was studied to cover all cases of probable perturbation combinations with oblate earth and controlled venting effects. One trajectory was for oblate effect only; one trajectory for combined oblate and venting effect; and the other eight trajectories for various Δv, Δr, and $\Delta\theta$ effects on the basis of oblate earth and controlled venting vehicle. The details of the trajectory composition for the parking orbit perturbation are listed in figure 7.

Results of all ten cases were studied, analyzed, and compared. Evaluated results indicated that the initial insertion velocity error, Δv, was most influential and represented the controlling input. Figure 8 is a composite diagram designed to illustrate this point. Outer and inner ellipses (see figure 8) represent the energy range of the perturbed

orbit. They are based on initial Δv variations and they envelop other ellipses which are based on Δr variations. With this controlling initial Δv at insertion as input, the resulting perturbations of Δv, Δr, and $\Delta\theta$ in the re-ignition region were studied for a vented orbiting trajectory around an oblate earth. They are plotted in figure 9 showing Δr, Δv, and $\Delta\theta$ deviations at the time of re-ignition of the third-stage vehicle due to the initial insertion error of Δv (for a vented orbiting trajectory and an oblate earth). As shown in figure 9, an insertion Δv error of $\pm$ 2 m/sec will cause a total variation of approximately $\pm$ 10 km in altitude, $\pm$ 8 m/sec in velocity, and $\pm$ 0.05 degree in path angle in the area of the third orbit re-ignition.

In addition to this parking orbit perturbation (which may be represented by velocity variations, $\pm \Delta v$, at insertion), there are three other types of perturbations: launch window or launch time variation; orbital residence or waiting period variation; and thrust I_{sp} variation during third stage post-orbital boost. These are illustrated in figure 10 and tabulated in figure 11 (table). This 3^3 set means that a total of 27 trajectories will give a fair coverage of all possible perturbation combinations for studies prior and up to third-stage re-ignition. In order to cover fairly the various perturbation combinations for studies of post-orbital boost, 27 x 5 = 135 trajectories are used. These perturbed trajectories may be seen pictorially in figure 10. Illustrated in figure 10 are launch windows, parking orbit windows, and Δr, Δv, $\Delta\theta$ at re-ignition due to insertion Δv error. Also illustrated in figure 10 are the 3-dimensional post-orbital boost perturbations and the spread of the end earth-moon transit which is due to the combined effect of these perturbations and the shifting of the transit following the moon's motion.

3-DIMENSIONAL TWISTED POST-ORBITAL-BOOST AND RE-IGNITION TIMING

As previously mentioned, the post-orbital-boost trajectory may be optimized by variational calculus with both ends variable. It starts from the perturbed parking orbit and ends on the earth-to-moon transit trajectory at third stage final cut off. Such a space or osculating conic for nominal flight may be based on the nominal earth-to-moon transit trajectory computed by the 6-body JPL program. To cover the 4-hour window of third-stage re-ignition (2/3 orbit, 1-2/3 orbit, 2-2/3 orbit with variations of early, nominal, and late launching for each orbit), a total of 9 earth-to-moon transit trajectories corresponding to different time of third-stage final cutoff and different time of arrival at Moon were computed and plotted in figure 10-A. The time-varying earth-to-moon transit may be further transformed into time-varying space or osculating conic passing the final cutoff point as illustrated in figure 10-B. The orbital elements of this osculating conic is tabulated in figure 10-C.

As this table is further expanded to cover more osculating conics at smaller time intervals, these orbital elements may be plotted and curve-fitted as time varying functions. These functions, therefore, represent one of the two end conditions for the above-mentioned variational calculus optimization. The other end condition, of course, may be represented by the perturbed parking orbit in the neighborhood of third-stage re-ignition.

In view of the fact that the earth-moon transit plane forms only a very small angle with the due-east parking orbit plane from Cape Canaveral, the analysis for third-stage re-ignition may be approached by a 2-dimensional approximation. (See figure 12.) Through variational calculus optimization, both the time duration of the third-stage re-burning, t_b, and the swept angle by the post-orbital boost, β_{incl}, were computed on the basis of various cutoff points on the transit or various range angles between "cutoff points on the transit and perigee of the

transit, " ϕ_p. Graphs of t_b vs. ϕ_p and β_{incl} vs. ϕ_p, as shown in figure 13, indicate a first-cut information concerning optimal re-ignition point.

By this approximated location of re-ignition point, a rescheduling by the venting may be made. In order to provide a clear and smooth operation for the astronaut within 500 seconds prior to re-ignition, it was programmed to reschedule or to advance the last venting in order to have a 500-second no-venting coasting prior to the third-stage re-ignition. It is important, therefore, to record the space angular orientation of the vehicle at this particular time: time of "start of no-venting program" or t_{sonvp}, the details of which are shown in figure 14.

Simultaneously, the parking orbit perturbation was re-studied on the basis of this rescheduling of the last venting. Δv, Δr, and $\Delta\theta$ variations at the time of "start of no-venting program" (t_{sonvp}) due to initial insertion error of Δv were re-calculated.

With the values of real time of t_{sonvp} together with the corresponding Δv, Δr, and $\Delta\theta$, several 3-dimensional calculus of variations (30V) optimal paths were studied with different no-venting costing, Δt, along the last 500 seconds, plus or minus a few seconds, of the parking orbit. As also illustrated in figure 14, the optimal $t_{re\text{-}ignition}$ was located after three such trials for each of the 27 trajectories to cover all probable perturbation combinations prior to re-ignition, as mentioned in previous sections and tabulated in figure 11.

In detail, the 3-dimensional MSFC V-30 deck and calculus of variations optimal program were used with state variables at real time t_{sonvp} and corresponding Δv, Δr, and $\Delta\theta$ as inputs. It started with an assumed parking orbit no-vent coasting of about 500 seconds, then proceeded through re-ignition, and 3-dimensional optimal boost to final

cut off on transit. The procedures were repeated until the optimal $t_{re\text{-}ignition}$ was found for each of the above mentioned 27 trajectories (minimum time duration for post-orbital boost).

DEVELOPMENT OF GUIDANCE EQUATIONS: $t_{re\text{-}ig}$, X_p, X_y, $t_{cut\ off}$*

Once all 27 optimal trajectories are established to cover all probable combinations of perturbations prior to third-stage re-ignition, each of these trajectories may be examined prior to re-ignition at each of its time intervals. As the programed no-vent coasting from t_{sonvp} lasted about 500 seconds, at 5-second intervals, a total of $\frac{500}{5}$ x 27 or 2700 points existed. At each of these 2700 points, we may note and tabulate corresponding time remaining to re-ignition together with vehicle's state variables x, y, z and $\dot{x}$, $\dot{y}$, $\dot{z}$. This is the guidance function of "time remaining to re-ignition" expressed in tabular form. In order to handle the case by on-board computers, this large table is further reduced by functional approximation through least square procedure into 32-term polynomials of state varialbes. In other words, we have developed a statistical and representative model of the 27-element volume trajectory. In theory, this 32-term polynomial should fairly represent all of these 2700 points and should be capable of computing the "time remaining to third-stage re-ignition," $t_{re\text{-}ig}$, based on instantaneous sensing of the vehicle's state variables. Figure 15 shows this 32-term equation. The units for x, y, z; $\dot{x}$, $\dot{y}$, $\dot{z}$; and t are m, m/sec, and sec, respectively.

An overall re-examination at each of these 2700 points was made in terms of the difference between the actual value and the value computed by the polynomial. This examination revealed that the root-mean-square value of all of these differences is equal to 1.3758 seconds. In a way, this RMS value indicates how well the polynomial represents these 27-element volume trajectories and the corresponding 2700 points as their representative statistical model.

Once this polynomial guidance equation for "time remaining to re-ignition" is obtained, each of the 27 trajectories may be re-run from the time of "t_{sonvp}" through the polynomial-calculated time of re-

ignition, then, through the 5-perturbation combination for post-orbital boost (see figure 11). A total of 27 x 5 or 135 trajectories was computed.

Using the same procedure as described in previous sections and based on these 135 trajectories for post-orbital boost period of about 350 seconds at 5-second intervals, a total of approximately $135 \times \frac{350}{5} = 9000$ points may be tabulated. At each point, there are corresponding X_p, X_y,* and "time remaining to final cut off," $t_{cut\ off}$, and corresponding state and performance variables of the vehicle: x, y, z, $\dot{x}$, $\dot{y}$, $\dot{z}$; and F/m, $\dot{m}$/m, and t. By least-square curve fitting, a 43-term polynomial for X_p, a 42-term polynomial for X_y, and a 42-term polynomial for $t_{cut\ off}$ were developed and are tabulated in figures 16, 17, and 18. RMS values representing the polynomials' accuracy are 0.455°, 0.105°, and 0.600 seconds, respectively. The units used for these guidance equations are m, m/sec, m/sec^2, 1/sec, and sec for x, $\dot{x}$, F/m, $\dot{m}$/m, and t, respectively.

---

* Note: X_p, X_y represents pitch steering angle with respect to plumbline vertical and yaw steering angle measured from X, Y plane as shown in figure 6.

ERROR ANALYSIS AND EVALUATION

Finally, the accuracy of these guidance polynomials in terms of the difference between the cutoff position and velocity vectors of the vehicle when steered by these polynomials and those obtained if steered by theoretical functions of variational calculus optimization have been examined.

In order to do so, 15 simulated flights were made, 5 from each orbit with 2-sigma value deviations of $\triangle F$, $\triangle I_{sp}$, $\triangle w$, $\triangle t$, and zero deriations (nominal). These 15 simulated trajectories, as tabulated in figure 19, were run by both adaptive guidance polynomials and by theoretical calculus of variations (COV) optimization. Each of the 15 cases was examined in terms of cut-off r, v, θ, and $\bar{N}$ (altitude, velocity, path angle, and angular difference between normals of trajectory planes or transit planes). These 15 values of differences were again expressed in RMS errors. Figure 20 illustrates the details of the comparison. Respective RMS errors at cutoff are about 2 km for altitude, 5 m/sec for velocity, 0.06 degree for path angle, and 0.008 degree for transit plane deviation.

CLOSING REMARKS

1. This study represents only the first cut investigation to illustrate the feasibility of the adaptive guidance technique in guiding the Saturn V third-stage vehicle through post-orbital boost to earth-moon transit. No attempt was made to carry out overall optimization of the problem.

2. Attempts were made to illustrate the 3-dimensional feature of the guidance technique. There was angular difference between the parking orbit plane and the transit plane for each of the 135 trajectories studied. The plane difference ranged from 0.9 degrees up to 1.4 degrees with 1.2 degrees for nominal case. It is to be noted that none of the five reference planes; MEP (earth-moon plane), equational, ecliptic, transit, and parking orbital; are co-planar.

3. It is to be repeated that this paper was based on: (1) assumed initial errors at parking orbit insertion, (2) assumed relationships for space conics at the third stage final cut-off, (3) approximated re-ignition timing. It is planned that the study will be repeated with refined and actual inputs in three areas: (1) actual errors instead of assumed errors at the time of parking orbit insertion, (2) refined time-varying functions of the corresponding space conic elements in the region of third-stage final cutoff, and (3) refined and iterated re-ignition timing. Area (1) is presently pursued by launching phase study group. Area (2) is to be pursued in a manner as illustrated by figures 10-A, 10-B, and 10-C. Area (3) will be pursued in a manner as described in the second half of the section "3-Dimensional Twisted Post-Orbital Boost and Re-ignition Timing." The optimal re-ignition timing will be determined by variational calculus with both ends variable. As mentioned previously, one end will be represented by last section of the refined parking orbit with adjusted venting schedule together with 500-second no-venting costing. The other end will

be represented by the refined time-varying-functions of the earth-to-moon transit conics.

4. In error analysis, this accuracy was based on cutoff errors at final cut off on the earth-moon transit: 2 km in altitude, 5 m/sec in velocity, 0.06 degree in path angle, and 0.008 degree in trajectory plane deviation. It is expected that these errors will be further reduced in the projected refined study. Furthermore, mid-course correction will further correct whatever the final error may be in order to arrive at the moon in the desired manner.

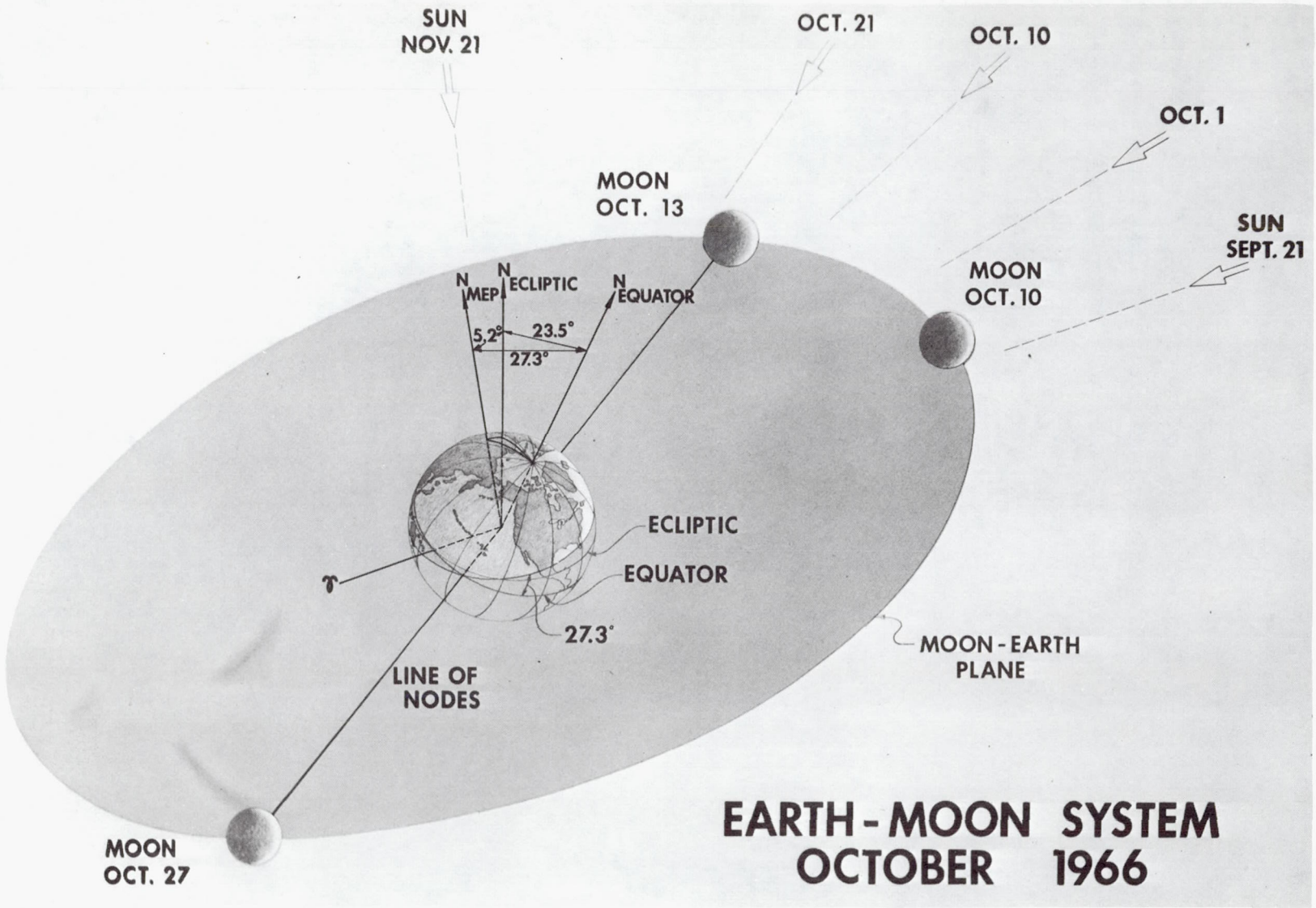
SUN
NOV. 21
OCT. 21
OCT. 10
OCT. 1
MOON
OCT. 13
SUN
SEPT. 21
MOON
OCT. 10
N
MEP
N
ECLIPTIC
N
EQUATOR
5.2°
23.5°
27.3°
ECLIPTIC
EQUATOR
27.3°
LINE OF
NODES
MOON - EARTH
PLANE
MOON
OCT. 27
EARTH - MOON SYSTEM
OCTOBER 1966

FIGURE 1

SIMPLIFIED VIEW OF PRE-SELECTED NOMINAL TRAJECTORY

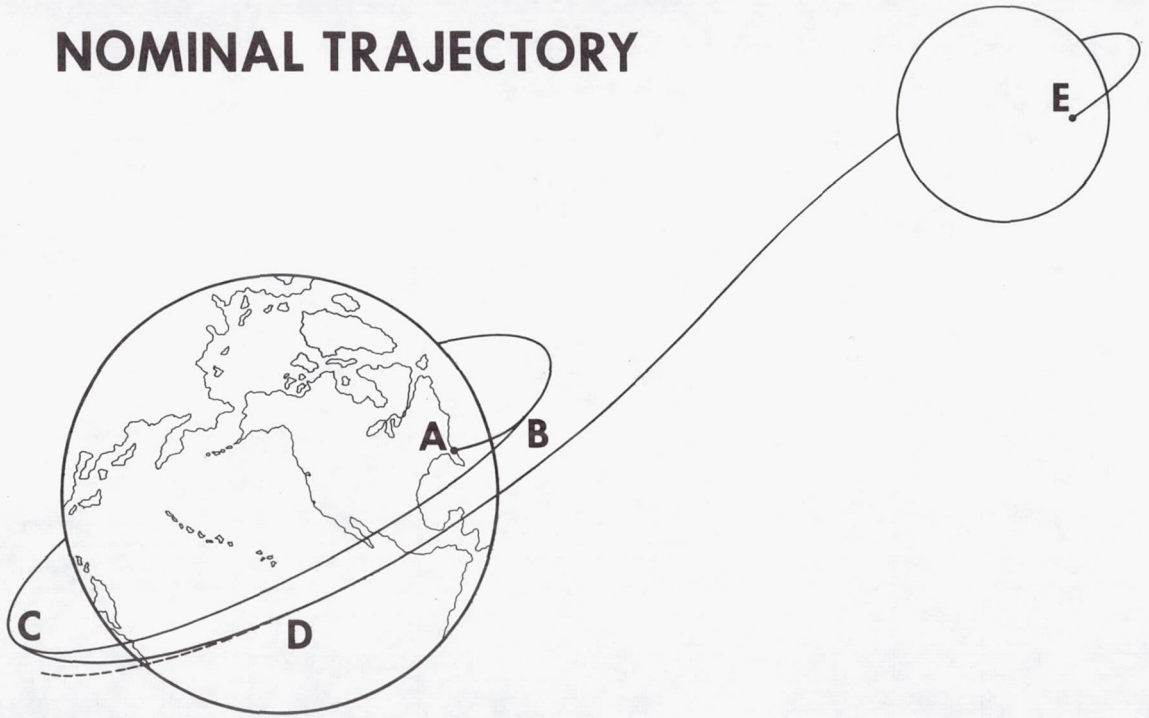

Figure 2

SATURN V
S-IVB STAGE AND APOLLO-LEM PAYLOAD

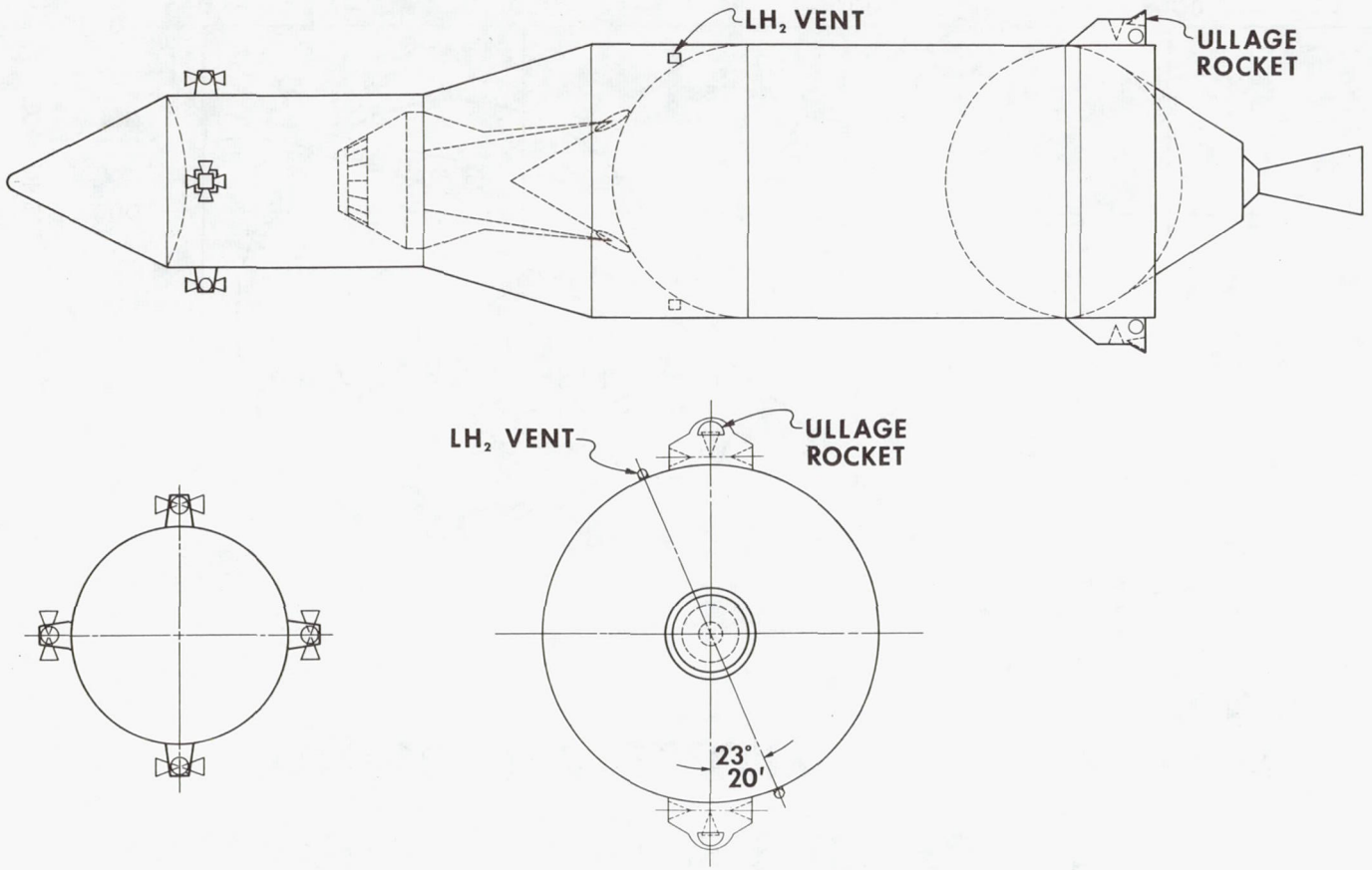

Figure 3

ULLAGE-VENTING THRUST AND PITCH STEERING ANGLE

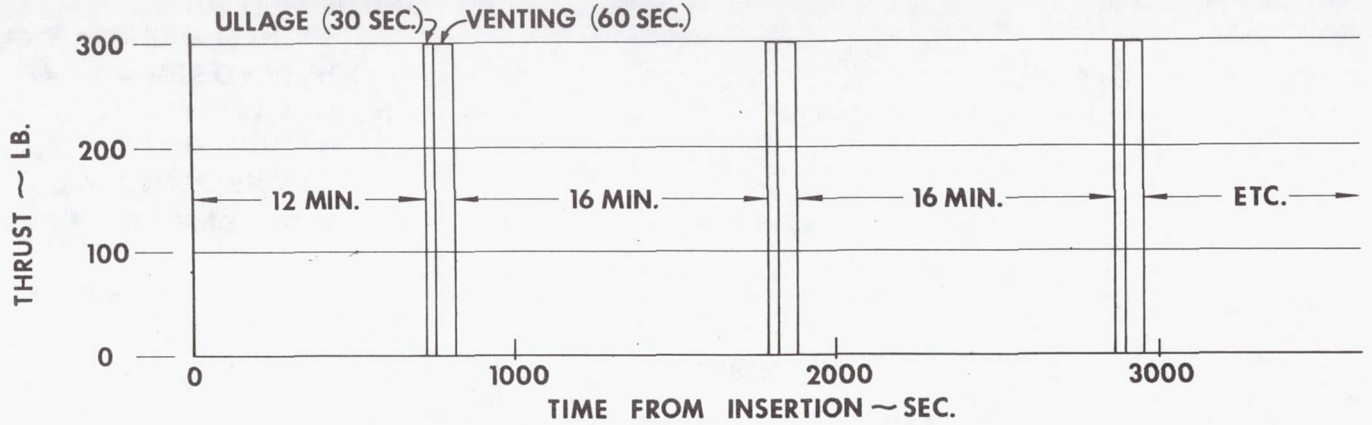

ULLAGE-VENTING SCHEDULE

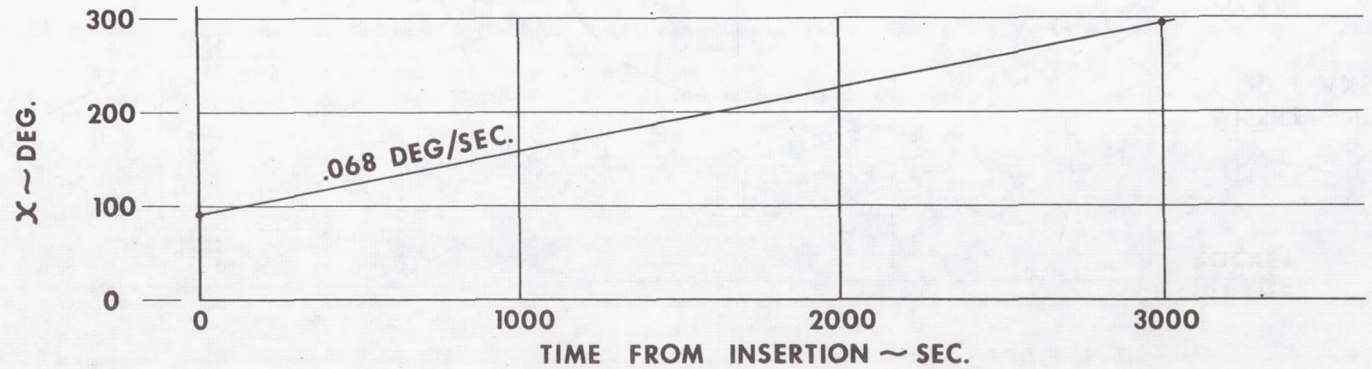

PITCH STEERING ANGLE

Figure 4

ANGLES IN PITCH PLANE

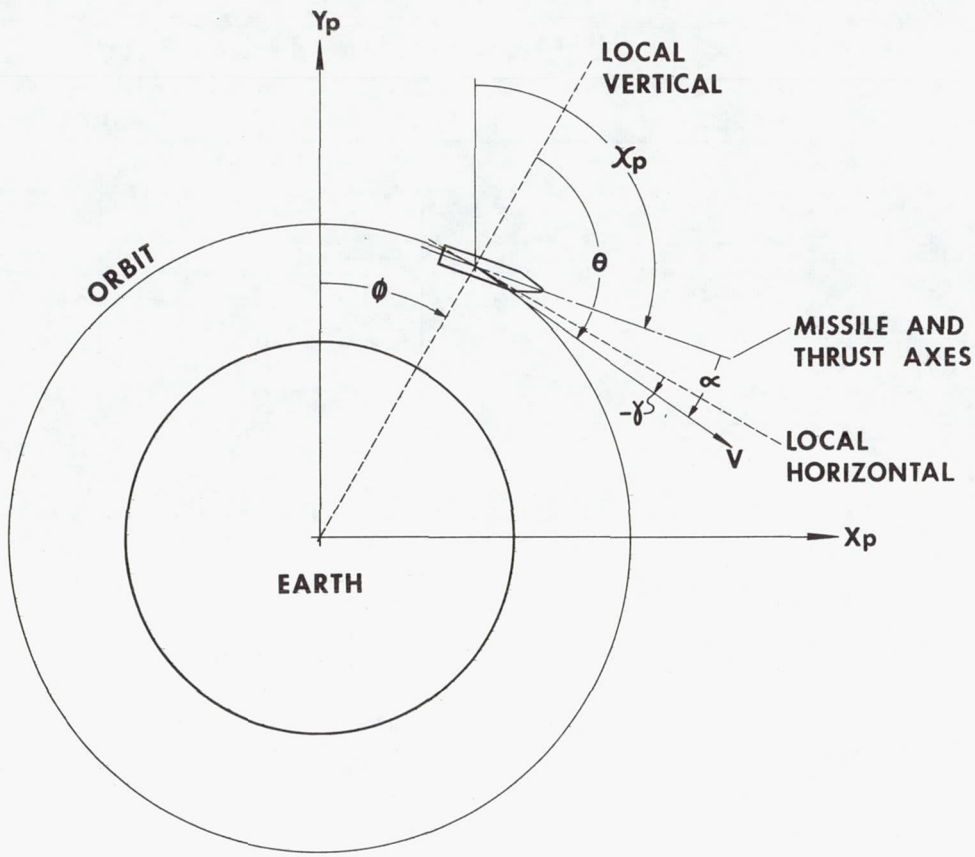

LEGEND –

X_p = STEERING ANGLE

ϕ = RANGE ANGLE

θ = FLIGHT PATH ANGLE LOCAL VERTICAL

α = ANGLE OF ATTACK

γ = FLIGHT PATH ANGLE LOCAL HORIZONTAL

$$X_p = \phi + \theta - \alpha$$

$$\theta = 90 - \gamma$$

Figure 5

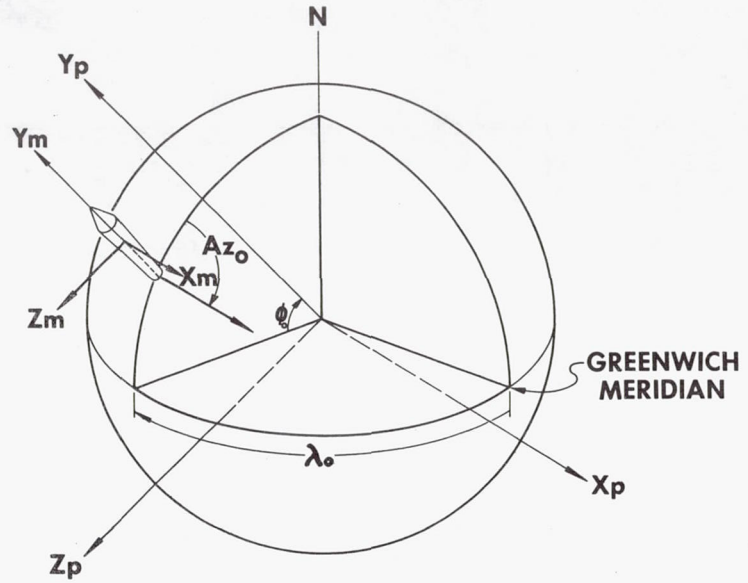

PLUMBLINE SYSTEM

EULER ANGLES

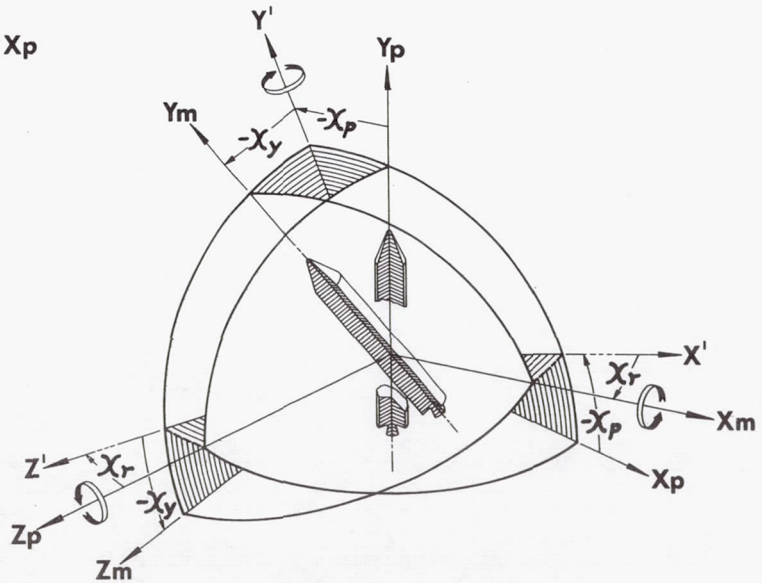

Figure 6

TRAJECTORY COMPOSITION FOR PARKING ORBIT PERTURBATION ANALYSIS DUE TO INSERTION & OTHER EFFECTS

(Listing of Initial Conditions)

Case	R(KM)	V(M/Sec.)	θ(Deg)	Variation	Venting
1	6558.4716	7794.72	90	-------	No
2	6558.4716	7794.72	90	-------	Yes
3	6557.4716	7794.72	90	$-\Delta R$	Yes
4	6559.4716	7794.72	90	$+\Delta R$	Yes
5	6558.4716	7792.72	90	$-\Delta V$	Yes
6	6558.4716	7796.72	90	$+\Delta V$	Yes
7	6558.4716	7794.72	89.98	$-\Delta\theta$	Yes
8	6558.4716	7794.72	90.02	$+\Delta\theta$	Yes
9	6558.9716	7795.72	89.99	$+\frac{\Delta R}{2}+\frac{\Delta V}{2}-\frac{\Delta\theta}{2}$	Yes
10	6557.9716	7793.72	90.01	$-\frac{\Delta R}{2}-\frac{\Delta V}{2}+\frac{\Delta\theta}{2}$	Yes

ΔR = 1 Kilometer

ΔV = 2 Meters/Sec.

$\Delta\theta$ = 0.02 Degrees

Figure 7

INNER AND OUTER ELLIPSES

COMPARATIVE STUDIES OF PERTURBATIVE EFFECTS DUE TO INSERTION ΔV, ΔR VARIATIONS

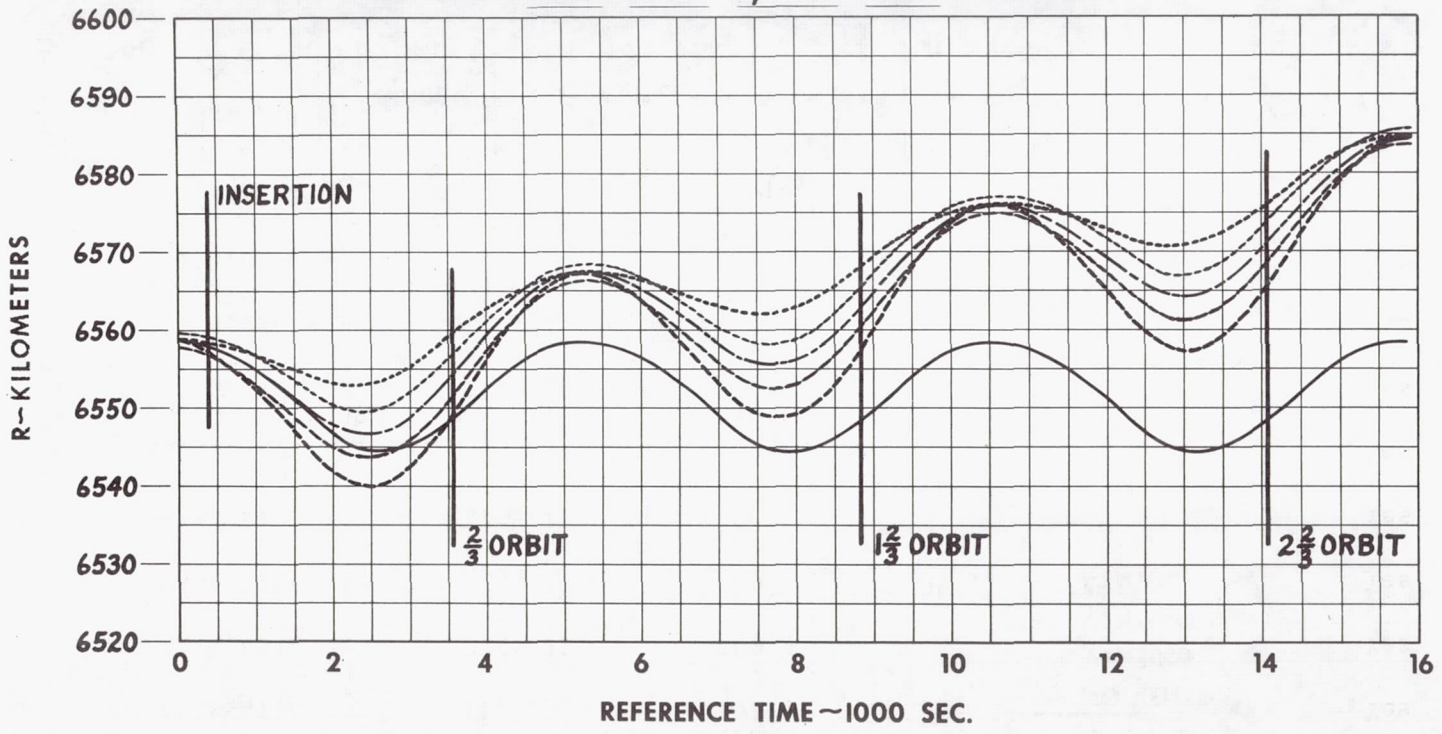

LEGEND –

—— NO VENTING

–––– VENTING

------- VENTING +ΔV

—— VENTING -ΔV

------ VENTING +ΔR

----- VENTING -ΔR

Figure 8

PERTURBATION DUE TO INITIAL VELOCITY VARIATION

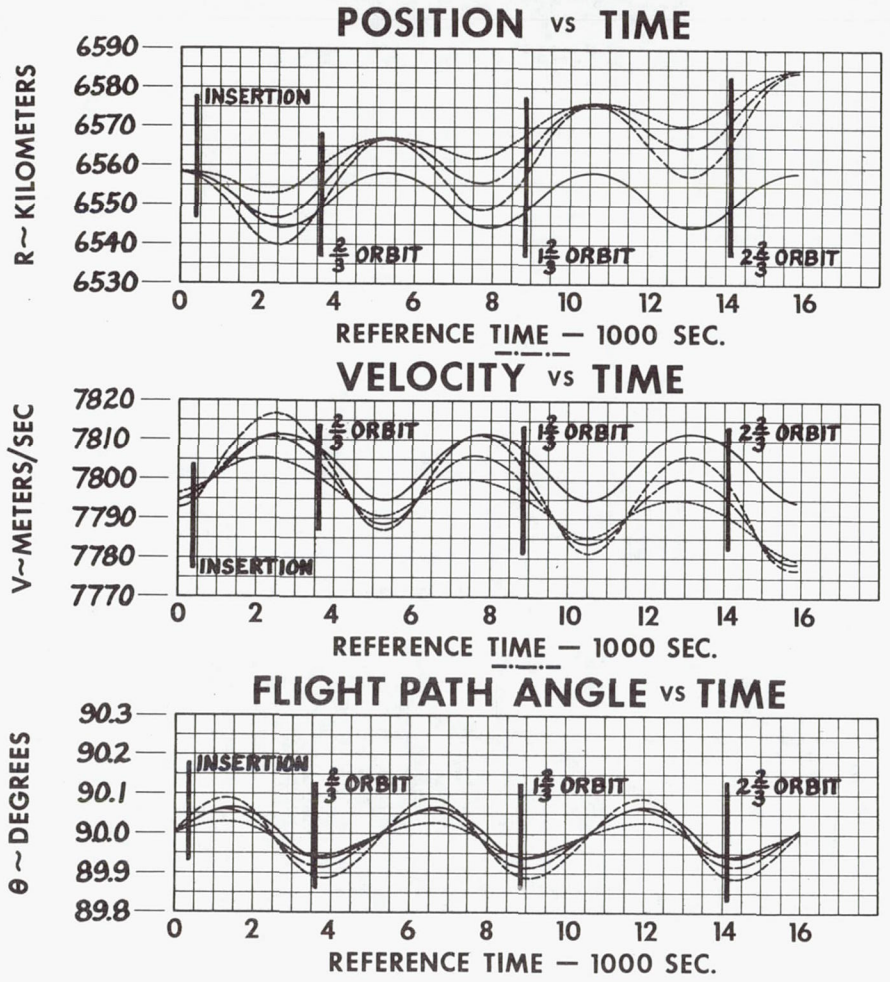

LEGEND –

—— NO VENTING

—·— VENTING

····· VENTING (+ΔV)

---- VENTING (−ΔV)

ALL STUDIES ARE FOR OBLATE EARTH

Figure 9

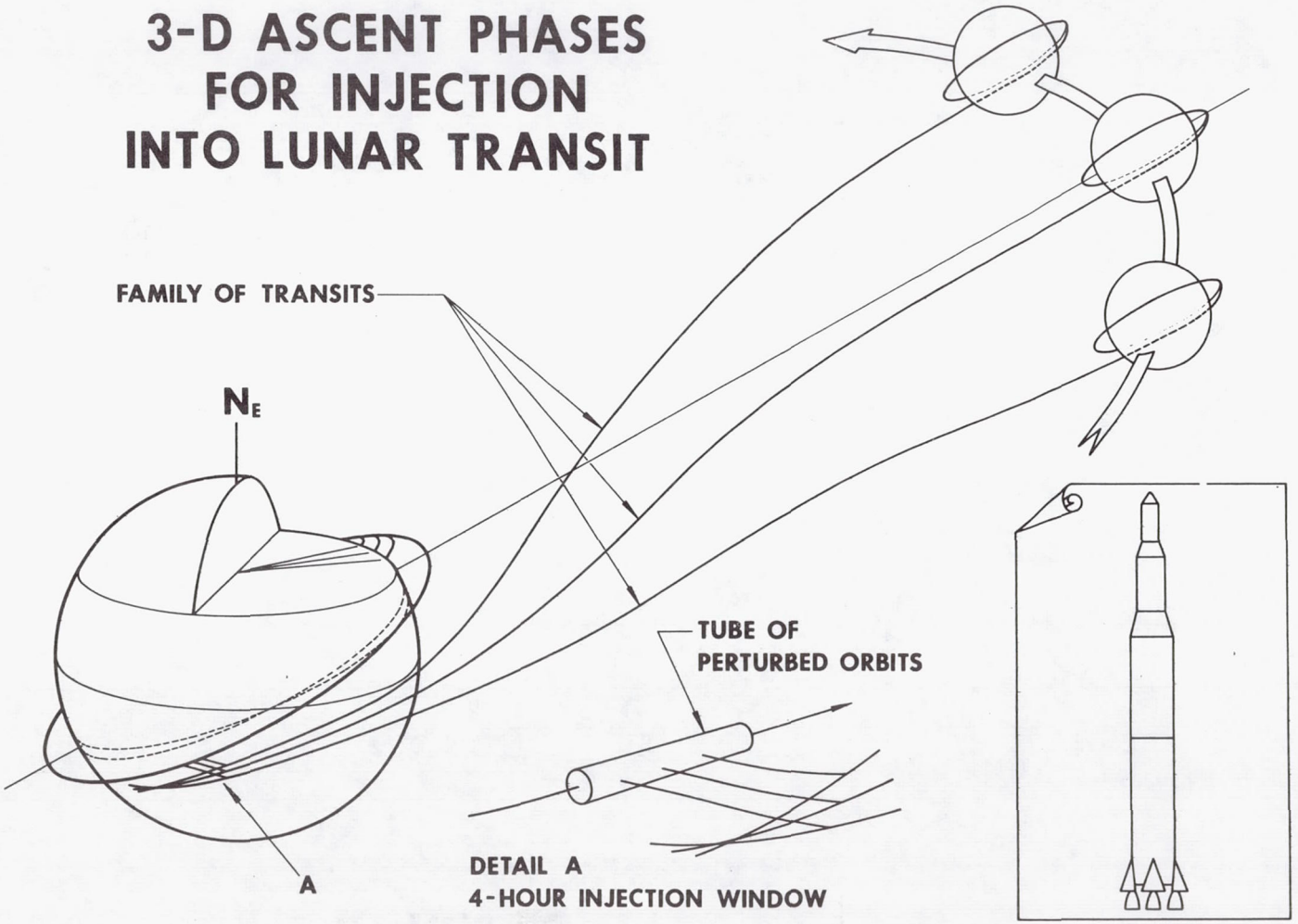
3-D ASCENT PHASES
FOR INJECTION
INTO LUNAR TRANSIT
FAMILY OF TRANSITS
N_E
TUBE OF
PERTURBED ORBITS
A
DETAIL A
4-HOUR INJECTION WINDOW

Figure 10

EARTH-TO-MOON TRANSIT TRAJECTORIES

IN EXPANDED SCALE

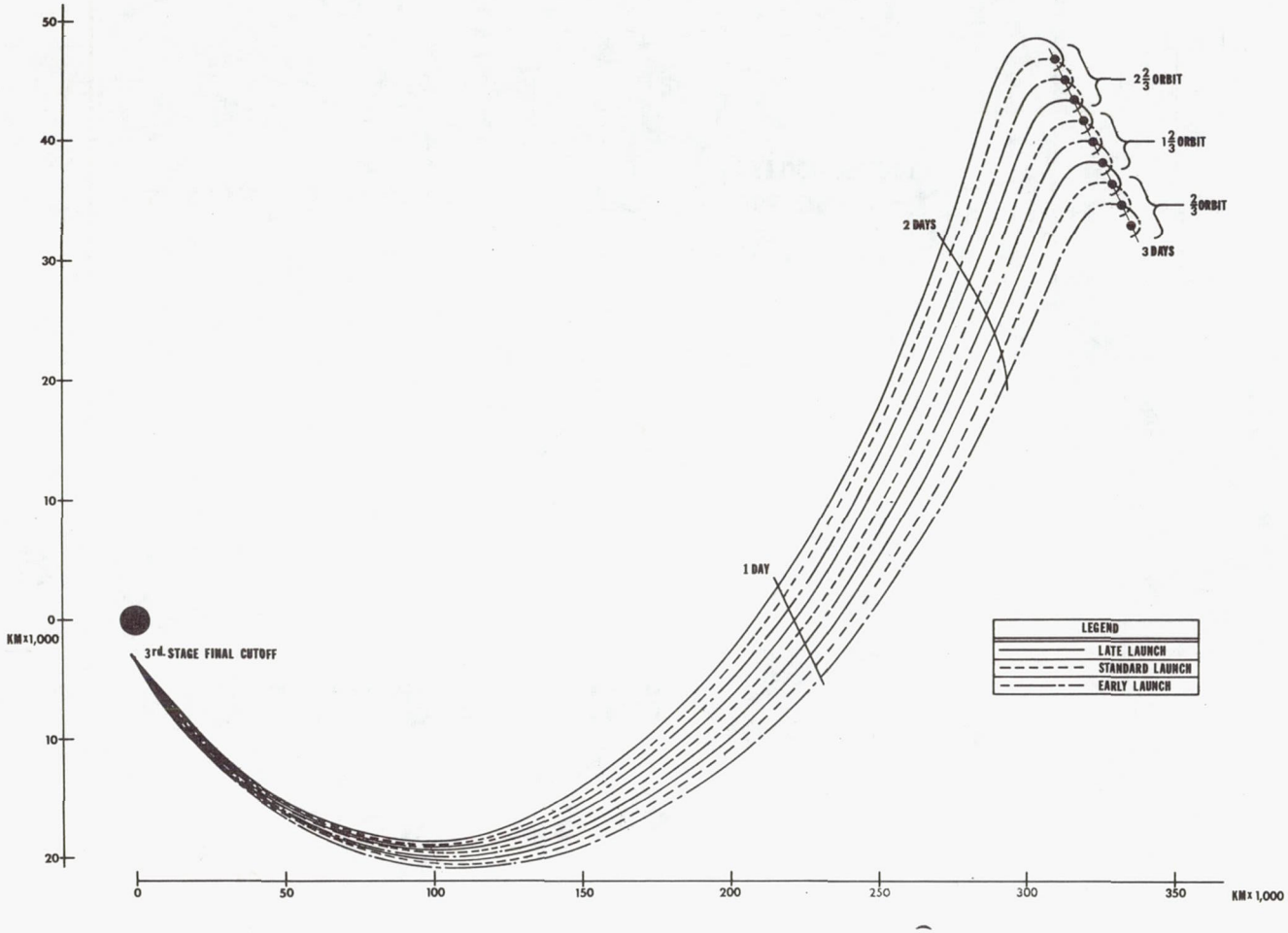

Figure 10A

EARTH-TO-MOON TRANSIT TRAJECTORY AND ITS OSCULATING CONIC

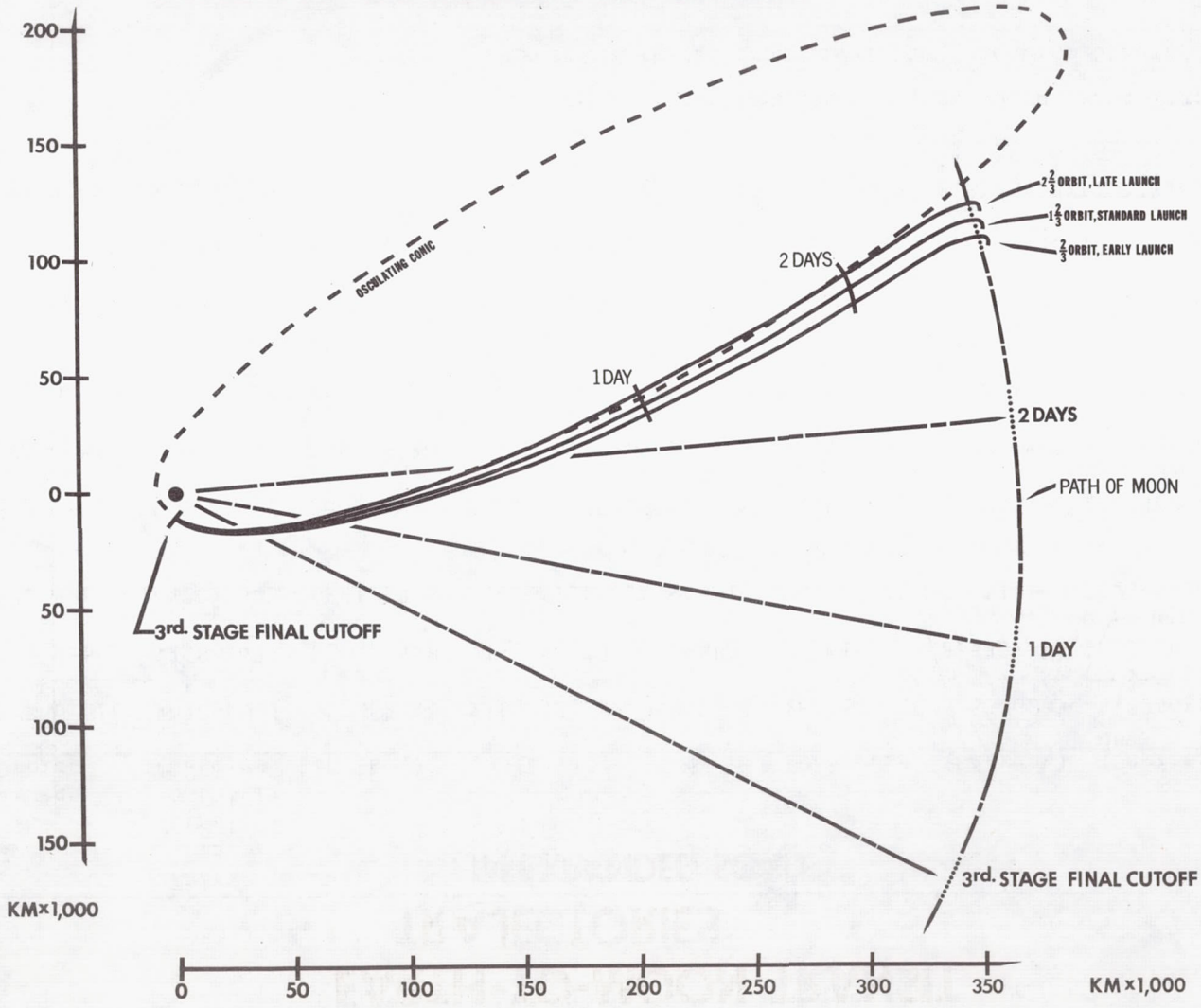

Figure 10B

ORBITAL ELEMENTS OF OSCULATING CONIC AT THIRD STAGE FINAL CUT OFF

Launch	Coast in Parking Orbit	Third stage final cut off (Seconds)	rp (km.)	a (km.)	e	i (Degrees)	Ω (Degrees)	ω (Degrees)	Time of Perigee Passage hr.	min.	sec.
E	2/3 orbit	40785.997	6603.1811	216,352.78	.96947956	28.587781	8.5506383	9.8240908	11	17	15.394
S	2/3 orbit	42580.437	6601.5446	216,364.77	.96948881	28.416395	8.5362614	10.151603	11	47	9.676
L	2/3 orbit	44205.445	6601.5940	216,361.80	.96948817	28.600123	8.5814669	10.398030	12	14	14.743
E	1-2/3 orbit	46198.599	6602.9947	216,370.05	.96948286	28.587475	8.5958230	10.737073	12	47	27.997
S	1-2/3 orbit	47990.947	6601.3528	216,283.78	.96947828	28.416078	8.5767595	11.083926	13	17	20.188
L	1-2/3 orbit	49617.133	6601.4055	216,378.48	.96949139	28.599867	8.6271262	11.310609	13	44	26.431
E	2-2/3 orbit	51611.055	6602.8070	216,385.56	.96948591	28.587154	8.6411123	11.650305	14	17	40.454
S	2-2/3 orbit	53400.350	6601.1611	216,408.32	.96949673	28.415755	8.6152130	11.986828	14	47	29.592
L	2-2/3 orbit	55028.666	6601.2160	216,403.23	.96949576	28.599537	8.6728923	12.223285	15	14	37.965

Note 1: E represents early launching; S, standard launching; L, late launching

Note 2: Times are measured from midnight (Greenwich Standard)

Figure 10C

LISTING OF SIMULATED TRAJECTORIES UNDER
VARIOUS CONDITIONS OF PERTURBATION COMBINATIONS

(A) INHERITED PERTURBATIONS
AT PARKING ORBIT INSERTION: LAUNCHING WINDOW → $\Delta T_{\text{LAUNCHING WINDOW}}$ { +30 MIN, 0, -30 MIN } 3

INSERTION ERROR
$\Delta V \pm 2$ m/sec.
$\Delta R \pm 1$ Km.
$\Delta \theta \pm 0.5$ deg.
NOMINAL

(B)
PARKING ORBIT
PERTURBATIONS:
→ INITIAL INSERTION ERROR
OBLATENESS
VENTING
} RESULTANT CONTROLLING PERTURBATION IN TERMS OF x, y, z & $\dot{x}, \dot{y}, \dot{z}$ AT 3rd STAGE RE-IGNITION AREA DUE TO ΔV AT INSERTION → ΔV { +2 m/sec., 0, -2 m/sec. } 3

PERTURBATION DUE TO PARKING
ORBIT RESIDENCE DURATION → ΔT_{ORBIT} { $\frac{2}{3}$ orbit, $1\frac{2}{3}$ orbit, $2\frac{2}{3}$ orbit } 3

$3 \times 3 \times 3 = 27$

(C)
THRUST PERTURBATION
DURING POST ORBITAL BOOST → ΔF { +3%, -3% }, ΔI_{sp} { +1.5%, -1.5% }, NOMINAL } 5

$5 \times 27 = 135$

Figure 11

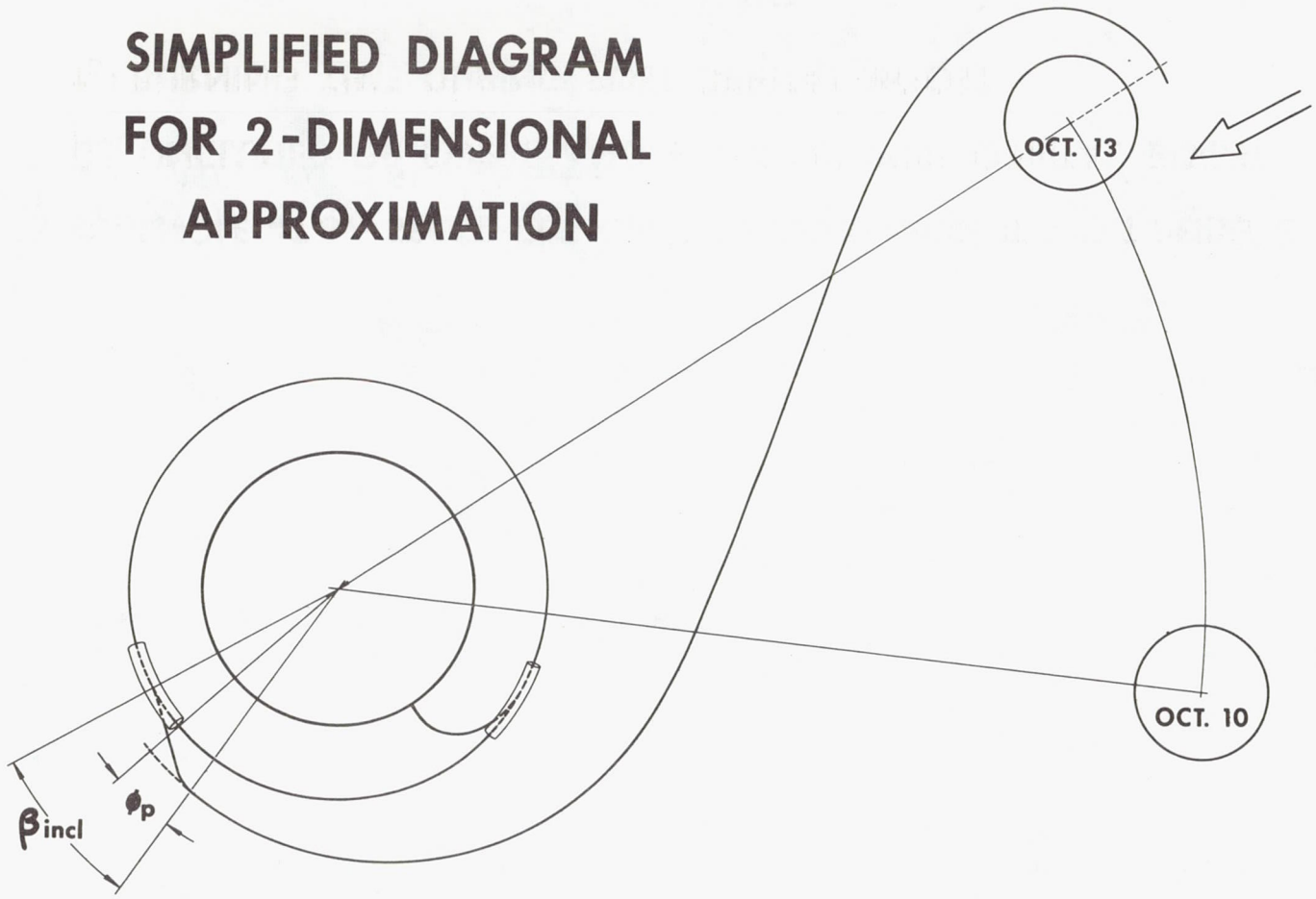
SIMPLIFIED DIAGRAM
FOR 2-DIMENSIONAL
APPROXIMATION
OCT. 13
OCT. 10
β_{incl}
ϕ_p

Figure 12

APPROXIMATED 2-D STUDY OF RE-IGNITION ANGLES ϕ_p & β_{incl}

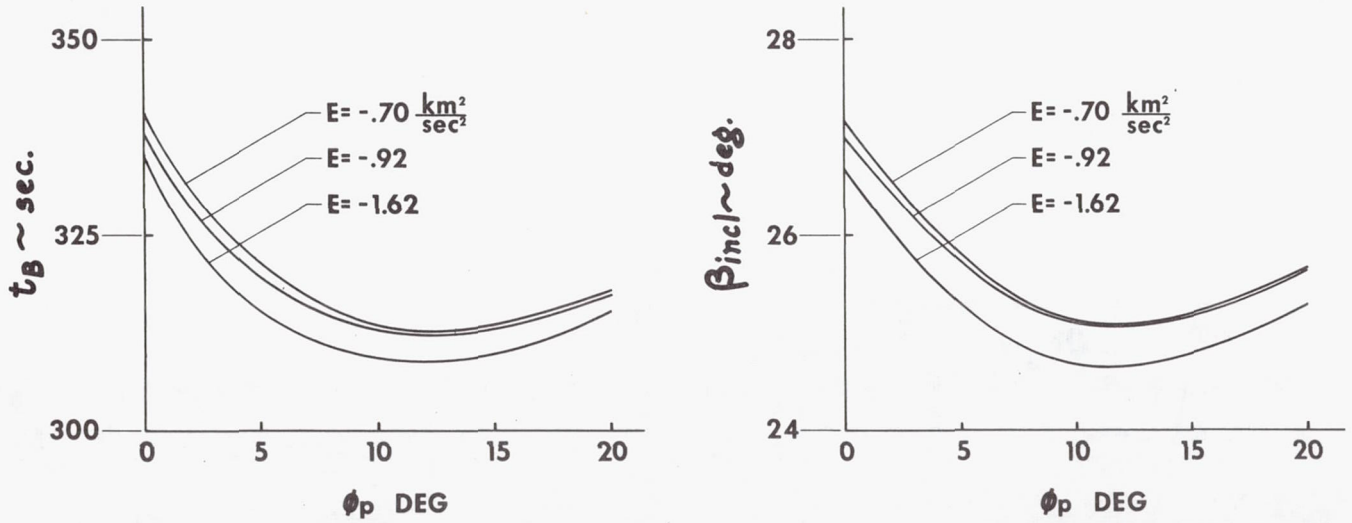

ϕ_p: ANGLE AT 3RD STAGE CUT-OFF MEASURED FROM TRANSIT PERIGEE

β_{incl}: INCLUDED OR SWEPT ANGLE DURING POST ORBITAL BOOST

t_B: BURNING TIME DURING POST ORBITAL BOOST

Figure 13

DIAGRAM FOR DETERMINATION OF

t_{sonvp} & $t_{opt.\ re\text{-}ign.}$

IN 3-D STUDIES

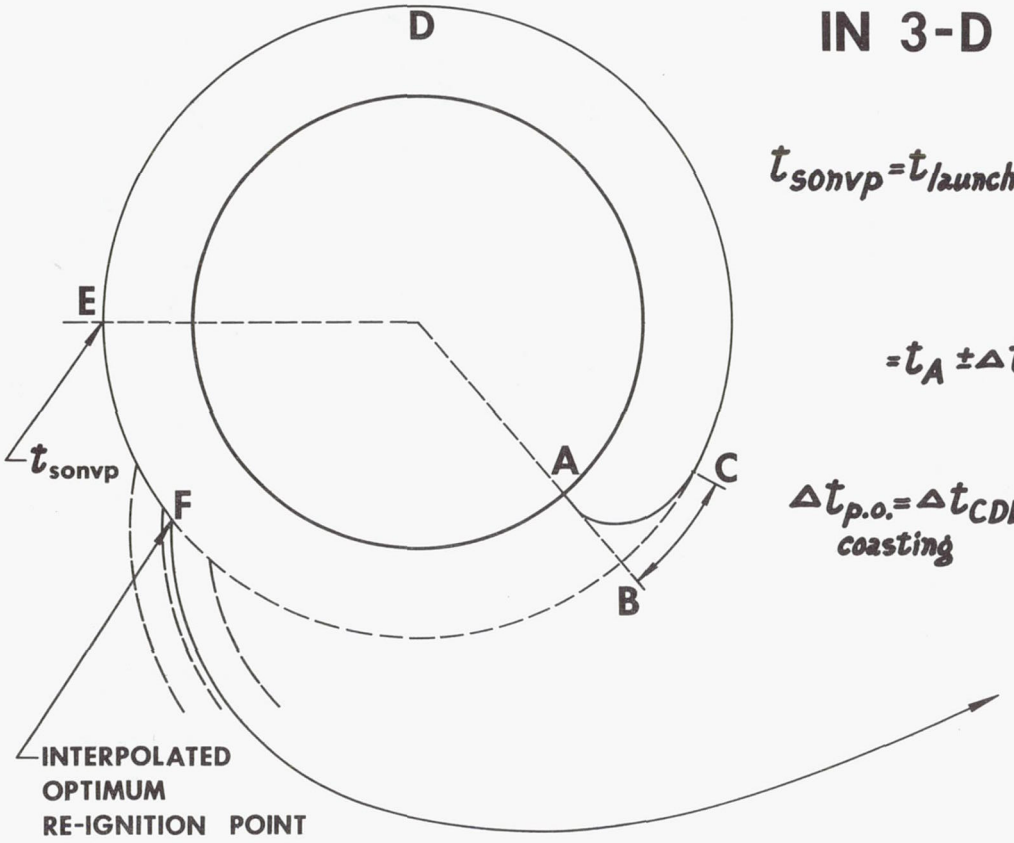

$$t_{sonvp} = t_{launch} \pm \Delta t_{\substack{launch \\ window}} + \Delta t_{\substack{boost\ from \\ launch\ pad}} + \Delta t_{\substack{p.o. \\ coasting}}$$

$$= t_A \pm \Delta t_{\substack{launch \\ window}} + \Delta t_{AC} + \Delta t_{CDE}$$

$$\Delta t_{\substack{p.o. \\ coasting}} = \Delta t_{CDE} = \Delta t_{\substack{tape \\ BCDE}} - \Delta t_{BC} \pm t_C \quad t_{\substack{tape \\ coast \\ period}} \quad t_{\substack{site \\ rotation}}$$

due to earth rotation

Δt_{AC}: approx. 700 sec.

Δt_{BC}: approx. 368 sec.

Δt_C : approx. $\pm$ 110 sec.

Figure 14

COEFFICIENTS OF 32 TERM POLYNOMIAL FOR TIME REMAINING TO 3rd STAGE RE-IGNITION

PARAMETER	COEFFICIENT	PARAMETER	COEFFICIENT
CONSTANT	$-.13704652\times10^{6}$	$\dot{y}^2$	$+.44265428\times10^{-2}$
x	$-.33913094\times10^{-1}$	$\dot{z}^2$	$+.24678161\times10^{+1}$
y	$-.95045687\times10^{-1}$	$\dot{x}T$	$+.11228720\times10^{-3}$
z	$+.11532524$	$\dot{y}T$	$-.11898984\times10^{-3}$
$\dot{x}$	$+.74598325\times10^{+2}$	$\dot{z}T$	$+.12146041\times10^{-1}$
$\dot{y}$	$-.22110806\times10^{+2}$	T^2	$-.12938048\times10^{-5}$
$\dot{z}$	$-.34006194\times10^{+3}$	x^3	$-.25857948\times10^{-16}$
T	$+.70403894$	y^3	$-.47954484\times10^{-17}$
x^2	$+.53586718\times10^{-8}$	x^2T	$-.16195811\times10^{-13}$
y^2	$-.92944665\times10^{-8}$	z^2T	$-.13650941\times10^{-10}$
z^2	$+.82798105\times10^{-6}$	$\dot{x}^2T$	$-.75418146\times10^{-8}$
$y\dot{x}$	$+.15053849\times10^{-4}$	$\dot{y}^2T$	$+.85701534\times10^{-8}$
$z\dot{x}$	$+.69324813\times10^{-5}$	$\dot{z}^2T$	$-.37418572\times10^{-4}$
$\dot{x}^2$	$-.79131437\times10^{-2}$	$\dot{x}T^2$	$-.15337463\times10^{-8}$
$x\dot{y}$	$+.12481051\times10^{-4}$	$\dot{y}T^2$	$+.51782550\times10^{-9}$
$z\dot{y}$	$-.14744844\times10^{-4}$	$\dot{z}T^2$	$-.91033639\times10^{-7}$

RMS Error = 1.376 sec.

Units: meters, seconds

Y transformation:

$Y = Y_p - 6373337.2$

Figure 15

COEFFICIENTS FOR 43 TERM POLYNOMIAL FOR χ_p STEERING ANGLE FOR POST ORBITAL BOOST

(BETWEEN 3rd STAGE RE-IGNITION AND FINAL CUT-OFF)

PARAMETER	COEFFICIENT	PARAMETER	COEFFICIENT
CONSTANT	$+.17228888\times10^{4}$	$\dot{x}\dot{y}T$	$-.20522858\times10^{-9}$
x	$+.42059390\times10^{-3}$	$\dot{y}\dot{z}T$	$+.10565799\times10^{-9}$
z	$+.87211159\times10^{-3}$	xT^2	$+.59936783\times10^{-14}$
$\dot{y}$	$+.32997921\times10^{-1}$	$\dot{x}T^2$	$+.11032575\times10^{-11}$
$\dot{z}$	$+.26336817\times10^{-1}$	$\dot{y}T^2$	$+.44512291\times10^{-10}$
F/m	$-.16548414\times10^{2}$	$(F/m)T^2$	$+.83364886\times10^{-9}$
y^2	$-.80986205\times10^{-10}$	T^3	$-.41239649\times10^{-11}$
$z\dot{y}$	$-.95790635\times10^{-7}$	$xz\dot{z}$	$-.12923623\times10^{-13}$
$y\dot{z}$	$-.57584052\times10^{-9}$	$z^2\dot{z}$	$-.75162203\times10^{-13}$
$\dot{z}^2$	$-.10765835\times10^{-5}$	$\dot{x}\dot{y}\dot{z}$	$-.96042316\times10^{-9}$
y^3	$-.45905236\times10^{-17}$	$\dot{y}\dot{z}\,(F/m)$	$-.85834128\times10^{-7}$
$y\dot{y}^2$	$-.10020367\times10^{-11}$	$y\,(F/m)^2$	$-.25781438\times10^{-8}$
$\dot{y}^3$	$-.12410749\times10^{-9}$	$z\dot{y}T$	$+.92378919\times10^{-12}$
$y\dot{z}^2$	$-.10953334\times10^{-12}$	zT	$-.90507301\times10^{-8}$
$xy\,(F/m)$	$-.22459561\times10^{-13}$	$xy\dot{x}$	$+.14758270\times10^{-14}$
$y\dot{x}\,(F/m)$	$-.33685724\times10^{-10}$	x^2y	$+.60773933\times10^{-18}$
$\dot{x}\dot{y}\,(F/m)$	$+.21107992\times10^{-6}$	xy	$+.66852788\times10^{-10}$
$y\dot{z}\,(F/m)$	$+.87729871\times10^{-9}$	yT^2	$-.32235049\times10^{-13}$
$\dot{z}\,(F/m)^2$	$+.21137200\times10^{-3}$	$y\dot{y}\,(F/m)$	$-.32476515\times10^{-9}$
x^2T	$+.16025891\times10^{-15}$	$xy\dot{y}$	$-.92053916\times10^{-15}$
xyT	$+.44030386\times10^{-15}$	$y^2\dot{y}$	$+.16106165\times10^{-14}$
$y\dot{y}T$	$+.93697273\times10^{-12}$		

RMS Error = .454481 deg.

Figure 16

COEFFICIENTS FOR 42 TERM POLYNOMIAL FOR χ_y STEERING ANGLE FOR POST ORBITAL BOOST

(BETWEEN 3rd STAGE RE-IGNITION AND FINAL CUT-OFF)

PARAMETER	COEFFICIENT	PARAMETER	COEFFICIENT
CONSTANT	$-.55451576\times10^{1}$	$\dot{x}^2(F/m)$	$+.31878416\times10^{-7}$
x	$-.24569037\times10^{-4}$	$\dot{y}^2(F/m)$	$-.21374055\times10^{-7}$
y	$-.81717797\times10^{-5}$	$\dot{z}^2(F/m)$	$-.13908632\times10^{-5}$
z	$-.14229007\times10^{-3}$	$x(F/m)^2$	$-.19652385\times10^{-6}$
$\dot{x}$	$+.11711731\times10^{-1}$	$y(F/m)^2$	$+.12585788\times10^{-6}$
$\dot{y}$	$-.14328470\times10^{-1}$	$z(F/m)^2$	$-.32572528\times10^{-5}$
$\dot{z}$	$-.59580151\times10^{-3}$	$\dot{x}(F/m)^2$	$-.38059335\times10^{-4}$
F/m	$-.73170173\times10^{1}$	$\dot{y}(F/m)^2$	$+.10337563\times10^{-4}$
T	$-.11775353\times10^{-1}$	$\dot{z}(F/m)^2$	$+.91509227\times10^{-4}$
xT	$+.71497338\times10^{-9}$	$x^2(F/m)$	$-.41717613\times10^{-12}$
yT	$-.52085995\times10^{-9}$	x^2T	$+.67472623\times10^{6}$
zT	$+.16484223\times10^{-8}$	xyT	$-.13662408\times10^{-15}$
$\dot{x}T$	$-.12479948\times10^{-6}$	y^2T	$+.17848923\times10^{-16}$
$\dot{y}T$	$+.21797780\times10^{-5}$	xzT	$+.11263465\times10^{-14}$
$\dot{z}T$	$-.98681255\times10^{-7}$	yzT	$-.14743902\times10^{-15}$
$(F/m)T$	$+.15835078\times10^{-3}$	z^2T	$+.16813058\times10^{-13}$
$xy(F/m)$	$+.36901049\times10^{-12}$	$\dot{x}^2T$	$+.17723451\times10^{-10}$
$y^2(F/m)$	$-.81917983\times10^{-13}$	$\dot{y}^2T$	$-.63407294\times10^{-10}$
$xz(F/m)$	$-.98159714\times10^{-11}$	$\dot{z}^2T$	$+.24681440\times10^{-9}$
$yz(F/m)$	$-.82648516\times10^{-12}$	$(F/m)^2T$	$-.41849798\times10^{-5}$
$z^2(F/m)$	$-.11876003\times10^{9}$	$(F/m)T^2$	$-.68188112\times10^{-9}$

RMS Error = .104736 deg.

Figure 17

COEFFICIENTS FOR 42 TERM POLYNOMIAL FOR TIME REMAINING TO 3rd STAGE FINAL CUT-OFF

PARAMETER	COEFFICIENT	PARAMETER	COEFFICIENT
CONSTANT	$+.15117779\times10^{4}$	$y\dot{y}T$	$+.33755174\times10^{-12}$
x	$+.15847417\times10^{-3}$	$\dot{x}\dot{y}T$	$-.25691452\times10^{-9}$
z	$-.47079464\times10^{-3}$	$\dot{y}\dot{z}T$	$-.14512354\times10^{-9}$
$\dot{y}$	$-.98350167\times10^{-1}$	xT^2	$+.21726636\times10^{-13}$
$\dot{z}$	$-.11470258$	$\dot{x}T^2$	$+.27085531\times10^{-10}$
F/m	$-.31102998\times10^{2}$	$\dot{y}T^2$	$+.29987208\times10^{-10}$
y^2	$-.24696235\times10^{-10}$	$(F/m)T^2$	$-.11443879\times10^{-8}$
$z\dot{y}$	$+.84347951\times10^{-7}$	T^3	$-.25401853\times10^{-11}$
$y\dot{z}$	$+.14166405\times10^{-9}$	$xz\dot{z}$	$-.19737880\times10^{-14}$
$\dot{z}^2$	$+.70466797\times10^{-5}$	$\dot{x}\dot{y}\dot{z}$	$+.10013529\times10^{-8}$
y^3	$-.88002863\times10^{-18}$	$\dot{y}\dot{z}(F/m)$	$+.15060145\times10^{-5}$
$y\dot{y}^2$	$+.33285183\times10^{-11}$	$y(F/m)^2$	$-.33524632\times10^{-7}$
$\dot{y}^3$	$+.27351149\times10^{-9}$	$z\dot{y}T$	$-.51960049\times10^{-11}$
$x\dot{z}^2$	$+.16045286\times10^{-11}$	zT	$+.35293851\times10^{-7}$
$xy\,(F/m)$	$-.27520983\times10^{-11}$	$xy\dot{x}$	$+.53516015\times10^{-15}$
$y\dot{x}\,(F/m)$	$+.32751373\times10^{-9}$	x^2y	$+.53671166\times10^{-17}$
$\dot{x}\dot{y}\,(F/m)$	$+.39695615\times10^{-6}$	xy	$+.60420857\times10^{-10}$
$y\dot{z}\,(F/m)$	$-.14052416\times10^{-8}$	yT^2	$-.42220395\times10^{-13}$
$\dot{z}\,(F/m)^2$	$-.49687572\times10^{-3}$	$y\dot{y}(F/m)^2$	$-.21320558\times10^{-8}$
x^2T	$+.12484709\times10^{-15}$	$xy\dot{y}$	$+.61804580\times10^{-14}$
xyT	$-.96327872\times10^{-16}$	$y^2\dot{y}$	$-.76178532\times10^{-16}$

RMS ERROR = .600 sec.

Figure 18

TRAJECTORY COMPOSITION FOR ERROR ANALYSIS AT 3rd STAGE FINAL CUT-OFF

CASE	ORBIT PASS	PERTURBATION	%	AMOUNT
1	1	NOMINAL	—	—
2	1	ΔF	-2%	-4000 LB.
3	1	ΔI_{sp}	-1%	-4.25 SEC.
4	1	ΔW	-1%	-1500 LB.
5	1	Δt	—	-20 MIN.
6	2	NOMINAL	—	—
7	2	ΔF	-2%	-4000 LB.
8	2	ΔI_{sp}	-1%	-4.25 SEC.
9	2	ΔW	-1%	-1500 LB.
10	2	Δt	—	-20 MIN.
11	3	NOMINAL	—	—
12	3	ΔF	-2%	-4000 LB.
13	3	ΔI_{sp}	-1%	-4.25 SEC.
14	3	ΔW	-1%	-1500 LB.
15	3	Δt	—	-20 MIN.

Figure 19

ERROR ANALYSIS
AT
3rd STAGE FINAL CUT-OFF

	R(km)		V (m/sec)		θ (deg)		δ (deg)
	COV	POLY	COV	POLY	COV	POLY	
1	6690.1741	6690.8219	10831.365	10834.519	83.442115	83.420415	+.0010
2	6698.1108	6698.9483	10824.850	10828.807	83.157496	83.111644	+.0041
3	6688.8060	6689.2301	10832.492	10834.666	83.492481	83.494433	+.0033
4	6688.1020	6688.7313	10833.070	10836.239	83.518534	83.502657	+.0037
5	6698.1325	6699.9530	10824.827	10817.804	83.186235	83.065223	-.0196
6	6691.3275	6688.1529	10830.388	10826.506	83.395387	83.463148	-.0065
7	6699.1740	6696.1955	10823.940	10821.178	83.116193	83.180323	-.0031
8	6689.9255	6686.6156	10831.542	10826.740	83.446588	83.532032	-.0052
9	6689.2511	6686.0780	10832.096	10828.178	83.471372	83.538444	-.0043
10	6701.0278	6701.0517	10822.413	10809.674	83.044272	82.993590	-.0191
11	6684.7007	6684.8955	10835.886	10832.276	83.636227	83.652244	-.0040
12	6692.1074	6693.4212	10829.794	10826.785	83.362414	83.364268	-.0008
13	6683.3109	6683.4316	10837.032	10833.187	83.688996	83.718001	-.0016
14	6682.6989	6682.6996	10837.536	10834.193	83.712415	83.728718	-.0010
15	6703.0711	6706.1235	10820.786	10815.344	83.025862	82.911277	+.0020
	RMS=1.9336		RMS=5.104		RMS=.060576		RMS=.0078

Figure 20

0425-702

THE BOEING COMPANY Seattle, Wash.
SATURN BOOSTER BRANCH
AEROBALLISTICS UNIT

RANGE CAPABILITY OF S-IVB AND SERVICE MODULE USED AS ABORT VEHICLES FROM SATURN V BOOST TRAJECTORIES

by
V. V. Moore and
F. G. Bourque

In ... 1963 p 71-88 refs
(See ...) OTS: $ ---

Huntsville, Alabama

THE BOEING COMPANY

SATURN BOOSTER BRANCH

AEROBALLISTICS UNIT

RANGE CAPABILITY OF S-IVB AND SERVICE MODULE USED AS ABORT VEHICLES FROM SATURN V BOOST TRAJECTORIES

by

V. V. Moore
F. G. Bourque

16524

SUMMARY

A

The minimum and maximum range capability of the S-IVB Stage and Service Module used as vehicles for powered abort from an expected volume of Saturn V boost trajectories has been determined. Abort is assumed to occur between the time of second stage ignition and a time near final lunar injection. Abort trajectories terminate at a re-entry altitude of 120 km with flight path angles of 94° and 99.5°.

AUTHOR

INTRODUCTION

During flight of the Saturn V vehicle, from lift-off to lunar injection, malfunctions may occur which would necessitate an abort. Abort may be defined as the reaction to malfunction which requires the immediate abandonment of primary and secondary missions.

Three flight modes may be considered for the Saturn V. They are:

1. Normal flight - no malfunctions

2. Abnormal flight - minor malfunction
   a. Primary mission may still be accomplished.
   b. Secondary missions may be accomplished if the primary mission cannot be completed.

3. Aborted flight - serious malfunction
   a. Unpowered abort.
   b. Powered abort.

Using the Apollo vehicle, unpowered abort can be accomplished with acceptable re-entry velocity and flight path angle for most sub-orbital abort initiation times. However, the low maneuverability of the Apollo does not allow a great degree of flexibility in landing site selection.

This study is concerned with powered abort using the S-IVB stage or Service Module. Initially, the study was directed toward obtaining a unique landing site accessible from all abort points. It soon became apparent that such a single site did not exist and the problem expanded to determining the range capabilities of the selected powered abort stages so that the minimum number of abort sites could be chosen. For a select group of landing sites, the final phase of the study will be to determine Path Adaptive Guidance steering polynomials for use during powered abort trajectories.

It is the purpose of this abort study to establish the two dimensional range capability of the S-IVB stage and the Service Module (SM) when used as abort vehicles between the time of S-II stage ignition and injection into lunar orbit. The ground rules imposed during this study were:

1) No coast would be considered from ignition of the abort vehicle until the re-entry point was reached.

2) No cross-range capability would be examined. The study would be two-dimensional.

3) Abort trajectories would originate from an envelope of likely boost trajectories as defined later in this report.

4) Abort trajectories would terminate with acceptable re-entry conditions at an altitude of 120 km.

The data contained in this report represents an extension of the study reported in Reference 1.

DEFINITIONS

- h - altitude
- v - velocity
- γ - flight path angle measured clockwise from local vertical
- ϕ - range angle measured from launch to the vehicle re-entry point along a spherical earth surface.
- α - angle of attack
- $\dot{\alpha}$ - time derivative of α
- $\ddot{\alpha}$ - time derivative of $\dot{\alpha}$

ANALYSIS

The Powered Abort Study consists of two parts, each characterized by the vehicle to be used during powered abort flight. Part one used the Service Module as the abort vehicle and part two used the S-IVB stage as the abort vehicle. In order to begin the abort study, a boost trajectory envelope was defined. Eighteen boost trajectories were generated by varying thrust, Isp and stage inert weights of all three stages of the Saturn V vehicle. The variations used are tabulated below.

Stage Variations for Boost Volume

	S-1C	S-II	S-IVB
Thrust (lbs)	± 450,000	± 100,000	± 20,000
Isp (sec)	± 4	± 4	± 4
Inert Wt. (lbs)	± 15,000	± 5,000	± 2,000

The descriptive characteristics of the base line Saturn V vehicle used in this study are given in Table I.

The two boost trajectories selected, from which abort was initiated, were the two which most closely represented the boundaries on an altitude-velocity graph of the eighteen boost trajectories. These two boost trajectories form the boost trajectory envelope shown in Figures 1 and 2, and are termed "boundary" trajectories.

For the Service Module, seven abort times were initially selected. Three of the abort times selected were during sub-orbital flight and four of the abort times were during super-orbital flight. Four sub-orbital abort times between second stage ignition and third stage ignition were selected for the S-IVB stage.

The abort times selected were as follows:

Service Module	S-IVB	Criteria
167 sec.	167 sec.	Near S-II ignition
	275 sec.	
395 sec.	395 sec.	
	503 sec.	Near S-II burnout
650 sec.		
790 sec.		Near S-IVB re-ignition
834 sec.		
874 sec.		
946 sec.		Near S-IVB final cut-off

As the study progressed, it was discovered that, under the established ground rules, abort with the SM at 946 seconds could not be accomplished. A time of 906 sec. appeared to be near the limit of SM superorbital abort time and, therefore, was used in the SM superorbital portion of this study. Later another time of 915 sec. was also studied in attempting to precisely locate the time limit. From each of the boundary trajectories, at each of the chosen abort times, it is desirable to fly the vehicle to a set of state variables as it approaches the earth's atmosphere. The set of variables is defined as a "re-entry window". These re-entry conditions define the terminal point of powered abort flight. For this study, the re-entry window is defined by an altitude of 120 km. and a flight path angle variation at this altitude from approximately 90° to 105°, depending upon the re-entry velocity. Abort trajectories were run on a 2-degree of freedom Calculus of Variations digital program which includes a mathematical scheme capable of isolating on pre-set conditions at burnout. (Reference 2)

In this study the end conditions were initially selected to be a re-entry altitude of 120 km and a flight path angle of 94 degrees. However, for the sub-orbital SM cases, isolations on 94° could not always be attained. This inability of the SM to attain a 94° re-entry from all abort points is due to the low thrust to weight ratio which is unable to modify the steep, high speed near ballistic path of the vehicle. Inability to isolate on γ = 94° for sub-orbital SM cases suggested that isolations from the entire boost trajectory at some higher γ might be possible. A value of 99.5 degrees was selected so that re-entry conditions for each powered abort flight were h = 120 km and γ = 94 or 99.5 degrees.

The technique of obtaining the maximum and minimum range angles for each abort time and from each trajectory consists of several steps:

1. A series of explicit Calculus of Variation (COV) trajectories were generated by specifying α_o and $\dot{\alpha}_o$ and using the transversality condition to specify $\ddot{\alpha}_o$. This entire set of runs was made with velocity extremalized and with range angle an open variable, i.e., no explicit control or optimization of ϕ was performed.

2. Each of the above series of trajectories was examined throughout its burn time for points that approached the desired re-entry window conditions. This selected burn time and the corresponding α_o and $\dot{\alpha}_o$ for that trajectory were then used as initial conditions for an isolation run on the exact desired re-entry window conditions. An "isolation" case is a series of explicit trajectory runs

in which the digital program automatically varies α_o and $\dot{\alpha}_o$ until altitude at burnout equals 120 km and the flight path angle equals either 94° or 99.5°, whichever is specified. After an isolation was obtained, the burn time was changed to either a larger or smaller value and a new isolation of the re-entry conditions was attempted. This time incrementation procedure was continued to establish the minimum and maximum burn times which would yield isolation on the desired end conditions. For the S-IVB stage, the maximum burn time to produce desired re-entry was taken as the propellant depletion time, although greater burn times would also produce acceptable re-entry. However, for the service module from some abort times, isolation on the desired re-entry window conditions could not be obtained for any vehicle burn time. As discussed previously, when this became apparent, the re-entry flight path was changed from 94° to 99.5°. Although this new γ value permitted successful trajectories from all abort times, for some abort times the maximum burn time achievable was less than the service module maximum burn time.

An example of the results from this part of the analysis is illustrated by Figure 3. For abort from a time of 503 sec. on the Boundary Boost Trajectory A, the data show the re-entry velocity and associated range angle for burn times from the minimum to the maximum for the S-IVB stage. For these data, range angle is unspecified and the COV analysis produces a maximum and a minimum velocity for each burn time. Both of these velocities are shown as well as the $\emptyset$ associated with each. Similar data for Boundary Boost Trajectory B are shown in Figure 4.

3. The final step consisted of incorporating an $\ddot{\alpha}_o$ term with the analysis as a parameter to be varied to determine the extreme range angles for a select abort stage burn time. This amounts to using the curves of Figures 3 and 4 as a starting point and varying $\ddot{\alpha}_o$ until maximum and minimum ranges are obtained. After carrying out the work for several abort times, it became apparent that for a given abort time the maximum range was obtained by performing this $\emptyset$ incrementation technique with the maximum burn time point (point (a) of Figure 3) and that the minimum range was obtained by incrementing the minimum burn time point (point (b) of Figure 3). Performing this procedure for a select abort time on boost Trajectories A and B provided the maximum and minimum range angles for that abort time.

RESULTS

As previously stated, only two boost trajectories have been used in this abort study. Therefore, for each abort time there exists two maximum and two minimum ranges, i.e., one for each trajectory.

The results presented below define the greater of the two maxima as the maximum and the smaller of the two minima as minimum range.

For the service module, Figure 5 gives the maximum and minimum ranges as a function of abort time. The abort times shown represent abort from sub-orbital conditions on the boost trajectory. After the curves were calculated, an evaluation of the resulting re-entry velocities and flight path angles was made to determine if the re-entries were "safe". A safe re-entry is defined to be one which does not exceed a pilot acceleration dose limit or one which does not skip out of the earth's atmosphere after re-entry initiation. (See Raytheon's "Re-Entry Corridor for Manned Lifting Vehicle" elsewhere in this report, for re-entry limits). The curves of Figure 5 were completed before these limits were available and, therefore, are independent of such constraints. It was found that for the maximum range curve, acceleration dose limit was exceeded for abort times greater than 606 seconds. For times greater than 606 seconds, the maximum permissible $\emptyset$ would be determined by the acceleration dose limit constraint. It is noteworthy that the limits are extremely sensitive to re-entry angles. For example, changing re-entry angle to 97° would result in exceeding neither an acceleration limit nor a skip-out limit.

Similar information for the sub-orbital abort with the S-IV B stage is given by Figure 6. The advantage of the higher thrust to weight of the S-IV B compared to the Service Module is evidenced by the greater re-entry range capability. As in Figure 5, the curves of Figure 6 are independent of acceleration or skip-out constraints. Later evaluation showed that for abort times greater than 352 seconds the maximum range would be determined by the skip-out constraint.

For service module abort from super-orbital conditions, Figure 7 gives the range capability. Super-orbital abort occurs after leaving the waiting orbit. However, the range angles shown are for powered flight only, i.e., $\emptyset$ during coast in orbit is assumed zero. The intersection of the two curves represents the maximum flight time from which no-coast abort with the service module is possible. This time is somewhat less than the full Saturn V burn time so that during the last few seconds abort cannot be accomplished with the service module. This conclusion is modified if coasting were permitted, if a different re-entry angle were used, or if a greater thrust to weight ratio were available.

CONCLUSIONS

1. The data presented here represents the abort no coast range capability envelopes of the Service Module and S-IVB stage from the selected boost envelope "boundary" trajectories with specified re-entry conditions.

2. Some desired re-entry conditions could not be reached when the SM was used as the abort vehicle for some booster flight times due to its low thrust to weight ratio.

3. Abort with the SM is impossible after a flight time of 938 seconds under the ground rules of this study.

4. It may be possible to extend the 2-dimensional range capability by investigating the other values of re-entry angle. Other re-entry angles also have a marked effect on range limits defined by excessive acceleration dose and skip-out.

RECOMMENDATIONS

The information of this report should be used to make a preliminary selection of desirable abort site locations along the AMR boost ground track. Once such sites are chosen, volumes of abort trajectories may then be generated from which the powered abort guidance equations may be produced.

Abort using coast and abort into a parking orbit should be considered as methods of extending the limiting abort time of the SM as established by this study.

ACKNOWLEDGMENTS

The assistance and constructive criticisms offered by Mr. W. B. Morgan during the course of this study, and efforts by several members of the Flight Mechanics Group in obtaining the necessary data, is sincerely acknowledged. The authors also appreciate the cooperative efforts of the Boeing Digital Computer Applications Unit and the Computation Division, Marshall Space Flight Center, where all numerical calculations were performed using IBM 7090 and 7094 digital computers.

TABLE 1

Stage I	
Sea Level Thrust (lbs.)	7,500,000
Sea Level Specific Impulse (sec)	*
Lift off Weight (lbs)	6,000,000
Propellants consumed (lbs)	4,242,362
Weight dropped at S-1C separation (lbs)	391,560
Azimuth Angle at Lift-off (deg.)	70
Stage II	
Vacuum Thrust (lbs)	1,000,000
Vacuum Specific Impulse (sec)	*
Lift-off weight (lbs)	1,366,078
Propellants consumed (lbs)	919,010
Weight dropped at S-II separation (lbs)	87,800
Stage III	
Vacuum Thrust	200,000
Vacuum Specific Impulse (sec)	*
Lift-off Weight (lbs)	359,268
Propellants consumed to orbit (lbs)	78,521
Weight lost in orbit (lbs)	5,000
Propellants consumed to injection (lbs)	146,831
Total propellants consumed (lbs)	225,352
Weight dropped at S-IVB separation (lbs)	23,100
Gross Payload (lbs)	105,815

* Specific impulse is classified.

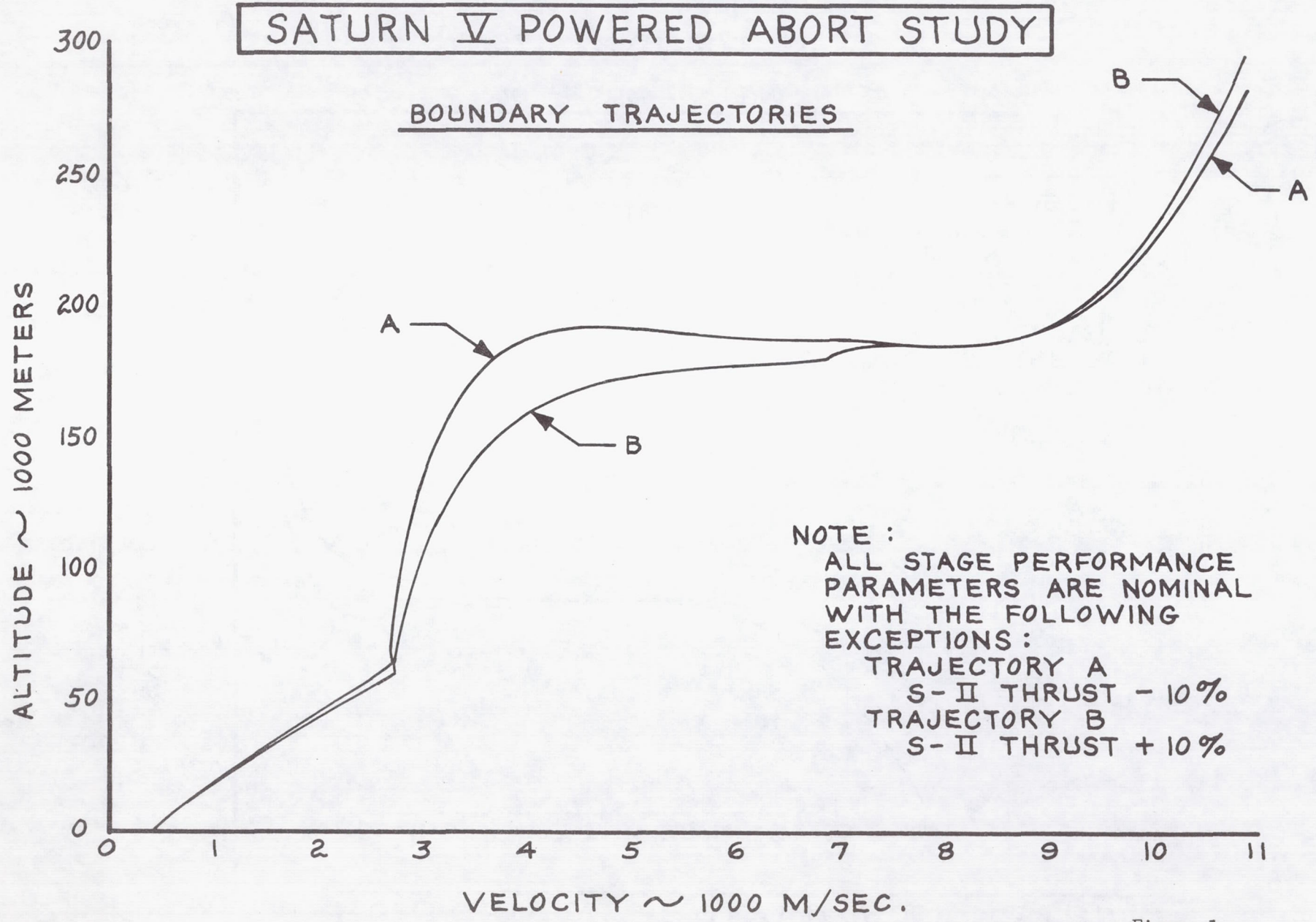
SATURN V POWERED ABORT STUDY
BOUNDARY TRAJECTORIES
ALTITUDE ~ 1000 METERS
300
250
200
150
100
50
0
0
1
2
3
4
5
6
7
8
9
10
11
VELOCITY ~ 1000 M/SEC.
A
B
B
A
NOTE :
ALL STAGE PERFORMANCE PARAMETERS ARE NOMINAL WITH THE FOLLOWING EXCEPTIONS :
TRAJECTORY A
S-II THRUST - 10%
TRAJECTORY B
S-II THRUST + 10%

Figure 1

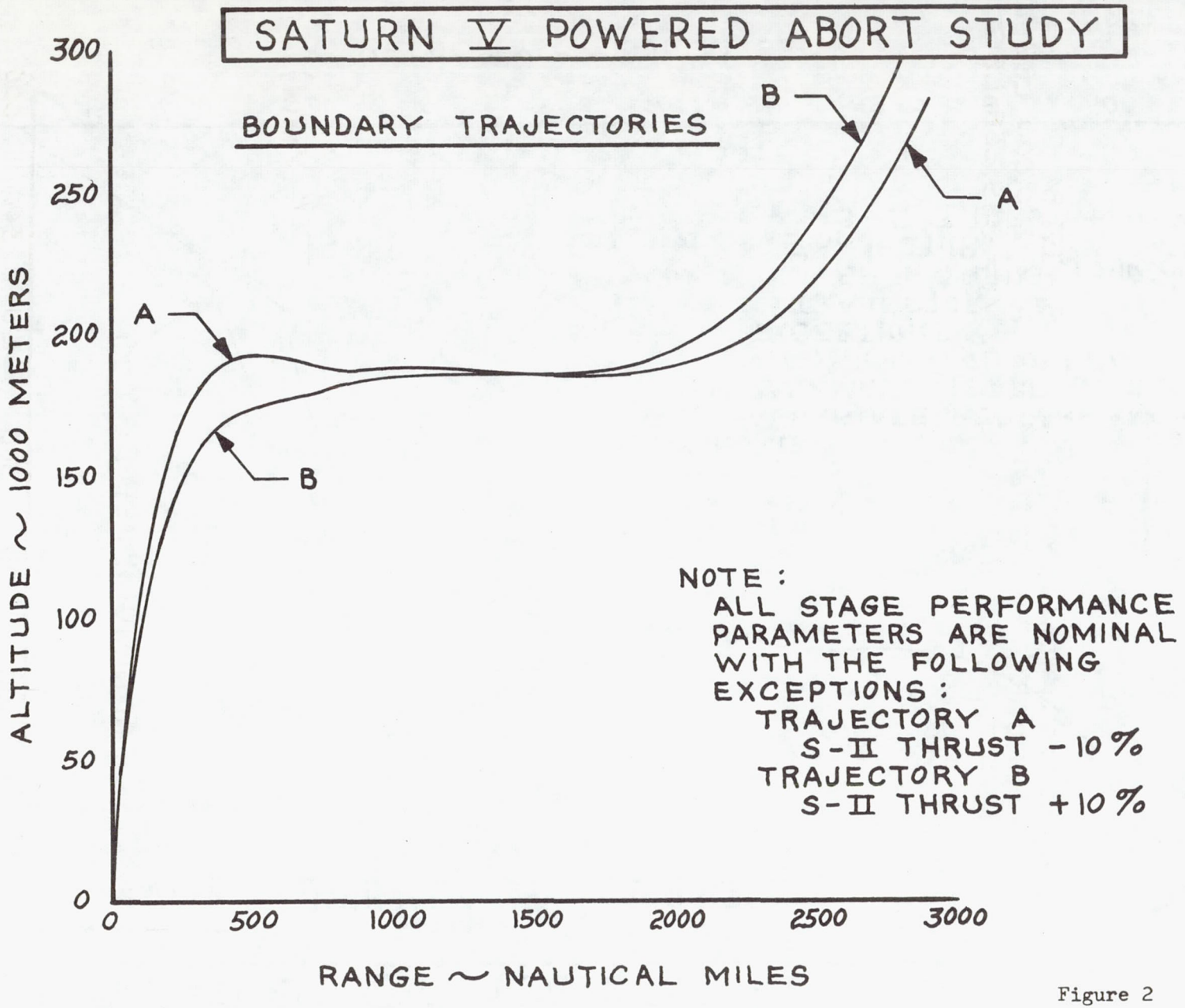
SATURN V POWERED ABORT STUDY
BOUNDARY TRAJECTORIES
B
A
A
B
300
250
200
150
100
50
0
ALTITUDE ~ 1000 METERS
0
500
1000
1500
2000
2500
3000
RANGE ~ NAUTICAL MILES
NOTE :
ALL STAGE PERFORMANCE PARAMETERS ARE NOMINAL WITH THE FOLLOWING EXCEPTIONS :
TRAJECTORY A
S-II THRUST -10%
TRAJECTORY B
S-II THRUST +10%

Figure 2

SATURN V POWERED ABORT

S - IV B

ABORT FROM UPPER BOUNDARY TRAJECTORY A
ABORT TIME = 503 SECS.

S - IV B
F = 200,000 LBS.
W_o = 359,268 LBS.

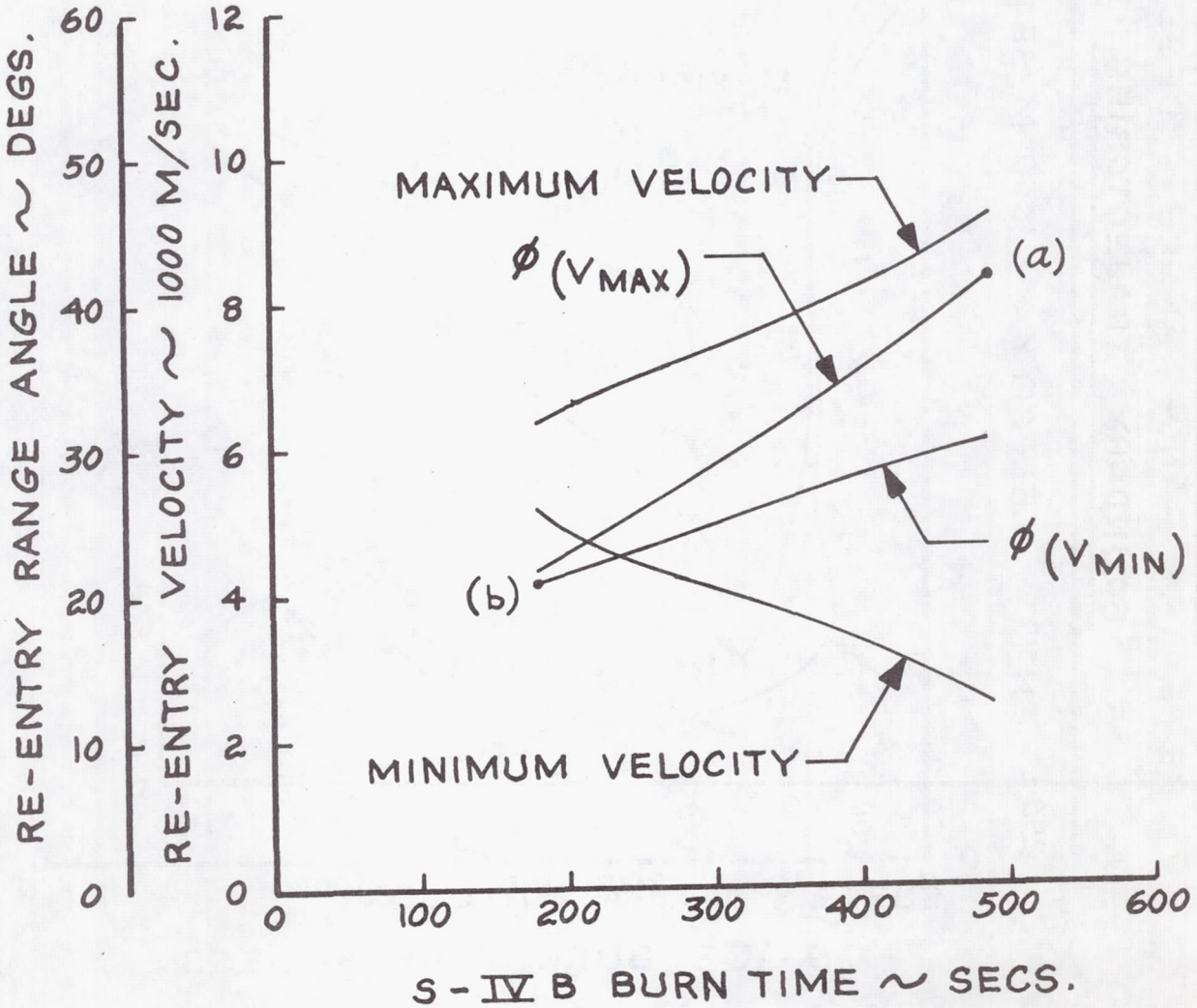

Figure 3

SATURN V POWERED ABORT

S - IV B

ABORT FROM LOWER BOUNDARY TRAJECTORY B
ABORT TIME = 503 SECS.

S - IV B
F = 200,000 LBS.
W_o = 359,268 LBS.

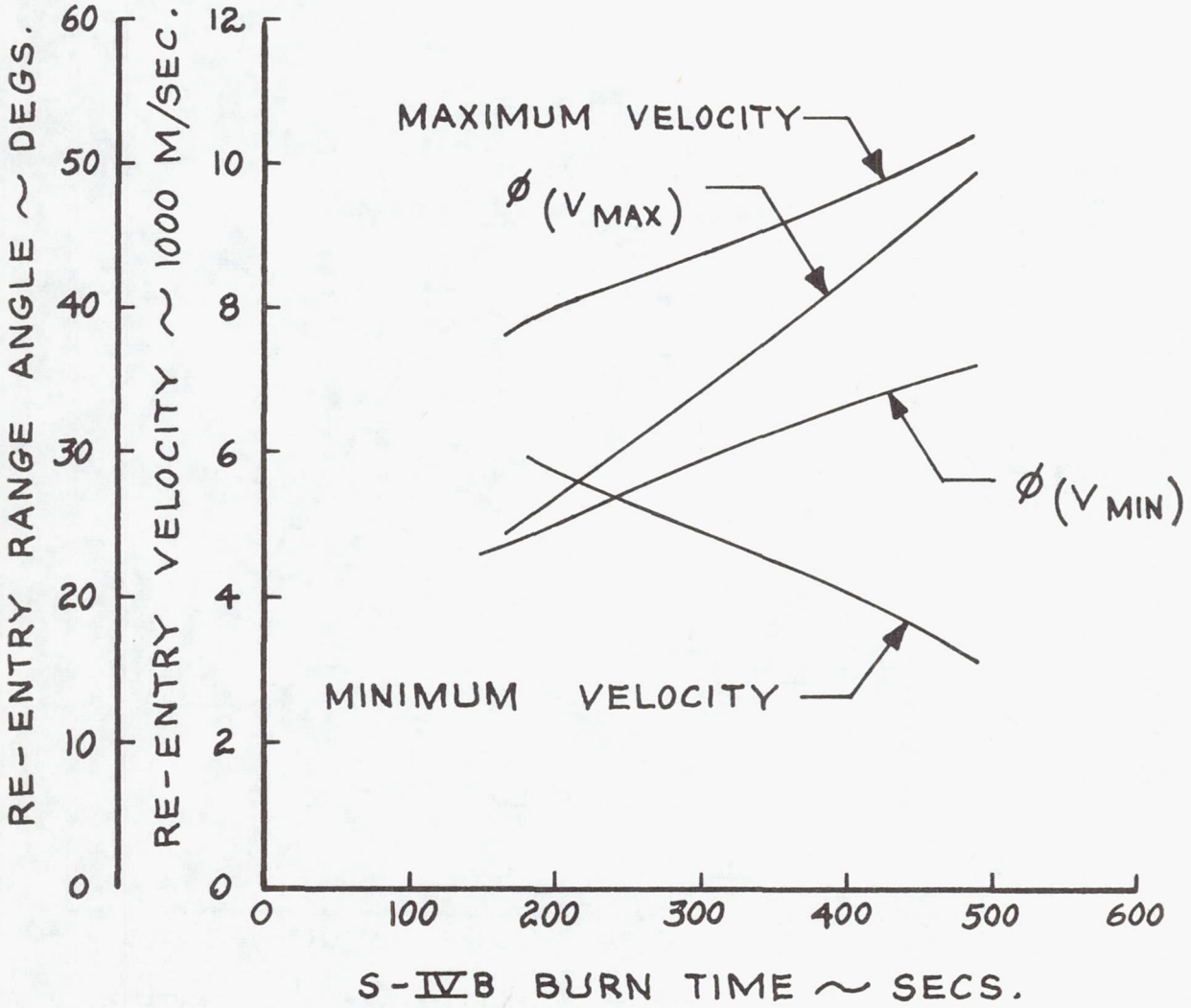

Figure 4

SATURN V POWERED ABORT

SERVICE MODULE

SERVICE MODULE
F = 21,500 LBS.
W_o = 61,120 LBS.

RE-ENTRY FLIGHT
PATH ANGLE = 99.5 DEGS.
RE-ENTRY
ALTITUDE = 120 KM.

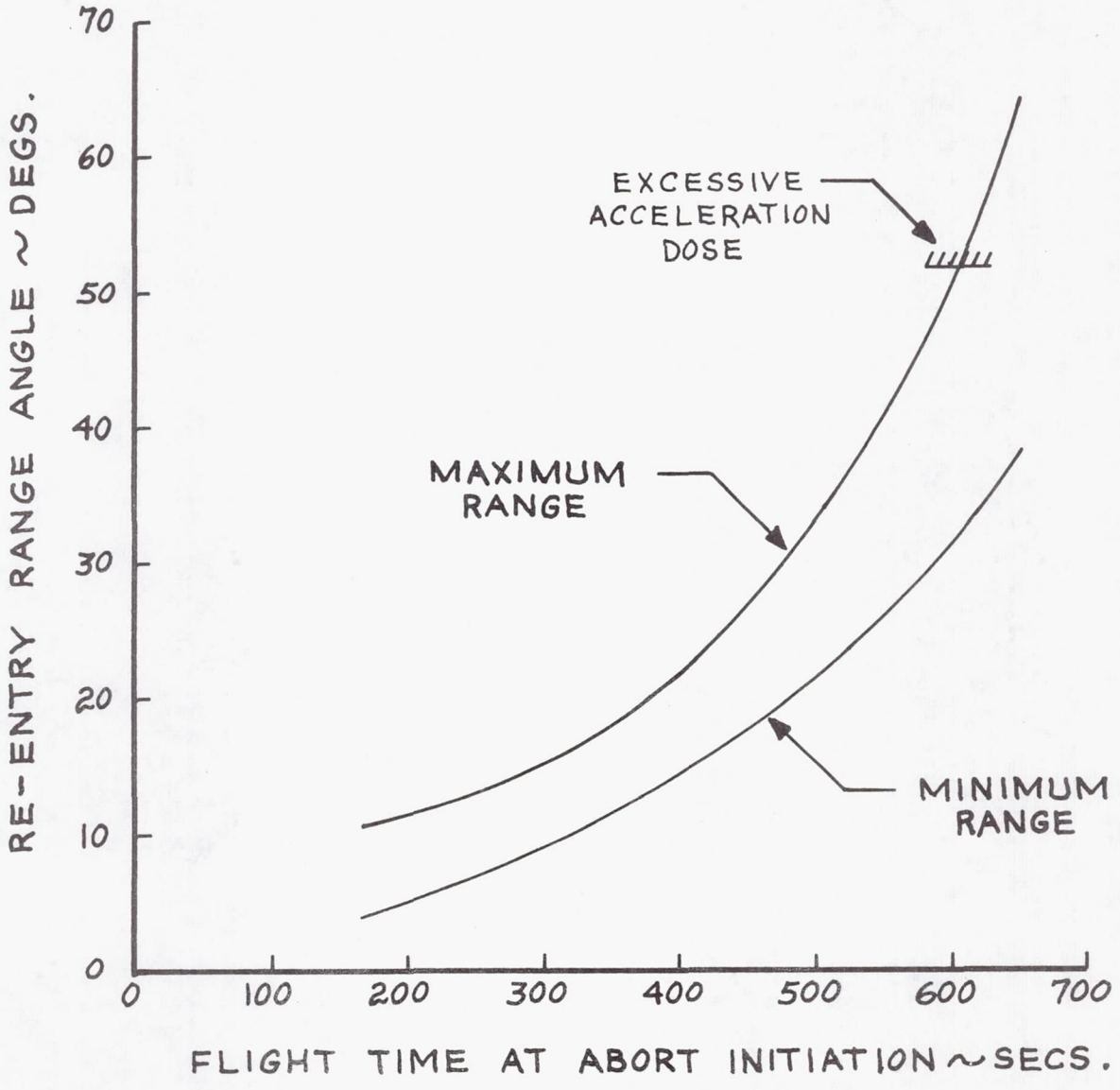

Figure 5

SATURN V POWERED ABORT

S - IV B

S - IV B
F = 200,000 LBS.
W_o = 359,268 LBS.

RE-ENTRY FLIGHT
PATH ANGLE = 94°
RE-ENTRY
ALTITUDE = 120 KM.

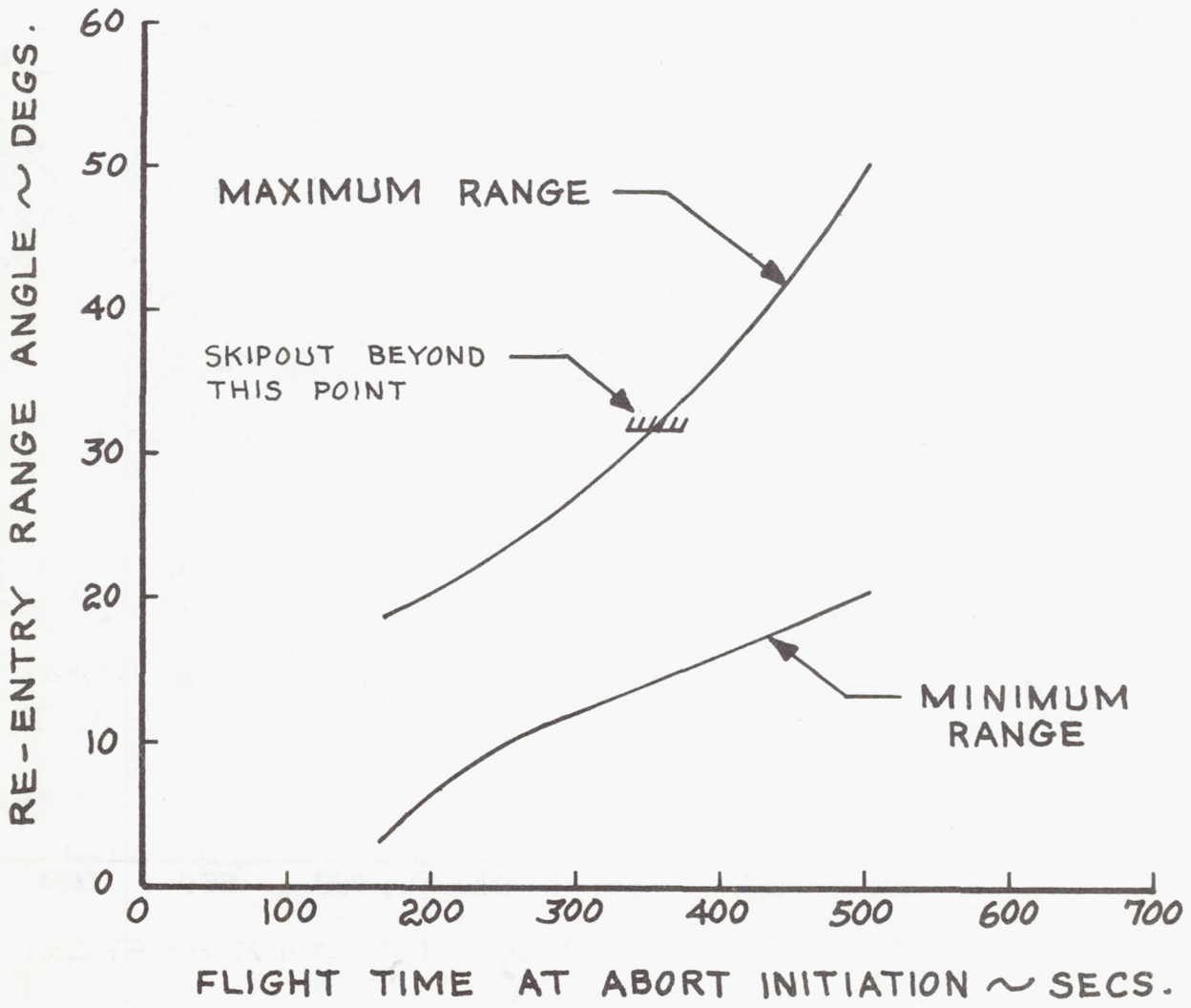

Figure 6

SATURN V POWERED ABORT

SERVICE MODULE

SERVICE MODULE
F = 21,500 LBS.
W_o = 61,120 LBS.

RE-ENTRY FLIGHT
PATH ANGLE = 94°

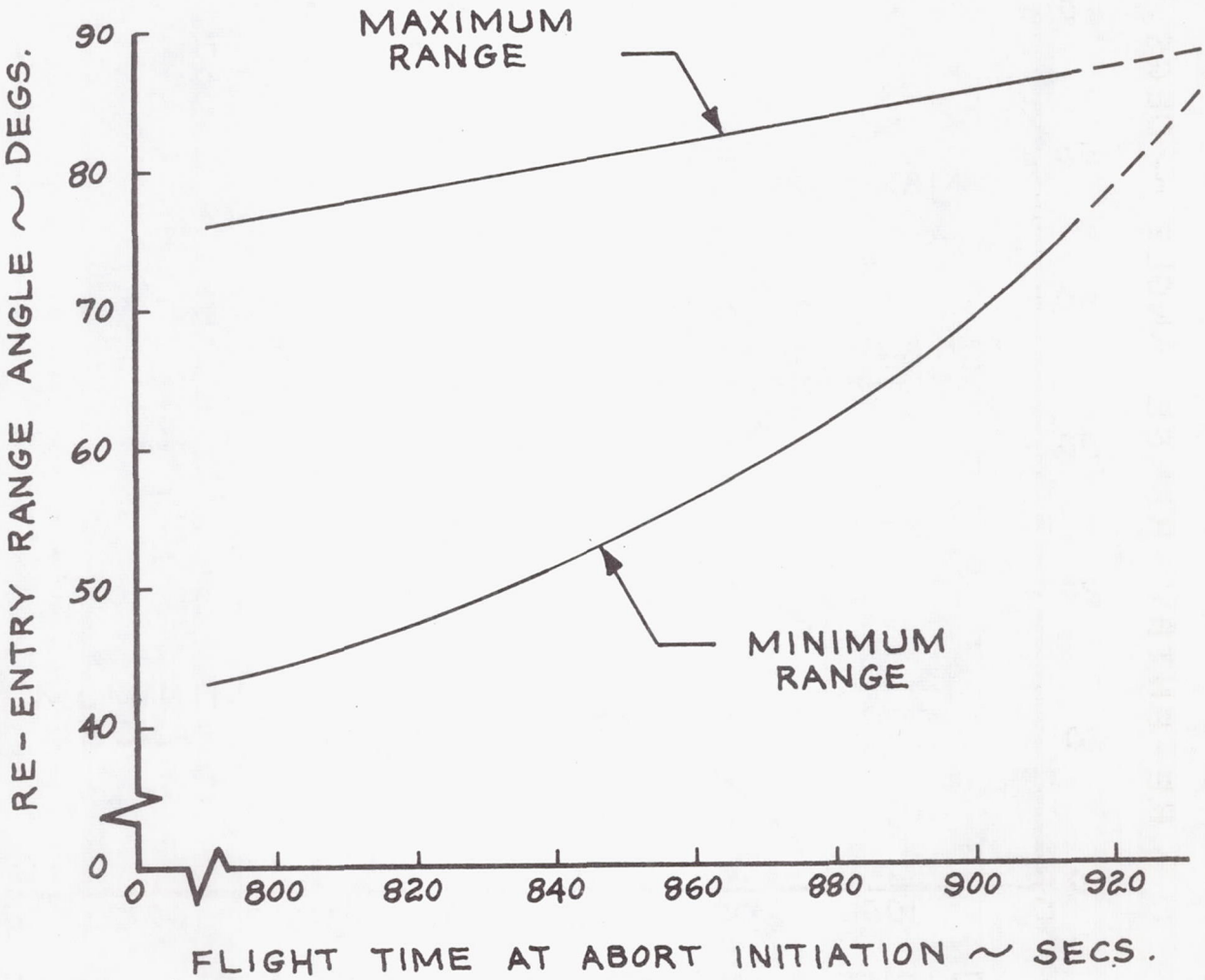

Figure 7

REFERENCES

1. Robinson, W.D., "Saturn V Powered Abort Study", Coordination Sheet AERO-H-186, Aeroballistics Unit, Saturn Booster Branch The Boeing Company, Huntsville, Alabama, May 17, 1963.

2. Albert L. Ayres, "Two Degree Dynamics (Calculus of Variations For Two Dimensional Vacuum Flight)", Boeing Document SH0001, Digital Computing Applications Unit, Saturn Booster Branch, The Boeing Company, November 13, 1962.

ANALYTICAL RESEARCH DEPARTMENT
RAYTHEON COMPANY
SPACE AND INFORMATION SYSTEMS DIVISION
BEDFORD, MASSACHUSETTS

RE-ENTRY CORRIDOR FOR MANNED LIFTING VEHICLE

by

Ann Muzyka and H. Elmore Blanton

Summary

A study has been made to determine the extreme re-entry flight-path angles, for various re-entry speeds, which permit safe, unpowered descent for a given manned lifting vehicle. Circular arcs, called entry arcs, were located at the initial altitude of 120 km. such that, for a specified initial speed and flight-path angle, entry at any point within the associated arc ensures the ability to arrive at the designated target on the surface of the earth.

I. INTRODUCTION

This study is part of the general abort re-entry problem. The trajectory of a space vehicle may include a boost phase which transports the vehicle through the atmosphere and into space, a powered and/or cruise phase through space, and a re-entry into the atmosphere followed by an unpowered descent to an altitude at which the landing

phase can begin. Somewhere along the powered phase of the trajectory a decision to abort may be necessary. The capability of a manned vehicle after an abort, especially its ability to re-enter the atmosphere safely, is of utmost importance.

This report is concerned with the re-entry corridor of a manned lifting vehicle descending through the atmosphere. Definition of this corridor requires finding the bounds on the re-entry velocity and position which permit a safe descent to a specified landing site. The acceptable initial conditions for re-entry and descent prescribe the terminal conditions for the exo-atmospheric phase of the trajectory. The results of the studies of the spatial and atmospheric phases of the trajectory must be combined to determine the situations from which successful aborts may be initiated.

II. LIST OF SYMBOLS

C_D	drag coefficient
C_L	lift coefficient
D	drag
L	lift
P	pilot penalty function
R	earth radius
S	reference area
T	final time
V	vehicle speed
V_o	initial (re-entry) vehicle speed
a	aerodynamic acceleration
g	gravitational acceleration
g_o	g at surface of the earth
h	altitude
m	vehicle mass
t	time
α	control variable, angle of attack
θ	flight-path angle
θ_o	initial (re-entry) flight-path angle
ρ	density of air
τ	pilot acceleration-endurance time
ϕ	angular displacement, range

III. PROBLEM DESCRIPTION

A. Dynamic Model

The vehicle is considered to be a particle of constant mass which moves in a plane with respect to a spherical, non-rotating earth. It is subject to the action of three forces: the inverse-square gravitational field of the earth, its lift, and its drag. The descent of the vehicle is controlled by varying the lift and drag forces. The variation of air density with respect to altitude is included. The force diagram is shown in Figure 1.

The weight of the vehicle is 8500 pounds and its reference area is 12.97 square meters. The aerodynamic coefficients are functions of the control variable, α, as shown in Figure 2. The maximum lift-to-drag ratio is 0.82 which occurs at $\alpha = 50°$. During this study, the angle of attack was constrained to the interval of $-70°$ to $70°$ because this interval includes the extreme variations in lift, drag, and lift-to-drag ratio.

Below Mach 2, the aerodynamic coefficients are functions not only of α but also of Mach number. In view of this consideration, a speed of Mach 2 served as the stopping condition for the computing. This speed occurs at altitudes compatible with the initiation of the landing phase.

B. Equations of Motion

$$m\dot{V} = -D - mg\cos\theta$$

$$mV(\dot{\theta} + \dot{\phi}) = -L + mg\sin\theta$$

$$(R + h)\dot{\phi} = V\sin\theta$$

$$\dot{h} = V\cos\theta$$

where

$$g = g_o\left(\frac{R}{R+h}\right)^2$$

$$D = \frac{1}{2} C_D(\alpha)\, \rho(h)\, V^2 S$$

$$L = \frac{1}{2} C_L(\alpha)\, \rho(h)\, V^2 S$$

and

$\rho(h)$ is given by ARDC Model Atmosphere 1956.

$C_D(\alpha)$ and $C_L(\alpha)$ are shown in Figure 2.

$g_o = 9.815$ m./sec^2

$R = 6.371 \times 10^6$ m.

$S = 12.97$ m.^{2}

$m = 393$ kg. sec^2/m.

C. Pilot Acceleration-Endurance Constraint

For a manned re-entry, α programs which produce excessive aerodynamic accelerations must be excluded. This condition is imposed during the solution procedure in the following way. A man's ability to remain usefully conscious is a function of both the aerodynamic accelerations he experiences and their durations. It has been shown that he can tolerate quite high accelerations if they are sufficiently brief. The dimensionless aerodynamic acceleration, a, is defined by

$$a = \frac{\sqrt{L^2+D^2}}{mg_o} .$$

Experiments have yielded the endurance limit $\tau(a)$ of experienced test pilots to given aerodynamic accelerations. By adding the equation

$$\dot{P} = \frac{1}{\tau(a)}$$

to the equations of motion, the "acceleration dose" or terminal value of the "pilot penalty function" is given by

$$P = \int_0^T \frac{1}{\tau(a)}\, dt,$$

where T is the time of flight. When this quantity becomes 1, the pilot is assumed to have had a full dose of acceleration; therefore, he should not be exposed to further accelerations that would increase this dose, if he is to function usefully. Thus, a terminal constraint is $P \leq 1$.

The pilot acceleration-endurance function, $\tau(a)$, used in this study is shown in Figure 3. This function was derived principally from information in References 1-3. The more recent data in References 4 and 5 reveal that the function of Figure 3 is conservative by factors from 2 to 5, in terms of permissible time for a given acceleration, if the pilot is oriented in the most favorable attitude. In the current study, however, the attitude of the vehicle is subject to wide variations in some maneuvers. If the pilot is exposed to similar variations in attitude, he may experience situations where, according to Reference 5, his endurance is significantly less than that shown in Figure 3. It is believed, however, that the $\tau(a)$ relation employed in the current study represents a reasonable compromise for the specification of pilot endurance to acceleration. As a refinement in the future, acceleration endurance might be introduced as a function of both aerodynamic acceleration and pilot attitude.

D. Procedure for Trajectory Optimization

The differential equations of motion together with the pilot penalty function form a non-linear system. The initial conditions are the altitude, 120 km., the re-entry speed, and the flight-path angle, the latter two being parameters of the study. The terminal condition is that the pilot not receive more than a full "dose" of acceleration, i.e. $P(T) \leq 1$. The control variable, $\alpha(t)$, occurs as an unspecified function.

For a given re-entry velocity (speed and flight path angle), the end points of the entry arcs are found from the maximum and minimum range trajectories. Several nominal α programs are assumed and the system is integrated by means of a high-speed digital computer for each one in turn. None will, in general, yield the extremal range nor satisfy the penalty constraint. The most promising α program is chosen and then subjected to successive improvements. A systematic procedure for producing such changes is the steepest-ascent method developed at Raytheon Company and described in Reference 6. It is a calculus of variations technique and alters the α program in such a way as both to improve the "pay-off" quantity that is being extremalized and to meet any terminal constraints. Thus a sequence of α programs is generated. This procedure is terminated when the terminal constraints are satisfied, and negligible gains in the pay-off quantity are produced by successive iterations.

For a given re-entry speed, the maximum re-entry flight-path angle can be found by increasing the initial flight-path angle until it becomes impossible to constrain the pilot penalty function to 1 either as a terminal constraint in an extremal-range series of iterations or, in more difficult cases, as the pay-off quantity in a minimal-pilot-penalty series of iterations. The minimum re-entry flight-path angle

is established theoretically at 90° for subcircular entry speeds and at an angle that exceeds 90° by an arbitrarily small amount for circular entry speed. For a supercircular entry speed, the minimum re-entry angle can be estimated using the work of References 7 and 8, and verified by decreasing the initial flight-path angle until, using maximum negative lift, the vehicle rises above the specified maximum altitude following the initial pass through the atmosphere.

IV. RESULTS

The results are tabulated in Table 1. For a given entry velocity, the angular distance between the target and the re-entry point nearest to the target is indicated in the Minimum Range column. If the vehicle enters the atmosphere at this distance from the target, the descent must be made using the α program associated with the minimum-range trajectory. An entry closer to the target will cause overshoot because the steepness of the trajectory is limited by the pilot penalty function. Similarly, the numbers in the Maximum Range column indicate the farthest from the target that entry may occur. The entry arc is the circular arc at the specified initial altitude of 120 km. joining the nearest and farthest possible re-entry points. Entry at any point within this arc with the associated initial speed and flight-path angle ensures the ability to arrive at the target. The entry flight-path angle, which is the direction of the initial velocity vector measured counterclockwise from the local vertical, can be confined to lie between 90° and 180°. The trajectory for an entry flight-path angle lying between 180° and 270° is the same as for its mirror image in the 90° to 180° range.

Table 1. Tabulation of Results

Entry Speed (m./sec.)	Entry Flight-Path Angle (degrees)	Minimum Range (degrees)	Maximum Range (degrees)	Entry-Arc Length (degrees)
750	90 180	0.93 0	1.05 ±0.05	0.12 0.10
3500	90 110	4.8 2.3	7.3 3.1	2.5 0.8
7833	90.50 101.75	46 8	138 16	92 8
11080	94.71 99.8	22 15	160* 110*	138 95

*See discussion in text.

The re-entry corridor, as it appears in the initial-flight-path-angle, initial-speed plane, is shown graphically in Figure 4.

For the lowest entry speed studied, 750 m./sec., there is no restriction on the initial flight-path angle. The vehicle can enter the atmosphere with a horizontal velocity or one which is straight down, but the range and entry-arc length are so small as to be negligible when compared with the performance at higher speeds.

The steepest entry angle for an entry speed of 3500 m./sec. is approximately 110°. At this entry angle, the pilot penalty constraint can be held to 1 for maximum and minimum ranges through appropriate modulation of the α program. A critical search was not made to verify the possibility of steeper entries because available information concerning the entire abort-trajectory problem indicated that re-entries for initial speeds of roughly 3500 m./sec. most likely will occur for angles less than 110°. The range and entry-arc capabilities at this speed may be of some significance for an entry at an angle of 90° but they both decrease drastically as the entry angle becomes steeper.

For true circular entry speed, the shallowest possible entry angle is undefined. A horizontal circular velocity, $\theta_o = 90°$, results in a circular orbit and consequently no entry if the effects of aerodynamic drag are absent. Any initial flight-path angle greater than 90° will result in re-entry, and the closer this angle is to 90°, the larger the maximum range. Similarly, a slight reduction in initial speed and/or the presence of slight aerodynamic drag at the specified initial altitude will lead to entry. For the solutions obtained during this study, the initial speed was circular for the entry altitude, but the atmospheric density, and hence drag, were defined to above this altitude in accordance with the ARDC Model Atmosphere, 1956.

In the circular-speed-entry studies, an arbitrarily selected shallow initial angle of 90.50° was found to lead to a maximum range of only 138°. As the entry angle becomes steeper, the maximum range decreases until it is only 16° for steepest permissible entry, $\theta_o = 101.75°$. The minimum ranges and the entry-arc lengths also are markedly less for the steeper entry angles. This situation is illustrated in Figure 5. It is significant to note that the entry arcs for the extreme entry angles do not overlap; consequently, several target areas will be necessary to effect successful recovery of space vehicles re-entering at circular speed if initial flight-path angles lie anywhere between the limits of 90° and 101.75°.

When a vehicle travelling at supercircular speed re-enters the atmosphere at a shallow flight-path angle, the aerodynamically produced deceleration may be insufficient to prevent the vehicle from rising above a specified altitude limit. Thus, the re-entry problem

reduces to the determination of the shallowest initial angle that leads to the satisfaction of the altitude restriction when the vehicle is flown with maximum negative lift. Through the use of results of theoretical analyses, as verified by numerical solutions, it was established that, for an entry speed of 11,080 m./sec. (essentially escape speed), acceptable re-entry can be accomplished for an entry angle as shallow as 94.71°, but not for one of 94.55°, when the altitude limit is 150 km. In lieu of attempting to define θ_o more exactly within this narrow range, 94.71° was taken as the shallowest initial flight-path angle at this speed.

The steepest entry angle at escape speed is limited by the pilot acceleration dose during the initial dive into the atmosphere. This dose is critically dependent on the precise modulation of the angle-of-attack program. For an entry angle of 99.8° an acceptable pilot-penalty value was achieved for both minimum and maximum range trajectories. Among the many trajectories evolved during the study of performance for steeper initial flight-path angles, none yielded an acceleration dose as low as 1.

Minimum-range capability for escape-velocity entries also is limited by the pilot acceleration dose. For the entry angles studied, this range decreased from 22° for 94.71° to 15° for 99.8° In the case of the shallow entry angle of 94.71°, a sufficient margin of negative lift was available to prevent the minimum-range trajectory from leaving the atmosphere following initial entry. Of course, for the actual shallowest permissible entry angle, which is between 94.55° and 94.71°, the minimum-range trajectory would include a rise to the specified maximum altitude of 150 km. and the resulting range would be substantially greater than 22°.

The computation of the maximum range for entries at escape speed becomes particularly difficult as the steepness of the entry angle increases. In these situations, the angle-of-attack program during the first 10% or less of the total flight time must be modulated extremely accurately in such a way that both the pilot-penalty and maximum-altitude restrictions are satisfied in a manner compatible with maximization of the range. The total pilot penalty is realized during roughly 2% of the flight time shortly after initial entry into the atmosphere, and the maximum altitude restriction, 150 km., occurs later in the flight during a long interval when the aerodynamic forces are negligible, thus complicating the solution process. During this study, the range capability was computed both by optimizing the performance during the entire time of flight and by combining extremal solutions for appropriately defined portions of the over-all trajectory. Cross checks were made to establish the compatibility of these approaches and to ensure the relative validity of the answers. The maximum ranges given in Table 1 represent

the "best" answers obtained. These ranges definitely are realizable under the specified conditions and perhaps can be increased through appropriate changes in the angle-of-attack program early in the flight.

The entry arcs for escape-speed entry are shown in Figure 6. For entry angles of 94.71° and 99.8°, the entry arcs overlap to a large extent indicating the feasibility of using a single recovery area.

In aborts during space missions, of course, the re-entry velocities are not subject to close control; they will lie between broad limits which are determined by many factors. Based on the results given in Table 1, if the speeds may be anywhere in range from zero up to escape and entry flight-path angles are unrestricted, recovery facilities would have to be provided on a continuous basis throughout possible re-entry areas. As the range of expected speeds decreases, and as probable flight-path angles are defined, projections may be made as to the discrete number of landing sites needed to effect successful recovery.

V. CONCLUSIONS

As re-entry speeds increase from 750 m./sec to escape speeds, restrictions arise on the possible re-entry flight-path angles. The shallowness of the entry, for supercircular entry speeds, is limited by the tendency of the vehicle to skip out; the steepness of the entry for all except the lowest speeds, by the acceleration-dose constraint. Stringent restrictions on initial flight-path angles which occur for escape-speed entries are coupled with wide tolerances on re-entry position. Re-entry speeds and flight-path angles must be limited more than indicated by the results reported here if a small number of landing sites is to offer a high probability of successfully recovering aborted spacecraft.

The results of this study define extreme re-entry conditions for the specified vehicle when subject only to pilot-acceleration-dose and altitude constraints. The re-entry corridor may be changed if any of the following considerations are included: the total heat and/or heating rate is constrained; the pilot-acceleration-endurance function includes pilot attitude dependence; or the magnitude of the angle of attack is limited.

ACKNOWLEDGMENT

The encouragement and assistance rendered during the course of this work by Mr. W. E. Miner, Future Projects Branch, Aeroballistics Division, Marshall Space Flight Center, and Dr. F. Wm. Nesline, Jr., Analytical Research Department, Space and Information Systems Division, Raytheon Company, and by staff members of these two groups is gratefully acknowledged. The authors also sincerely appreciate the cooperation received from the personnel of the Computation Division, Marshall Space Flight Center, where all numerical calculations were carried out using IBM 7090 and 7094 high-speed computing facilities.

REFERENCES

1. Bryson, A. E., and Denham, W. F., "Guidance Scheme for Supercircular Re-Entry of a Lifting Vehicle," American Rocket Society Journal, Vol. 32, No. 6, June 1962, pp 894-898.

2. Konecci, E. B., "Manned Space Cabin Systems," Chapter 4 of Advances in Space Sciences, Vol. 1, R. I. Ordway III, ed., Academic Press, N.Y., 1959.

3. Hegenwald, J., and Oishi, S., Human Tolerance to Acceleration, North American Aviation, Inc., 1957.

4. Creer, B. Y., Smedal, H. A., and Wingrove, R. C., Centrifuge Study of Pilot Tolerance to Acceleration and the Effects of Acceleration on Pilot Performance, National Aeronautics and Space Administration, Technical Note NASA TN-D-337, 1960.

5. Chambers, R. M., and Hitchcock, L., Jr., "Effects of High G Conditions on Pilot Performance," Proceedings of the National Meeting on Manned Space Flight, co-sponsored by National Aeronautics and Space Administration and Institute of the Aerospace Sciences, St. Louis, April 30 - May 2, 1963, pp 204-217.

6. Bryson, A. E., and Denham, W. F., "A Steepest-Ascent Method for Solving Optimum Programming Problems," Trans. of ASME, Series E: Journal of Applied Mechanics, Vol. 29, No. 2, June 1962, pp 247-257; also Raytheon Company, Report BR-1303, Aug. 10, 1961.

7. Chapman, D. R., An Approximate Analytical Method for Studying Entry into Planetary Atmospheres, National Aeronautics and Space Administration, Technical Report NASA TR R-11, 1959.

8. Chapman, D. R., An Analysis of the Corridor and Guidance Requirements for Supercircular Entry into Planetary Atmospheres, National Aeronautics and Space Administration, Technical Report NASA TR R-55, 1960.

FORCE DIAGRAM

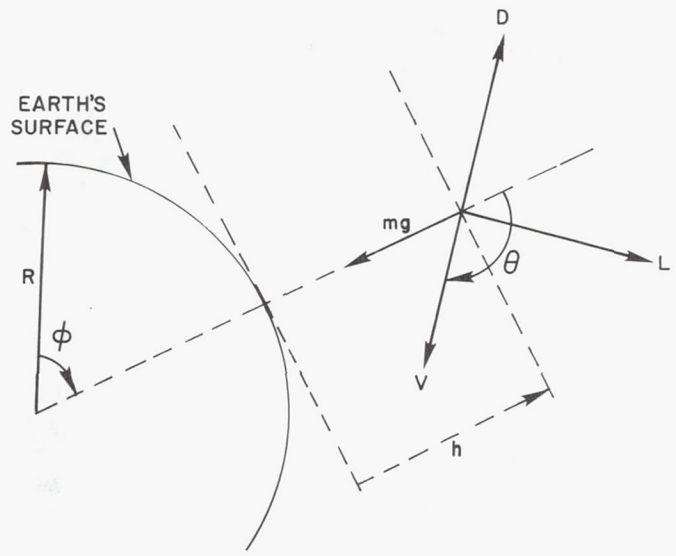

FIGURE 1

LIFT AND DRAG COEFFICIENTS
VS ANGLE OF ATTACK

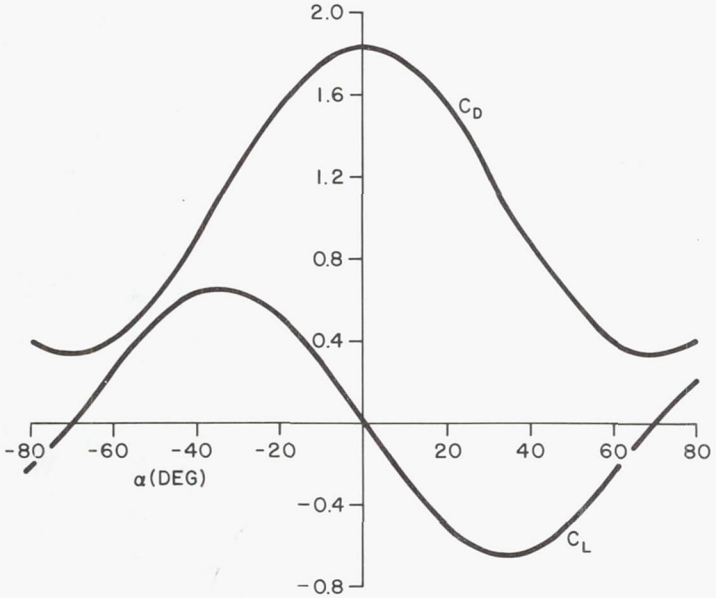

FIGURE 2

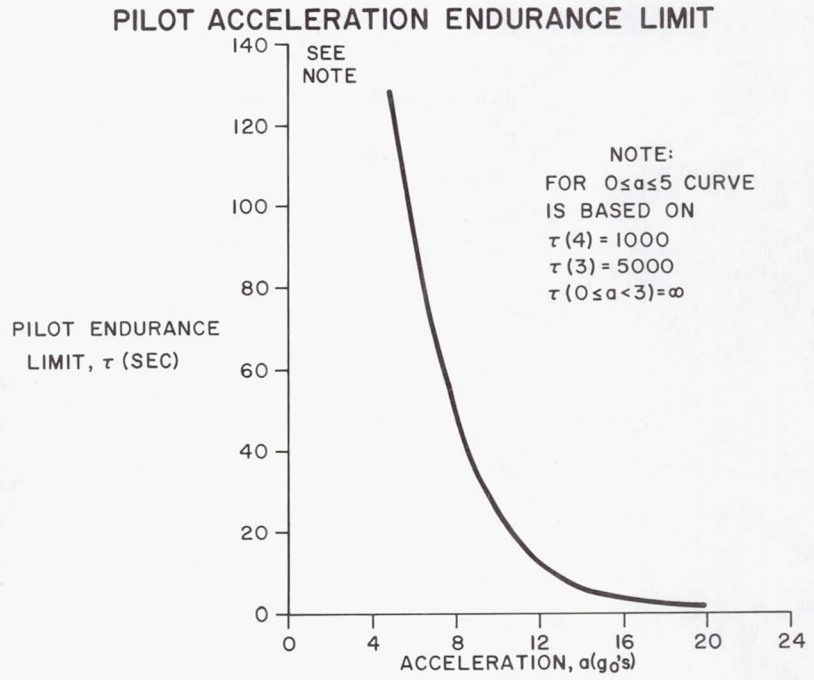

FIGURE 3

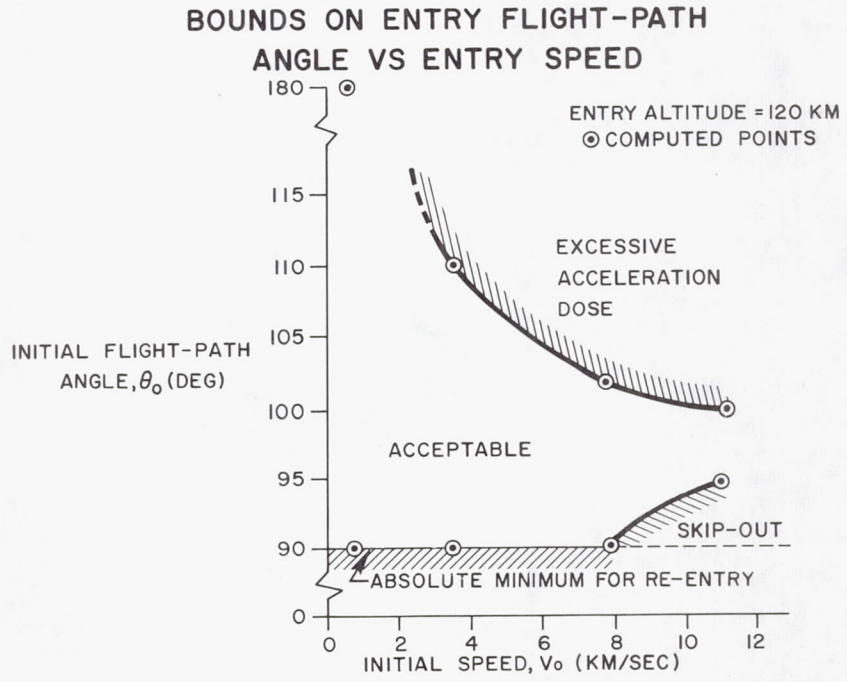

FIGURE 4

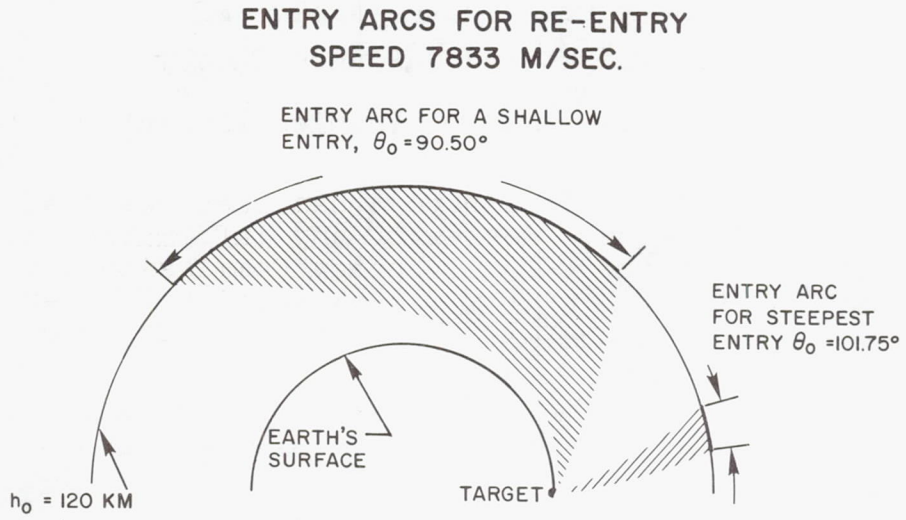

FIGURE 5

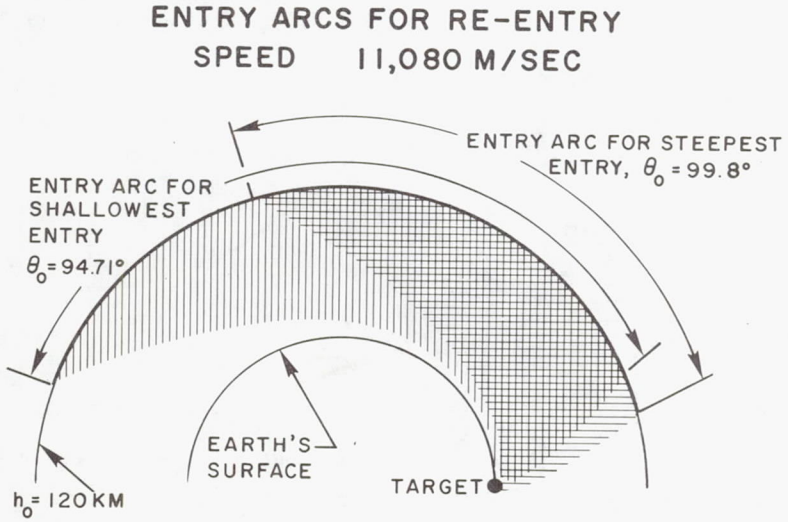

FIGURE 6

APPROVAL

IMPLEMENTATION REPORT NO. 1
on Studies in the Fields of
Space Flight and Guidance Theory

Sponsored by Aero-Astrodynamics Laboratory

The information in this report has been reviewed for security classification. Review of any information concerning Department of Defense or Atomic Energy Commission programs has been made by the MSFC Security Classification Officer. This report, in its entirety, has been determined to be Unclassified.

APPROVED

W. E. MINER, Deputy Chief
Astrodynamics & Guidance Theory
Division

E. D. GEISSLER
Dir, Aero-Astrodynamics Laboratory

DISTRIBUTION LIST

INTERNAL

DIR

DEP-T

CC-P

MS-H

MS-IPL (8)

AST-P, Mr. Hardee

MS-IP, Mr. Ziak
Mr. Scott

R-AERO, Dr. Geissler
Dr. Hoelker
Mr. Miner (80)
Mr. Braud
Mr. Ingram
Mr. Schmieder
Mr. Tucker
Mr. Dearman
Mr. Winch
Mr. Schwaniger
Mr. Teague
Mr. Lisle
Dr. Sperling
Dr. Heybey
Mr. Cummings
Mr. Thomae
Mr. Baker
Mr. Kurtz
Mr. Lovingood
Mr. Hart
Mrs. Chandler
Mr. deFries
Mr. Callaway
Mr. Jean
Mr. Telfer
Mr. McDaniel
Mr. Goldsby
Mr. Felker
Mr. Martin

I-I/IB, Col. James
Mr. Bramlet

R-P&VE, Mr. Swanson
Mr. Burns
Dr. Krause

R-ASTR, Mr. Brandner
Mr. Moore
Mr. Richard
Mr. Gassaway (4)
Mr. Taylor
Mr. Brooks
Mr. Hosenthien
Mr. Scofield
Mr. Woods
Mr. Digesu
Mrs. Neighbors
Mr. R. Hill
Mr. Thornton

R-COMP, Dr. Arenstorf
Mr. Harton
Mr. Iloff
Mr. Schollard
Mr. Seely
Mr. Davidson

DISTRIBUTION LIST (CONT'D)

EXTERNAL

Minneapolis-Honeywell Regulator Company
Military Products Group
Aeronautical Division
2600 Ridgway Road
Minneapolis 40, Minnesota
ATTN: Mr. J. T. Van Meter
Mr. William C. Marshall
Mr. Dahlard Lukes

Space Sciences Laboratory
Space and Information Systems
North American Aviation, Inc.
Downey, California
ATTN: Dr. D. F. Bender
Mr. Gary McCue
Mr. H. A. McCarty

Mr. T. W. Scheuch
North American Aviation, Inc.
Holiday Office Center
Huntsville, Alabama
ATTN: Mr. S. E. Cooper

Dr. Daniel E. Dupree
Department of Mathematics
Northeast Louisiana State College
Monroe, Louisiana

Dr. Steve Hu
Northrop Corporation
Box 1484
Huntsville, Alabama

Raytheon Company
Missile and Space Division
Analytical Research Department
Bedford, Massachusetts
ATTN: Dr. F. William Nesline, Jr.
Miss Ann Muzyka

DISTRIBUTION LIST (CONT'D)

EXTERNAL

Mr. Frank J. Carroll
Raytheon Company
Equipment Division
Systems Requirement Department
40 Second Avenue
Waltham, Massachusetts

Mr. J. R. Bruce
Northrop Corporation
3322 Memorial Parkway, S. W.
Huntsville, Alabama

Southern Illinois University
Department of Mathematics
Carbondale, Illinois
ATTN: Dr. Robert W. Hunt
Mr. Robert Silber

Dr. Henry Hermes
Research Institute of Advanced Study
7212 Bellona Avenue
Baltimore 12, Maryland

Analytical Mechanics Associates, Inc.
941 Front Street
Uniondale, New York
ATTN: Mr. Samuel Pines
Dr. H. J. Kelley

Dr. W. A. Shaw
Mechanical Engineering Department
Auburn University
Auburn, Alabama

Bendix Systems Division
The Bendix Corporation
3322 Memorial Parkway South
Huntsville, Alabama
ATTN: Mr. William Green
Mr. Robert Glasson

Dr. Rudolph Kalman
Research Institute for Advanced Study
7212 Bellona Avenue
Baltimore, Maryland

DISTRIBUTION LIST (CONT'D)

EXTERNAL

The Boeing Company
P. O. Box 1680
Huntsville, Alabama
ATTN: Mr. Richard Hardy, Box AB-38
Mr. Wes Morgan, Box AB-49

Mr. Oliver C. Collins
Mail Stop 15-12
Organization 2-5762
Flight Technology Department
The Boeing Company
Seattle 24, Washington

Chrysler Corporation Missile Division
Sixteen Mile Road and Van Dyke
P. O. Box 2628
Detroit 31, Michigan
ATTN: Mr. T. L. Campbell
Mr. R. J. Vance
Dept. 7162
Applied Mathematics

Mr. George Westrom
Astrodynamics Section
Astrosciences Department
Aeronutronic Division ofFord Motor Company
Ford Road
Newport Beach, California

Astrodynamics Operation
Space Sciences Laboratory
Missile and Space Vehicle Department
General Electric Company
Valley Forge Space Technology Center
P. O. Box 8555
Philadelphia 1, Pennsylvania
ATTN: Mr. J. P. deVries
Dr. V. Szebehely
Mr. Carlos Cavoti (8)

Auburn Research Foundation (2)
Auburn University
Auburn, Alabama

DISTRIBUTION LIST (CONT'D)

EXTERNAL

Dr. I. E. Perlin
Rich Computer Center
Georgia Institute of Technology
Atlanta, Georgia

Research Department
Grumman Aircraft Engineering Corporation
Bethpage, L.I., New York
ATTN: Mr. Hans K. Hinz
Mr. Gordon Pinkham
Mr. Gordon Moyer

Grumman Library
Grumman Aircraft Engineering Corporation
Bethpage, Long Island, New York

Jet Propulsion Laboratory
4800 Oak Grove Drive
Pasadena 3, California
ATTN: Mr. Howard Haglund
Mr. W. G. Melbourne
Dr. John Gates

Mr. Harry Passmore
Hayes International Corporation
P. O. Box 2287
Birmingham, Alabama

Mr. J. S. Farrior
Lockheed
P. O. Box 1103
West Station
Huntsville, Alabama

Dr. Charles C. Conley
University of Wisconsin
Department of Mathematics
Madison, Wisconsin

Mr. Robert Reck
Martin Company
3313 S. Memorial Parkway
Huntsville, Alabama

DISTRIBUTION LIST (CONT'D)

EXTERNAL

Dr. John W. Carr, III
Department of Mathematics
University of North Carolina
Chapel Hill, North Carolina

Mr. J. W. Hanson (20)
Computation Center
University of North Carolina
Chapel Hill, North Carolina

Dr. M. G. Boyce (3)
Department of Mathematics
Vanderbilt University
Nashville 5, Tennessee

University of Kentucky
College of Arts and Science
Department of Mathematics and Astronomy
Lexington, Kentucky
ATTN: Dr. Eaves
Dr. Krogdahl
Dr. Pignani
Dr. Wells

University of Kentucky Library (10)
University of Kentucky
Lexington, Kentucky

Space Flight Library (4)
University of Kentucky
Lexington, Kentucky

Mr. Robert E. Allen
Manager, Huntsville Sales Office
A. C. Spark Plug of General Motors
Holiday Office Center
Huntsville, Alabama

Dr. Hermann M. Dusek
A. C. Spark Plug of General Motors
950 N. Sepulbeda Blvd.
Elsegundo, California

DISTRIBUTION LIST (CONT'D)

EXTERNAL

Mr. Rigdon
VITRO Laboratory
14000 Georgia Avenue
Silver Springs, Maryland

Mr. Donald Jezewski
Guidance Analysis Branch
Spacecraft Technology Division
Manned Spacecraft Center
Houston, Texas

Mr. Fred D. Breuer
General Dynamics/Astronautics
Lunar Systems
Department 580-3
Mail Zone 580-30
San Diego, California

Mr. Ralph W. Haumacher
A2-863: Space/Guidance & Control
Douglas Aircraft Corporation
3000 Ocean Park Blvd.
Santa Monica, California

Dr. B. Paiewonsky
Aeronautical Research Associates of Princeton
50 Washington Road
Princeton, New Jersey

Dr. Cheng Ling
Principle Staff Engineer
Systems Research Section, R & A T Dept.
Electronic Systems and Products Division
Martin Company
Baltimore 3, Maryland

The Martin Company
Space Systems Division
Mail # 3072
Baltimore 3, Maryland
ATTN: Mr. William E. Wagner
Mr. A. H. Jazwinski

DISTRIBUTION LIST (CONT'D)

EXTERNAL

Douglas Aircraft Corporation
3000 Ocean Park Blvd.
Santa Monica, California
ATTN: R. E. Holmen A2-263
Guidance & Control Section

Dr. Byron D. Tapley
Department of Aerospace Engineering
University of Texas
Austin, Texas

Langley Research Center
Hampton, Virginia
ATTN: Mr. Hewitt Phillips
Librarian (2)

Mr. Robert Chilton
Manned Spacecraft Center
Houston, Texas

Mr. Howard S. London
Bellcomm, Inc.
Room 910-E
1100 17th Street, N. W.
Washington 6, D. C.

Mr. Paul T. Cody
76 Central Street
Peabody, Massachusetts

Mr. George Cherry
Massachusetts Institute of Technology
Cambridge, Massachusetts

Mr. F. A. Hewlett
Manager of Documentation
IBM Federal Systems Division
6702 Gulf Freeway
Houston 17, Texas

Mr. T. Perkins
Chrysler Corporation
HIC Building
Huntsville, Alabama

DISTRIBUTION LIST (CONT'D)

EXTERNAL

Dr. R. M. L. Baker, Jr.
Lockheed-California Company
A Division of Lockheed Aircraft Co.
Burbank, California

Corporate Systems Center
United Aircraft Corporation
Windsor Locks, Connecticut
ATTN: Mr. Robert Gregoire
Mr. Samuel P. Altman

Mr. Roger Barron
Adaptronics, Inc.
4725 Duke Street
Alexandria, Virginia

Dr. Ray Rishel
Physics Technical Department
Organization No. 25413, Box 2205
The Boeing Company
Box 3707
Seattle 24, Washington

Scientific and Technical Information Facility (2)
ATTN: NASA Representative (S-AK/RKT)
P. O. Box 5700
Bethesda, Maryland

NASA Ames Research Center
Mountain View, California
ATTN: Librarian

NASA
Goddard Space Flight Center (2)
Greenbelt, Maryland
ATTN: Librarian

Office of Manned Space Flight
NASA Headquarters
Federal Office Building #6
ATTN: Dr. Joseph Shea
Mr. Eldon Hall
Mr. A. J. Kelley
Mr. J. I, Kanter

DISTRIBUTION LIST (CONT'D)

EXTERNAL

NASA
Launch Operations Directorate (2)
Cape Canaveral, Florida
ATTN: Librarian

NASA
Lewis Research Center (2)
Cleveland, Ohio
ATTN: Librarian

NASA Manned Spacecraft Center (2)
Houston 1, Texas
ATTN: Librarian

NASA
Wallops Space Flight Station
Wallops Island, Virginia
ATTN: Librarian (2)

Dr. George Nomicos, Chief (5)
Applied Mathematics Section
Applied Research and Development
Republic Aviation Corporation
Farmingdale, Long Island, New York

NASA Goddard Space Flight Center
Greenbelt, Maryland
ATTN: Dr. Peter Musen
Mr. Ken Squires, Bldg. 1

Dr. Dirk Brouwer
Yale University Observatory
Box 2023, Yale Station
New Haven, Connecticut

Smithsonian Institution Astrophysical Observatory
60 Garden Street
Cambridge 38, Massachusetts
ATTN: Dr. Imre Izsak
Dr. Yoshihide Kozai

Mr. Ken Kissel
Aeronautical Systems Division
Applied Mathematics Research Branch
Wright-Patterson Air Force Base
Dayton, Ohio

DISTRIBUTION LIST (CONT'D)

EXTERNAL

Mr. Jack Funk
Manned Spacecraft Center
Flight Dynamics Branch
N. A. S. A.
Houston, Texas

Dr. Paul Degrarabedian
Space Technology Laboratory, Inc.
Astro Science Laboratory
Building G
One Space Park
Redondo Beach, California

Mr. George Leitmann
Associate Professor, Engineering Science
University of California
Berkeley, California

Mr. Theodore N. Edelbaum
Senior Research Engineer
Research Laboratories
United Aircraft Corporation
400 Main Street
East Hartford, Connecticut

Dr. J. B. Rosser
Department of Mathematics
Cornell University
Ithaca, New York

Dr. Jurgen Moser
Progessor Mathematics
Graduate School of Arts and Science
New York University
New York City, New York

Dr. Lu Ting
Department of Applied Mathematics
Polytechnic Institute of Brooklyn
333 Jay Street
Brooklyn 1, New York

Dr. O. R. Ainsworth
Department of Mathematics
University of Alabama
University, Alabama

DISTRIBUTION LIST (CONT'D)

EXTERNAL

Mr. E. L. Harkleroad
Office of Manned Space Flight
NASA, Code MI
Washington, D. C.

Mr. E. M. Copps, Jr.
MIT, Instrumentation Labs
68 Albany Street
Cambridge 39, Massachusetts

Dr. M. L. Anthony
Mail Number A-95
The Martin Company
Denver, Colorado

Dr. R. P. Agnew
Department of Mathematics
Cornell University
Ithaca, New York